**CAD/CFD Integration System for Flow Control Product Optimization**

by

Lei Li

A thesis submitted in partial fulfillment of the requirements for the degree of

Doctor of Philosophy

Department of Mechanical Engineering
University of Alberta

# Abstract

Computational fluid dynamics (CFD) has been extensively used for fluid flow simulation and thus, guiding the flow control device design. However, CFD simulation requires explicit geometry input and complicated solver setup, which is a barrier in case of the cyclic CAD/CFD integrated design process. So far, tedious human interventions are inevitable to fill the gap. To fix this issue, this research proposes a theoretical framework where the CFD solver setup can be intelligently assisted by the simulation intent capture. Five innovative feature concepts are proposed. The fluid functional feature is used to capture the design intent while the fluid physics feature and dynamic physics feature present the simulation intent. The inter-feature associations are established by CAE boundary features and effect features. These feature concepts are defined based on the need of CAD/CFD integration and intelligent CFD solver functions for steam simulation. A prototype software tool has been developed for intelligent CAD/CFD integration, where the design intent and CFD simulation intent are associated seamlessly. An outflow control device (OCD) model, used in the steam assisted gravity drainage (SAGD) process, is studied by applying this prototype, and the target performance of this design is effectively reflected and virtually improved. The optimization result is further validated by a realistic OCD model from the industry, which confirms the software tool can provide design guidance for better steam even distribution. Therefore, it proves that the proposed method is capable of supporting complex design optimization in practice.

# Preface

This thesis is my original work. Some parts of this thesis have been published or accepted by the journals or conferences listed below.

1. Li, Lei, Yongsheng Ma, Mahdi Mahmoudi, Vahidoddin Fattahpour, and Carlos F Lange. 2018. "Steps toward Designing the Optimum Outflow Control Device for SAGD Using Computational Fluid Dynamics Simulation." In *SPE Canada Heavy Oil Technical Conference*. Society of Petroleum Engineers.

2. Li, Lei, Carlos F Lange, and Yongsheng Ma. 2018. "Artificial Intelligence Aided CFD Analysis Regime Validation and Selection in Feature-based Cyclic CAD/CFD Interaction Process." *Computer-Aided Design and Applications*.

3. Li, Lei, Yongsheng Ma, and Carlos F Lange. 2017. "CFD Expert System for Steam Simulation." In *Proceedings of the 25$^{th}$ Annual Conference of the Computational Fluid Dynamics Society of Canada*. Windsor, Canada: CFD Society of Canada.

4. Li, Lei, Carlos F Lange, and Yongsheng Ma. 2017. "Association of Design and Computational Fluid Dynamics Simulation Intent in Flow Control Product Optimization." *Proceedings of the Institution of Mechanical*

*Engineers, Part B: Journal of Engineering Manufacture*: 0954405417697352. doi:10.1177/0954405417697352.

5. Li, Lei, Carlos F Lange, and Yongsheng Ma. 2016. "CFD Modelling of Outflow Control Device Applied in Steam Assisted Gravity Drainage." In *Proceedings of the 24th Annual Conference of the Computational Fluid Dynamics Society of Canada*. Kelowna, Canada: CFD Society of Canada.

6. Li, Lei, and Yongsheng Ma. 2016. "CAD/CAE Associative Features for Cyclic Fluid Control Effect Modeling." *Computer-Aided Design and Applications* 13(2): 208–20. doi:10.1080/16864360.2015.1084190.

7. Li, Lei, Yongsheng Ma, and Carlos F Lange. 2016. "Association of Design and Simulation Intent in CAD/CFD Integration." *Procedia CIRP* 56: 1–6. doi:10.1016/j.procir.2016.10.006.

# Acknowledgements

This thesis is completed under the guidance of my co-supervisors, Dr. Yongsheng Ma and Dr. Carlos F. Lange, who are not only outstanding researchers but also excellent educators in University of Alberta. I would like to express my sincere gratitude to their dedicated instructions and prompt help during my doctoral program. They have unlocked the door to rigorous research for me, which will be the treasure of my life.

The financial support from China Scholarship Council (CSC), Natural Sciences and Engineering Research Council of Canada (NSERC), Alberta Innovates Technology Futures (AITF), RGL Reservoir Management, and University of Alberta is greatly appreciated. With the support provided, I could immerse myself in this research deeply, which guarantees the quality of my work.

The useful suggestions from my supervisory committee members, Dr. Ming J. Zuo and Dr. Rafiq Ahmad, are also gratefully acknowledged here. In addition, I want to thank my colleagues in University of Alberta and the researchers in RGL Reservoir Management, who have helped me address the problems in my research.

Special thanks go to my parents who always support me no matter what kind of difficulty I am faced with. This considerate support bridges the distance between us and keeps me moving forward toward my goals.

# Table of Contents

# List of Tables

# List of Figures

# Chapter 1 : Introduction and Objectives

## 1.1 Research Background and Motivation

Simulation Based Design (SBD) has been extensively used in recent years to meet the increasing demand for the product performance. To conduct SBD, CAD and CAE are the commonly used tools: the former for product modeling while the later for physical simulation. They are expected to be seamlessly integrated, where the communications among the participators involved are supposed to be highly effective (Zheng et al. 2008). However, there are evident gaps in practice that design intent embedded in CAD is missing during model transfer into CAE, e.g., the designable geometric parameters cannot be identified in CAE and thus, design changes cannot be accurately determined through analyzing the simulation results. In addition, CAD and CAE are still operated by different groups of engineers because of their distinctive expertise (Shephard et al. 2004). Plenty of information communications are required to maintain a consistent product development process; however, this complicates the product development process and severely delays the design cycle time, especially given the cyclic characteristic.

To bridge this gap, a primary idea is to remove the barrier through realizing CAD/CAE integration (J. Liu, Duke, and Ma 2015; J. Liu et al. 2015). So far, the integration can be categorized into two aspects: maintaining the geometric information consistency and automating the CAE solver setup. Both aspects have

been extensively studied, but a mature integration solution is still vacant, especially coming to the field of computational fluid dynamics (CFD), which requires rich experience and strong background knowledge to identify the flow regime and properly select the physics models.

In this research, a CAD/CFD integration system is developed, with which a design engineer without deep knowledge in CFD is expected to be able to conduct the flow control device development independently. Meanwhile, the mechanism of design and simulation intent interaction is deeply explored. A few novel feature concepts are proposed, where fluid physics features and dynamic physics features are used to convey simulation intent; fluid functional features are used for defining design intent (L. Li, Ma, and Lange 2016). In addition, the CAE boundary features and CAE effect features (L. Li and Ma 2016) are proposed to establish inter-feature associations. More descriptions of these feature classes will be given in the following sections.

The literature review in the following section introduces the development history of CAD/CAE integration systems to facilitate SBD and CFD expert systems to assist solver setup. The optimization techniques in an integrated envionment are also reviewed. The feature modeling technology, CFD simulation and best practices, and approximation-based optimization algorithms are applied as the methods to conduct this research, which are detailed in section 1.3. Section 1.4 presents the objectives of this research. The structure of this thesis corresponding to the research objectives is specified in section 1.5.

## 1.2 Literature Review

### 1.2.1 CAD/CAE Integration

From the early 1980s to 2000, CAD and CAE researchers focused on the geometry conversion and simplification. During that period, semantic information related to the CAE geometry meshes was missed during the conversion, and redundant efforts were needed to recover the lost information, i.e. the boundary conditions. Therefore, the efficiency was low, especially for cyclic design processes.

To remedy this deficiency, there are two common approaches proposed: one is to develop an integrated system with both CAD and CAE modules, for which the feature-based techniques are supposed to maintain the semantic information during model conversion; the other is to develop a unified feature model incorporating with both CAD and CAE information, with which both CAD and CAE views could be extracted and the information consistency could be easily sustained (Willem F Bronsvoort and Jansen 1993).

For the first approach, Kao et al. (2006) introduce an integrated system to generate thread rolling die-plate geometry. The design parameters are linked to SolidWorks through Microsoft Excel. Matin et al. (2012) put forward a feature-based CAD/CAE integration system for mold design. With the commercial CAD software Pro/Engineer, the specific mold design module guarantees rapid mold modification. The simulation module determines the injection molding parameters.

Lin and Kuo (2008) build an integrated CAD/CAE/CAM system for automobile stamping die development. In this system, STRIM is used as 3D surface construction CAD software, CATIA as CAD/CAE software, DYNAFORM as stamping formability analysis software and CADCEUS as CAM software. Johansson (2014) develops a prototype system to integrate SolidWorks, ANSA and LS-Dyna simulating the behavior of ski-racks during car collision. For the latter, Deng et al. (2002) propose the CAD/CAE feature concept to incorporate both CAD and CAE information. CAD/CAE features are related to both design and analysis processes. The geometric information derived from CAD features is assigned to CAD/CAE features. The design intent is transformed to the CAE portion of the CAD/CAE features. The integration can be established once all the CAD/CAE features are created. Lee (2005) develops a feature-based single model for CAD and CAE integration. It is unique for the multi-resolution and multi-abstraction modeling techniques making it capable of a wide range of applications. Cuillière and Francois (2014) establish a unified topological model to integrate CAD, FEA and topology optimization. This originally developed environment and database organization enable multi-source model utilization, automatic meshing, reanalysis corresponding to remeshing, and topology optimization.

CAE analysis is carried out to check whether the design is satisfactory. If not, the reasoning of the analysis results is significant in guiding the following design modifications. This actually forms the reverse process of CAD/CAE integration. Different methods are available to properly interpret the analysis results. Merkel

and Schumacher (2004) utilize response surface methods in the CAE driven product development. Park and Dang (2010) use commercial CAD and CAE software constructing an integrated system to achieve structural optimization with metamodeling techniques including response surface method and radial basis function. Robinson et al. (2012) propose a method to obtain optimized design by adding new parameters or features to CAD model incrementally.

There have been commercial software tools providing integration support. For example, SolidWorks has a CFD module embedded in the software environment. ANSYS Workbench is capable of carrying out modeling, meshing, simulation and optimization in a single environment. TOSCA is integrated into this environment as the optimization module (Sun, Yang, and Tian 2013). It has a wide range of application in solid and fluid mechanics. The optimization result can be remeshed automatically to get validated. However, the CFD module in SolidWorks is not comprehensive due to its limitation in mesh type and solver. The usability of the modeler in ANSYS Workbench is not sufficiently powerful and flexible. Moreover, the optimization process is not fully automated. In these commercial and integrated packages, high-level feature information is still not explicitly managed in the CAD/CAE interaction conversion cycles (Uddin and Ma 2015). In general, there are some limitations both in the research and application of CAD/CAE integration. CAE-oriented design information cannot be fully described. The CAE calculation accuracy which has not obtained enough emphasis is actually a critical factor in the design optimization. In addition, the

research conducted in the fluid domain is not sufficient. As a result, further research on this issue is needed.

### 1.2.2 CFD Expert System

Seen from the developing history, CAD/CAE integration is a demanding research topic in the past two decades, as interfacing design and simulation tools for intelligent product development is still widely recognized as a technical gap without a general solution. Besides the effort of synchronizing the CAD and CAE models and interpreting the CAE results, the CAE model setup should be highlighted as a vital component which affects the simulation accuracy greatly. The question of how to create a correct CAE model automatically poses another barrier for seamless CAD/CAE integration. This situation becomes even worse when CFD is needed to analyze the flow field because the CFD model requires special expertise and rich experience to deal with the nonlinearity.

To assist the CFD solver setup, an effective approach is to embed knowledge into the CFD system. The knowledge is represented as rules and coded into the system. Such kind of rule-based system is also known as expert system which is the simplest form of artificial intelligence (Grosan and Abraham 2011). Dating back to 1980s, Kutler and Mehta (1984) investigated the potential impact of artificial intelligence on aerodynamic simulation. One of the first implemented AI/CFD systems was an expert cooling fan design system called EXFAN proposed by Tong (TONG 1985; ANDREWS 1988). EXFAN is a rule-based

system developed on top of a Fortran CFD code. The EXFAN system starts with a primary input and gradually modifies it through iterative CFD analysis till the design objective satisfaction. The rules are repetitively followed during the iterations. Dannenhoffer and Baron (1987) establish a hybrid system which incorporates both conventional and expert systems to conduct local compressible flow analysis. Their hybrid system is coupled at a lower level leading to the separation of processing and control, which turns out to be a major benefit. Aided by artificial intelligence, Shelton et al. (1993) use a design shell coupled with a CFD solver to optimize the airfoil design. Rubio et al. (2012) use the artificial neural network to create an expert system which can be used to predict the time required for the convergence of a CFD problem.

Another type of expert system is developed to diagnose problems, aid decision making and provide best practices in the CFD environment. Wesley et al. (1998) bring forward a CFD expert system by integrating AI and CFD to monitor the user input and inspect unreasonable combinations. Thus, wasted simulation runs could be reduced. Stremel et al. (2007) implement Best Practices eXpert (BPX), an expert system, to guide the CFD projects. Users can receive sufficient information about flow properties, object configuration, grid generation, solver selection and guidelines to make decisions and obtain accurate results with less uncertainty. Though helpful to novice users, such kind of systems can only facilitate the CFD solver setup, instead of providing full automation. So far, automated CFD solver functions are still insufficient and urgently needed.

CFD expert systems drew research attention when the solvers were in the form of in-house codes, which required special knowledge and training. With the evolution of CFD, more and more commercial systems have been developed and equipped with graphical user interface (GUI) to be user-friendly. Even so, the knowledge behind the solvers is still nontransparent to junior users. In fact, relying on experts also makes it difficult to develop the CAE-driven optimization programs (Gelsey 1995; J. Liu, Cheng, and Ma 2016). Ideally, the implementation of intelligent CFD solver should inherit the design information from the design stage and transform it into the best-fit simulation model and then, in turn, generate accurate results. Thus, the integration of CAD/CFD will be prompted to a higher level of robustness and efficiency.

### 1.2.3 Optimization Techniques in an Integrated Environment

CAD/CFD integration is expected to eliminate many tedious intermediate procedures during the cyclic design loops, e.g. repeated meshing and solver setup, which greatly improves the design efficiency. In addition, a critical factor to further enhance the efficiency is using optimization methods.

Generally, the optimization in an integrated environment can be performed using gradient-based algorithms, stochastic algorithms and metamodeling based algorithms (Bonte, Boogaard, and Huétink 2008). The gradient-based algorithms are classical search and optimization techniques in which the first and/or second order derivatives of the objective function and/or constraints are used to guide the

search process (Onwubolu and Babu 2004). Edke and Chang (2006) use the finite difference method to calculate the gradients of the objective function and constraints, and then determine the design changes in the shape optimization of heavy load carrying components. Comparing to the direct search methods, the gradient-based algorithms are more efficient. However, they are not efficient in non-differentiable or discontinuous problems.

There are various tools, such as genetic algorithms, differential evolution, simulated annealing, etc., for stochastic algorithms to optimize a system where the relationship between the independent variables and the objective function is not known in advance (Onwubolu and Babu 2004). Take genetic algorithms for example, the algorithms start with an initial generation of individual solutions generated randomly. The individuals evolve through generations created by genetic operators including reproduction, crossover, and mutation. This process continues until the stopping criteria are met (Sakawa 2002). Corriveau et al. (2009) report that the genetic algorithms are used to reduce the static stress in critical regions of a hydroelectric turbine. The stress can be reduced by 10.7% with the optimization of six design variables. Nevertheless, the process of conducting the genetic algorithms is time-consuming, especially when CAE is used to measure the performance of a configuration.

The metamodel is a simple model that approximates computation-intensive functions in complex systems. Optimization can be conducted based on a metamodel to search for the optimum (G. G. Wang and Shan 2007). Among those

introduced optimization techniques, metamodeling shows advantages of high efficiency compared to stochastic algorithms and more general applicability, given problems where the gradient information is nontrivial to calculate (Park and Dang 2010). Metamodeling has a broad application in simulation-based optimization where the simulation is treated as numerical experiments (Ayancik et al. 2017; Luo et al. 2017; W. Wang et al. 2017). Meanwhile, the computational cost may be reduced dramatically (Papalambros 2002). Because the metamodel provides an approximated view of the entire design space, it can detect the errors in simulation (G. G. Wang and Shan 2007). Therefore, the metamodeling techniques can be well fitted in the CAD/CFD integration system where design and simulation are associated seamlessly.

## 1.3 Research Methodology

### 1.3.1 Feature Modeling Technology

In the early development of feature modeling technology, features are specifically designated as form features which are generic shapes for product development purposes (Shah 1991). For example, there may be form features like the hole, slot, pocket and chamfer in a product model. Later, features are used to model the non-geometric product properties which are useful in the whole product lifecycle. In this case, the feature definition is usually driven by a specific application in product development (Sanfilippo and Borgo 2016). However, this is still insufficient. A generic feature definition is needed to associate product geometry

and engineering knowledge (Ma, Chen, and Thimm 2008). Generic feature is defined as the most basic feature entity template in an object-oriented software engineering approach to abstract the semantic patterns for different applications in engineering (Tang, Chen, and Ma 2013).

In this work, for product modeling, the *fluid functional feature* is defined as a class managing the design intent of fluid devices. Typical attributes are composed of design parameters and functional descriptions, as well as functional geometry which is controlled by those attributes (L. Li, Ma, and Lange 2016). So, the design intent can be effectively conveyed by fluid functional features. For CFD simulation phase, the *fluid physics feature* is defined as an object class representing a characteristic set of fluid simulation setup parameters with a generic data structure and related methods (L. Li, Ma, and Lange 2016). By this definition, the physical modeling information is embedded in fluid physics features.

Li et al. (Y. Li et al. 2012) define the interim features between various manufacturing operations as dynamic features. Based on this concept, a novel operation planning method is developed for the machining of complex structural parts (X. Liu, Li, and Tang 2015). Applying the similar dynamic feature concept, in this research for CFD model generation in the simulation phase, the *dynamic physics features* are defined as the intermediate states of the fluid simulation model including flow properties, grid distribution, and discretization scheme (L. Li, Ma, and Lange 2016). The dynamic physics features help to generate a robust

simulation model which produces the convincible results to be processed by the optimization module.

For cyclic CAD/CAE integrated design process, CAD/CAE model synchronization is important. For this purpose, the associative feature concept proposed by Ma and Tong (2003) is the right mechanism to realize the seamless synchronization. An associative feature is defined as a set of semantic relationships which can be both geometric and non-geometric among different geometries or applications. The associative feature is a new concept which is distinguished from traditional form features (Ma et al. 2007). The associative feature can not only manage fixed relations but also the developing ones which are derived from them. Features which are based on the volume of material are just specific types of associative features. More importantly, different from form features, associative features can be independent of volume. This is the key characteristic explaining the reason why associative features can also reveal and manage the relations embedded in different applications.

Based on the concept of associative feature (Ma and Tong 2003), this work proposes the CAE boundary feature and the CAE effect feature to establish the inter-feature associations. A *CAE boundary feature* is defined as a class of features that contains the mapping relations of geometrical dependencies between CAD entities and their associated CAE mesh representations as well as non-geometrical dependencies, such as inherited properties, like fluid properties, fluid space body face names, tags, constitutional structures, and conceptual constraints

to apply CAE boundary conditions (L. Li and Ma 2016). On the other hand, the *CAE effect feature* is introduced by extracting the sensitivity information from a series of CAE run results. Such extracted information is necessary for identifying proper design modification direction. The functionalities of the proposed feature concepts will be presented in chapter 2 and chapter 3 in detail.

### 1.3.2 CFD Simulation and Best Practices

CFD is widely used to analyze the fluid flow problems. The solving space is usually a fluid domain bounded by boundary conditions. The domain can be created by CAD software, and defeaturing is required for a good quality CFD solution (García et al. 2015). Besides, the domain size will affect the simulation time and accuracy, which should be carefully tested especially for new problems.

The domain needs to be discretized into elements for the numerical calculation. There are two types of mesh, namely structured mesh and unstructured mesh. Even though the unstructured mesh tends to have larger artificial diffusion and takes more time to solve, it is the most used mesh type because it is more efficient in preparing an adequate grid. The quality of the mesh is significant to the accuracy of the solution. Ideally, the mesh should provide evenly distributed levels of truncation error. The truncation error is proportional to the grid spacing, which can be reduced by refining the mesh. The refinement over the entire domain is at high computational cost and not necessary because large error only appears in small regions in most cases. As a result, local mesh

refinement is the right approach to increase the accuracy at specific locations. For example, mesh inflation should be applied along solid walls to have the grid surfaces aligned with the boundary layer flow approximately. The mesh can be further refined by adaptive meshing, which is based on the preliminary solutions (Bathe and Zhang 2009).

In addition to discretization, the fluid domain should also be confined by boundary conditions. Boundary conditions are properties and values assigned to the fluid boundaries. A fluid boundary is an external surface of a fluid domain which supports the inlet, outlet, opening, wall and symmetry boundary conditions. The inlet boundary condition is the most important one, where the fluid predominantly flows into the domain. Correspondingly, the outlet specifies the area where the fluid flows out of the domain. Either velocity or pressure can be set at those boundaries. Among all the possible combinations, the inlet with velocity assigned and outlet with static pressure assigned lead to the most robust boundary condition setup ("ANSYS CFX-Solver Modeling Guide" 2013). The opening boundary should be applied if the direction of the flow is uncertain, which means the fluid can flow in and out of the domain at the opening boundary simultaneously. It is suggested to use this boundary type only as part of the preliminary investigation because it introduces an increased uncertainty in the solution. The wall boundary defines the area where the fluid cannot penetrate. Especially for the no-slip wall boundary, the fluid has zero velocity relative to the boundary. If there is a plane that satisfies both geometric and physical symmetry,

the symmetry boundary condition can be applied at this plane where the diffusive flux is zero.

Before the solving stage, appropriate physical models need to be specified for the solver. The flow regime, such as laminar or turbulent flow and flow compressibility should always be checked first to select the correct model. At the beginning of the simulation, instead of using higher order schemes and advanced turbulence models, first order schemes and $k$-$\varepsilon$ turbulence model should be chosen in favor of convergence.

After the pre-processing is done, the simulation can be started and it will stop when the convergence criteria are met or the maximum number of iterations is reached. On condition that there is no error occurring, the post-processing can be conducted to analyze and visualize the solution. If there is a convergence problem found after the solving stage, only one modification in the model configuration should be made to identify the key factor. In such situations, more robust schemes, such as Upwind Differencing Scheme (UDS) for advection, Euler Implicit for time, $k$-$\varepsilon$ for turbulence, should be considered. If a steady simulation diverged, switching to transient simulation helps to test whether the flow is unsteady.

Approaching the end of the whole calculation, higher order schemes are preferred to increase accuracy. Because there is no universal turbulence model, the effect of different turbulence models should be tested, if the flow is turbulent. Before performing these actions, the mesh should be refined accordingly. At last,

if an analytical or experimental result is available, the numerical solution should be validated by comparing with the existing solution (Oberkampf and Trucano 2002).

### 1.3.3 Approximation-Based Optimization

Metamodeling approximates the empirical relationship between the objective function and the design variables, based on a group of experimental or numerical tests, where design of experiments (DOE) is extensively adopted to reduce the total number of tests (Simpson et al. 2014). This is very meaningful, especially when computationally expensive CFD simulations are used to provide test results. A general approximation-based optimization problem can be formulated by Equation (1).

$$\text{Min } \hat{f}(x)$$

Subjected to

$$\hat{g}_i(x) \leq 0, i = 1, \dots, l \tag{1}$$

$$\hat{h}_j(x) = 0, j = 1, \dots, m$$

$$x_L \leq x \leq x_H.$$

Some widely-used metamodeling methods include the response surface method (RSM), the radial basis function (RBF) based method and the kriging method (Simpson et al. 2014), where the RBF-based and kriging methods are

more suitable to explore highly-nonlinear design space (Park and Dang 2010), and RSM fits better for engineering problems with a small group of design variables and a relatively regulated design space (Simpson et al. 2014). Moreover, RSM is a very robust technique which is often selected when other optimization methods fail (Gosavi 2015). In this work, RSM is adopted and the response surface is approximated by quadratic polynomials (Zhang et al. 2016). To be specific, the quadratic response surface is mathematically described as follows

$$y = \beta_0 + \sum_{i=1}^{k} \beta_i x_i + \sum_{i=1}^{k} \beta_{ii} x_i^2 + \sum_{i=1}^{k-1} \sum_{j=i+1}^{k} \beta_{ij} x_i x_j + \varepsilon \quad (2)$$

where $y$ is the response function, $x$ is the design variable, $k$ is the number of variables, $\varepsilon$ is the error and $\beta$ is the regression coefficients.

Based on the collected data, the coefficients in Equation (2) can be obtained through regression analysis. The quality of the fitted metamodel should be validated. Subsequently, the optimal combination of design parameters can be obtained by further optimizing the derived response function. By experiment or simulation, the performance of the metamodel-predicted optimum should be checked to verify the effectiveness of the metamodel (Barton and Meckesheimer 2006).

## 1.4 Research Objectives

In order to conquer the problems in SBD and associate the design intent and simulation intent seamlessly for finding optimum product design, the following objectives are proposed.

(1) Establish an effective CAD/CFD integration system, which makes the CAD and CFD tools seamlessly integrated to facilitate the cyclic product development.

(2) Develop intelligent CFD solver functions toward an expert system for steam simulation to assist the solver setup and the generation of the robust simulation model.

(3) Make the prototyped CAD/CFD integration system work for general flow control product optimization.

(4) Validate the optimization result by conducting the simulation of a realistic case with original and improved designs.

## 1.5 Thesis Structure

In chapter 2, the proposed CAD/CFD integration system is introduced. Based on the system, the novel CAE boundary feature and CAE effect feature are defined. The intelligent CFD solver functions for steam simulation based on the proposed fluid physics features and dynamic physics features are presented in chapter 3.

The design optimization of the simplified outflow control device (OCD) is conducted using the CAD/CFD integration system as the case study in chapter 4. To show the effectiveness of the optimization result, the detailed CFD simulation of a realistic OCD with original and improved designs is conducted in chapter 5. A conclusion of the contribution of this research and an outlook toward the future work are made at last.

# Chapter 2 : CAD/CFD Integration System

## 2.1 Introduction

Although a number of approaches have been studied, seamless CAD/CAE integration has not been fully realized. The majority of efforts focused on the front process of preparing the CAD model for CAE analysis effectively and efficiently. The close loop CAD/CAE interactions remain to be a research issue, and there are mainly two difficulties: how to synchronize the CAD and CAE models and how to interpret CAE results for design optimization. In order to overcome these difficulties, this chapter presents two new concepts. For the former difficulty, a CAE boundary feature concept is proposed to manage the geometric and semantic associations between CAD and CAE models based on the well-established associative feature concept (Ma and Tong 2003). This CAE boundary feature is defined as a software object class and its application is put forward as a robust tool to maintain analysis setup information consistency during the cyclic CAD/CAE information conversion. For the latter difficulty, another class, referred to as CAE effect feature, is introduced by extracting the sensitivity information from a series of CAE run results; such extracted information is necessary for identifying proper design modification direction. By introducing these concepts, a new CAD/CAE integration framework has been developed which covers both the forward and reverse integrations and supports more automated cyclic product development.

In the CAD/CFD integrated product development, the design intent and simulation intent are supposed to be associated tightly. Thus, the consistency of the original intent can be kept throughout the cyclic SBD process. To discover the mechanism of design and simulation intent interaction, their meanings are firstly explored in section 2.2. For general CAD/CAE integration issues, the CAE boundary feature and effect feature are proposed in section 2.3. As to this thesis's focus of CAD/CFD integration, an integration framework with some novel feature concepts associated is demonstrated in section 2.4.

## 2.2 Definition of Design Intent and Simulation Intent

Conventionally, the definition of design intent mainly focuses on geometric modeling aspects (Price et al. 2013). It involves the control of parametric, geometric and constrained relationships to define a part. However, this kind of view is not sufficient because it ignores function which is another constituent of design intent. Mun et al. (2003) define design intent as the functional requirement provided by customers, which is a set of geometric and functional rules satisfied by the final product. From this definition, it is obvious that the formation of design intent starts from the customer's requirement for functions. Designers fulfill the functional requirement based on engineering knowledge and develop the initial conceptual design using CAD model. CFD simulation should not only transform the CAD geometric model into a CFD mesh model, but also the

simulation conditions and setup parameters must be transmitted into a CFD meta model. The result should be coherently used by the analyst to run the simulation.

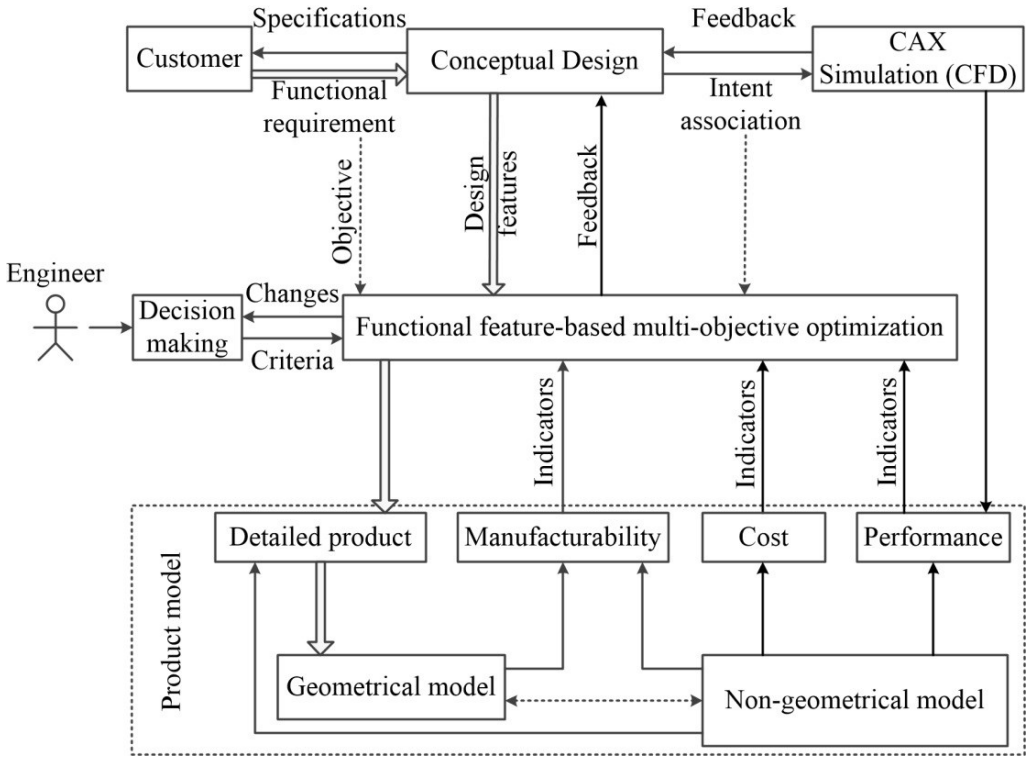


Figure 2.1: Product development routine.

Nolan et al. (2015) define simulation intent as a collection of all the analysis, modeling and idealization decisions, and all the parameters required to create an adequate analysis model from an input CAD geometry. Based on this definition, it is suggested that the generation of simulation intent should occur in the transition process where the association with design intent could be readily setup. Commonly, after the simulation is done, the result has to be used to check the initial design assumption validity and conduct design optimization. Subsequently, the design is further modified to meet the manufacturability and cost constraints.

Eventually, an acceptable design is returned to the customer for endorsement. Figure 2.1 presents this whole product development process, which may take many iterations before the final design is achieved.

## 2.3 Feature Concepts in CAD/CAE Integration

As mentioned earlier in chapter 1, the associative feature is capable of establishing and managing both geometric and non-geometric associations. Therefore, the associative feature concept is used in this chapter to interface the CAD and CAE tools, which synchronizes the different application models and guarantees the data consistency. The overall CAD/CAE integration scheme is shown in Figure 2.2. The feature concepts related to physical modeling will be introduced in chapter 3 in detail.

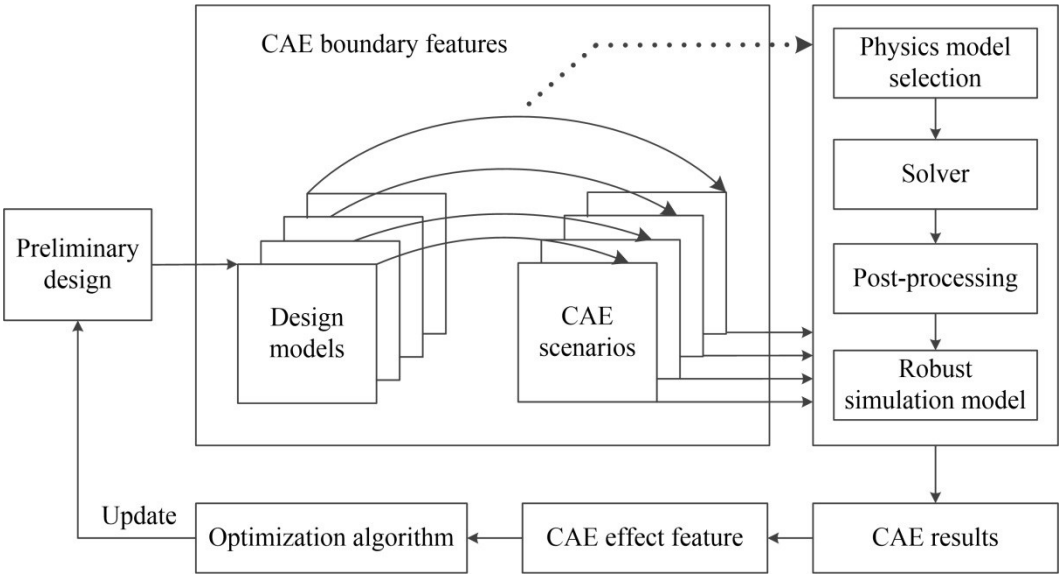


Figure 2.2: The overall CAD/CFD integration scheme.

The design flow starts from the conceptual design which preliminarily satisfies the design requirement. Given the optimality, the conceptual design is still immature and requires the simulation-based design modifications. The conceptual design model conveys both geometric and non-geometric information; therefore, it is significant to guarantee the complete information transfer between CAD and CAE tools. The CAD/CAE associative feature plays the roles in fulfilling this seamless integration. To be specific, all geometric entities from the CAD model and analysis model employ the one-to-one correspondence, and the semantic information useful for CAE analysis is also linked to analysis model. In this way, the CAE analysis pre-setup could be automatically completed without redundant model preparations.

The accuracy of CAE calculation is critical in the CAD/CAE integration because the calculation results will be the input of the optimization algorithm. Without high-quality input, the optimum will be hard to achieve. Proper application of boundary conditions is very important to obtain accurate results because they will not only affect the type of mesh generated but also the setup of the solver. Many research works are dedicated to the integration of CAD and CAE but rarely focus on the accuracy. However, if the results are not valid, the integration would be less meaningful. As a result, the CAE boundary feature is proposed to manage the relations among the geometry, boundary conditions and specific mesh type. For example, the velocity and pressure boundary in CFD simulation are assigned to the inlet or outlet of the geometry according to the

application situation. The walls formed by the faces of the fluid body geometry are subject to no-slip boundary condition. Particularly, mesh inflation should be applied along solid walls to pursue higher accuracy because it is capable of estimating the steep gradients in the boundary layer.

Generally, if the number of the meshes is increased, the computational cost will be higher accordingly. Here in this presented approach, the accuracy is not only guaranteed by the number of the meshes, but also by the type of meshes. As aforementioned, mesh inflation is applied along the wall boundary in order to obtain more accurate results. Thus, this approach can achieve higher accuracy without dramatically reducing computational speed. This is because of the use of correct mesh types, which is well-supported by the CAE boundary feature that maintains the consistency during CAD/CAE interactions. The reason why the importance of accuracy is paid so much attention is that the optimal design will not be achieved without rounds of accurate iterations. The proposed approach provides an efficient way to increase and maintain the CAE accuracy.

Smit and Bronsvoort (2009) suggest an analysis view which is an interface concept to interact with mesh generation, boundary conditions, analysis model, and solution methods in a multi-view feature modeling environment. In comparison, CAD model and CAE model are associated through the CAE boundary features in this research. Specifically, the CAE boundary feature expands its associations to the design model and the corresponding simulation

process in the integration loop. It is a robust tool to maintain information consistency during the iterations.

Currently, human intervention in the CAE analysis still plays an important role in decision making. To obtain a better design, specialists will usually make the decision on the modification and then process the change. This is a tedious process because the CAD model may be modified for hundreds of times and the CAE analysis should be conducted accordingly. In order to guide the design modifications based on CAE results, the concept of CAE effect feature is proposed here.

The CAE effect feature is defined as a class of features that represents the unique characteristics of interested measure changes for a physical behavior in the context of a CAE analysis scope; in other words, its applied instances explicitly express the influence on the physical performance of a defined function due to the changes in the associated CAD model. This concept is of significant importance to form the loop of CAD/CAE integration. Based on the initial design, the system will attempt to generate a series of designs that represent the design space as much as possible. Then, the CAE scenario will be updated synchronously according to the CAD model, resulting in corresponding CAE analysis results after the solving stage. CAE effect features will be extracted based on the analysis of these results. With the set of CAE effect features extracted, the interpretation can be carried out and the design improvement would be possibly achieved.

## 2.4 CAD/CFD Integration System

As to CAD/CFD integration, which is a special case of CAD/CAE integration involving fluid flow, in order to keep the consistency of design intent in different product development stages and to facilitate the correspondence of the design and simulation models, a CAD/CFD integration system is proposed here, which is depicted in Figure 2.3.

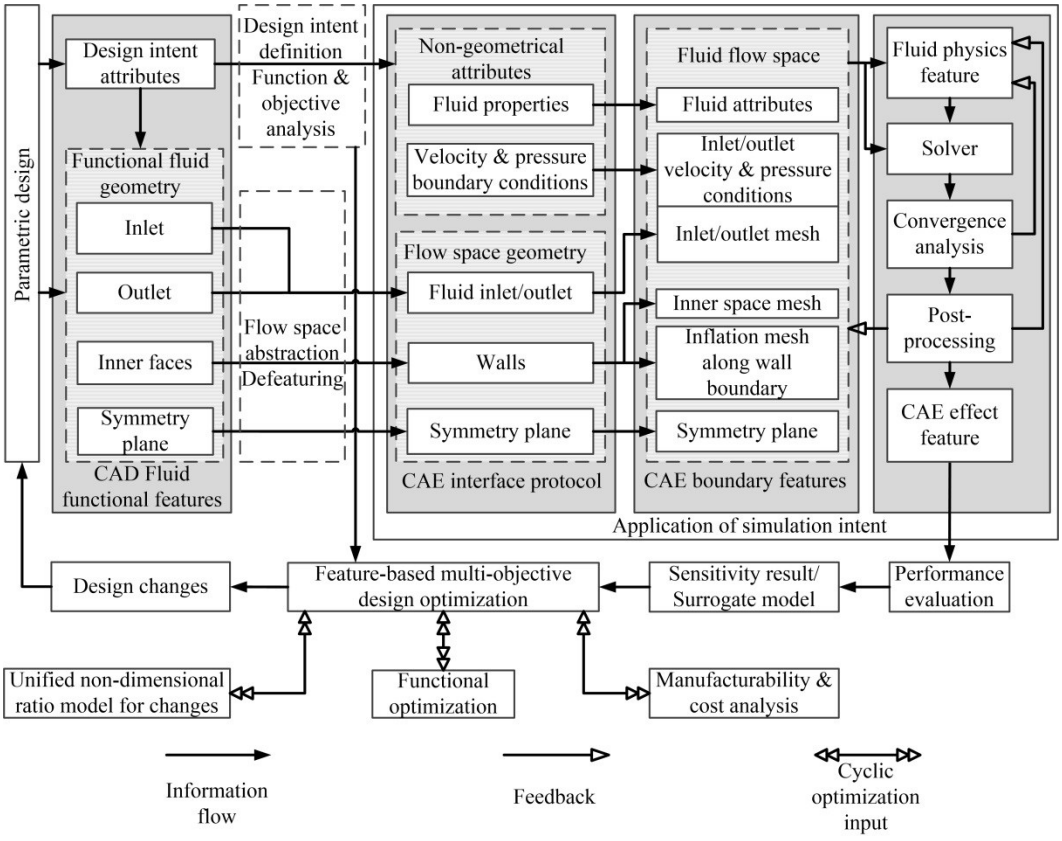


Figure 2.3: CAD/CFD integration system framework.

The design can be parameterized according to engineering knowledge. The parametric design enables a topology-based representation of the part, which

maintains the design intent consistently (Vosniakos, Benardos, and Lipari 2014). The parametric modeling of the design can be easily achieved by the built-in expression function library in a CAD package like SolidWorks and NX. By introducing appropriate constraints, a parametric model can be constructed in such a way that it can be readily integrated with automated optimization loops (Delap, Hogge, and Jensen 2006). The functional fluid geometry, which is derived from design intent attributes, can be itemized as the inlet, outlet, and inner faces enclosing fluid space and symmetry plane if there is any. In this way, the design intent can be fully conveyed by fluid functional features to the downstream analysis stage. The CAD model of the flow space can be extracted by Boolean operations. Because the face IDs in CAD system may differ from that in another system (Tierney et al. 2014), the IDs of fluid space faces will be assigned specific tags with attributions and boundary conditions attached. The tag is an identifier which can be recognized by both CAD and CFD systems. It works as part of the CAE interface protocol. The information of entities with tags is stored in the database for later processes. Table 2.1 shows the mechanism how the information is transmitted between different models, in which m, n, p, and q are the numbers of corresponding faces in the CAD model.

CAE boundary features are established to link geometry characteristic faces of the fluid body, meshes, corresponding boundary conditions and the specific mesh generation method. The fluid body geometric faces such as inlets, outlets, walls and symmetrical planes with unique tags will be indexed from the database

and assigned names with the type of boundary. Later in meshing stage, CAE boundary features also direct the mesh generation and refinement. For example, an inflation layer is applied along the wall boundary to capture the boundary layer accurately. Meanwhile, the boundary conditions are assigned accordingly. The fluid flow space including discrete geometry, boundary conditions and non-geometrical fluid attributes inherited from the design intent, is treated as the input of the solving stage. The solver invoked by the CFD module will automatically recognize the boundary with pre-defined IDs. As a result, after the CAD model is updated, the CFD model including both geometric and non-geometric information, can be synchronized accordingly. In this process, the non-geometrical parameters remain unchanged. CAD/CFD feature information sharing is achieved by the associations embedded within the CAE boundary features.

Table 2.1: Information transmission in CAD/CFD conversion.

| Tag | Attribute | Boundary condition |
|---|---|---|
| $I_1, I_2,\ldots, I_m$ | Inlet | Velocity or pressure inlet |
| $O_1, O_2,\ldots, O_n$ | Outlet | Velocity or pressure outlet |
| $W_1, W_2,\ldots, W_p$ | Wall | No-slip wall |
| $S_1, S_2,\ldots, S_q$ | Symmetrical plane | Symmetry |

At the upper-right corner of Figure 2.3, the fluid physics feature module models a set of rules to select the appropriate CFD solver regime applicable to each round of simulation. This module is also designed to implement knowledge

and best practices, which enable the conversion of input data, assist CFD solver setup and robust CFD model generation. Therefore, the simulation intent is embedded in the fluid physics feature instances. The detailed description of the fluid physics feature class will be illustrated in chapter 3 by introducing the intelligent CFD solver functions for steam simulation. Post-processing could be conducted based on any converged run. The CFD model including mesh and solver setup parameters could be updated iteratively, leading to a robust model setup. This is a unique requirement of CFD analysis which distinguishes it from linear engineering problems, such as stress analysis.

After achieving the robust CFD model, the initial design can be modified systematically to approach design objectives. Then, based on each new design, the updated CFD analysis will be obtained accordingly under the aforementioned scheme. Following that, a sensitivity or surrogate model could be obtained to provide optimization input. Coupling with optimization objectives derived from design intent, operational performance, manufacturability and cost analysis, the optimization process takes different constraints into consideration, which eliminates the redundant communications between designer and other stake holders. Here, a unified non-dimensional ratio model is proposed to calculate the weights of different design criteria and to enable the measurement of performance increments between different designs. In this process, the CAE effect features are extracted based on the sensitivity information derived from the optimization algorithm. Finally, a closed CAD/CFD loop forms, which links the CAD domain

and CFD domain consistently. Evidently, the design intent is adhered to throughout the whole process. The transfer of the design intent in this process is denoted by solid arrows which link the relevant blocks in Figure 2.3. At the same time, the design intent and simulation intent are associated through the control of fluid functional features, CAE boundary features, and fluid physics features.

Optimization is carried out based on the integrated CAD/CFD feature model with associated geometry and parameters, robust simulation models, accurate results, effective optimization inputs and prospective manufacturability constraints. The semantic definitions and their relations among the involved features are shown in Figure 2.4.

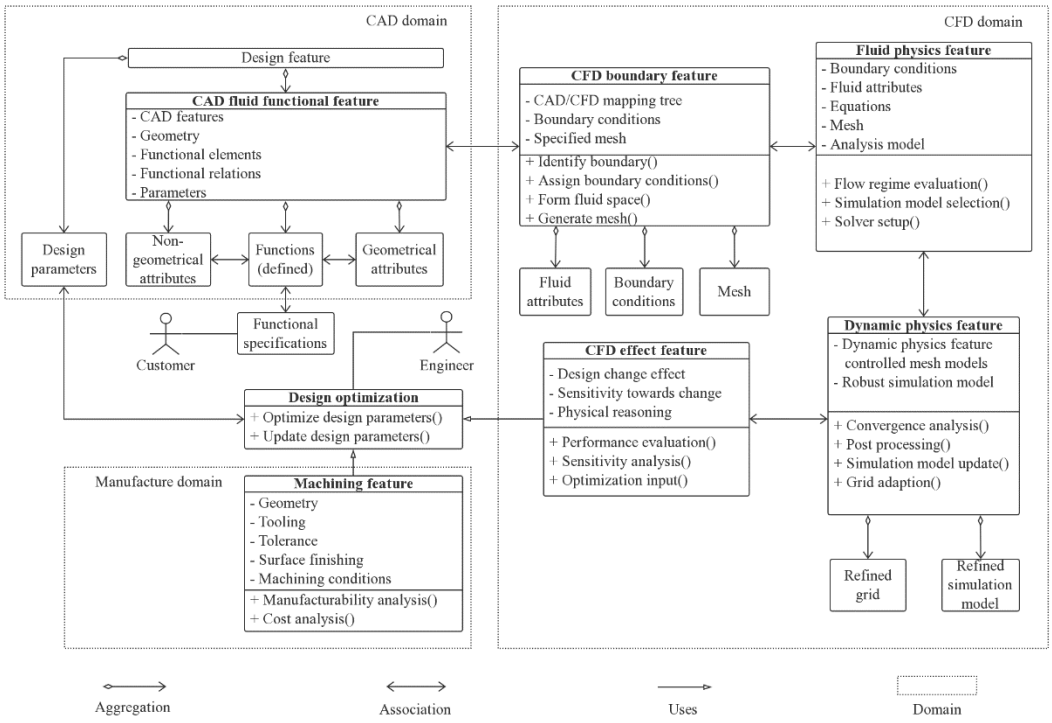


Figure 2.4: UML diagram representing inter-feature associations.

## 2.5 Summary

In order to keep the semantic consistency in product development, a CAD/CFD integration system is proposed in this chapter. With the implementation of the integration system, the design intent and simulation intent can be associated seamlessly. Based on the associative feature concept, the CAE boundary feature and CAE effect feature are put forward aiming to support the automatic CAD/CFD interactions with both geometric and semantic information. This chapter describes the general information flow in the product development based on the proposed CAD/CFD integration system. The fluid physics feature and dynamic feature concepts will be presented in the next chapter based on the intelligent CFD solver functions for steam simulation.

# Chapter 3 : Intelligent CFD Solver Functions

## 3.1 Introduction

With the development of feature modeling techniques, the application of features is not restricted to represent the generic shapes only. In the whole product lifecycle, features can also be used to model the non-geometric properties which are usually driven by different activities in product development (Sanfilippo and Borgo 2016). Each activity has its own way of looking at a product (Willem F. Bronsvoort et al. 1997). However, excessive subjective decisions and manipulations exist in this process, which reduces the consistency and efficiency (J. Liu et al. 2015). Multiple-view feature modeling provides a specific view for each product development phase and keeps the information consistency through view updating (W F Bronsvoort and Noort 2004). Specifically, for simulation-based design, the analysis view (Smit and Bronsvoort 2009) should be fully integrated with CAD models in a multiple-view product development environment. In the development of fluid flow products, CFD is increasingly used as an advanced support. However, the successful application of CFD requires special knowledge and rich experience, which is a barrier to the conversion from the design view to the analysis view, and the maintenance of information consistency. So far, the integrated analysis view with CFD involvement has not been well studied.

In order to conquer the barrier, intelligent CFD solver functions toward an expert system for steam simulation are introduced in this chapter. The proposed intelligent functions are expected to automatically propagate the changes in the design view so that the dependence on the experienced engineer can be reduced dramatically. The following section introduces different approaches to conduct multiple-view feature modeling. The feature model of the CFD analysis view based on the intelligent solver functions is described in section 3.3. In addition, the subroutine for the advanced turbulence model and the process of grid independence analysis and error estimation are developed to enhance the intelligent solver functions. The function of the proposed system is extended to wet steam modeling by expanding the knowledge base. Section 3.4 demonstrates the case study of a section of a contracted pipe, which is used to show the functions of the proposed feature-based system and compare the results obtained from this system with empirical results.

## 3.2 Multiple-View Feature Modeling Approaches

There have been several approaches to multiple feature views, which take advantage of design by features, feature recognition (Martino and Giannini 1998) and feature conversion (Willem F Bronsvoort and Jansen 1993; Suh and Wozny 1997). Cunningham and Dixon (1988) use design by features and feature conversion to create the feature model for the design view and the finite-element model for the analysis view, respectively (W F Bronsvoort and Noort 2004).

Anderson and Chang (1990) propose a geometric reasoning method called feature refinement to convert features in the design view into process planning procedures in manufacturing view for material removal operations. For injection moulding product, Deng et al. (2002) propose CAD-CAE features to capture both geometric and non-geometric information from the design view, which are used to establish the analysis view. Lee (1998) identifies the design view of the moulding product contains the form features and the mouldability features. Meanwhile, the manufacture view is focused on the design of the mould. The translation from the design view to the manufacture view is based on the geometric relationships between the product and the mould. Liu et al. (2016) propose the associative optimization feature model to build the structural optimization view of the product.

The aforementioned approaches fall into the one-way feature conversion in which features are usually derived from the original design view (Hoffmann and Joan-Arinyo 2000). Hoffmann and Joan-Arinyo (1998) put forward a master model which has domain-specific clients who have their own view of the product model. The CAD view, geometric dimensioning and tolerancing view, manufacturing process planning view and other downstream views can be coordinated by the master model under the control of the change protocol. Thus, multi-way feature conversion (de Kraker, Dohmen, and Bronsvoort 1995) is achieved and the consistency is maintained at the same time. Instead of focusing on the completely specified geometry and a single part, Bronsvoort and Noort

(2004) introduce a new multiple-view feature modeling approach which provides the conceptual design view, assembly design view, part detail design view and part manufacturing planning view. This approach not only supports the later phases of product development, but also the earlier phases. Thus, a designer is able to specify the product model from an arbitrary view, and the consistency is kept by automatic consistency checking and recovering algorithms.

Based on the multiple-view feature modeling approach, Smit and Bronsvoort (2009) propose that the analysis view should be a feature model to propagate the changes in a multi-directional manner. However, the current CFD solver structure does not support this generally. It should be noted that incorporating knowledge in the analysis process is essential for the integration of analysis with other activities in product development (Smit and Bronsvoort 2009). Therefore, by applying artificial intelligence, intelligent CFD solver functions can be used to capture the knowledge needed in CFD analysis and aid the automatic analysis regime validation and selection in response to the changes in the design view.

## 3.3 Structure of the Intelligent CFD Solver for Steam Simulation

### 3.3.1 Feature Model of the CFD Analysis View

Different from the static analysis, the CFD model requires special expertise and rich experience to deal with the nonlinearity. Thus, the solver configuration is a time-consuming process and prone to mistakes, which may lead to inaccurate

results. Here, the intelligent CFD solver functions for dry steam simulation are proposed, and the system is composed of different modules.

The data processing module of the intelligent CFD solver is depicted in Figure 3.1. The initial values are obtained from the fluid functional features in the design view. The parameters in the following steps can be derived using equations listed below

$$A = \frac{\pi d^2}{4} \tag{3}$$

$$\rho = \frac{p}{RT} \tag{4}$$

$$a = \sqrt{kRT} \tag{5}$$

$$Q = \bar{v}A \tag{6}$$

$$\mathrm{Re} = \frac{\rho \bar{v} d}{\mu} \tag{7}$$

$$\mathrm{Ma} = \frac{\bar{v}}{a} \tag{8}$$

where $\mu$ is the dynamic viscosity of steam, $p$ is the pressure of steam, $T$ is the temperature of steam, $R$ is the gas constant, $k$ is the specific heat ratio of steam, $\bar{v}$ is the average velocity of steam, $d$ is the inner diameter of duct, $\rho$ is the density of steam, $a$ is the speed of sound in steam, $A$ is the cross-sectional area of duct, $Q$ is the volumetric flow rate of steam, Re is the Reynolds number, and Ma is the Mach number. The Reynolds number and Mach number determine the flow

regime, and they can always be obtained regardless of the occurrence order of the other parameters if the initial data pool is sufficient.

If the Reynolds number exceeds the critical value (4000 for flow in the pipe), a turbulence model will be selected. Meanwhile, the Mach number judges whether the flow is compressible. If the compressibility effects cannot be ignored (Ma > 0.3), the total energy model will be selected and the reference pressure, as well as proper boundary conditions, will be setup to trigger the compressible flow simulation. In the preliminary stage of the simulation or at the time the simulation has convergence problems, lower order discretization schemes like UDS and Euler implicit, as well as *k*-*ε* turbulence model if applicable, are preferred to assist convergence. This physics model selection process is illustrated in Figure 3.2.

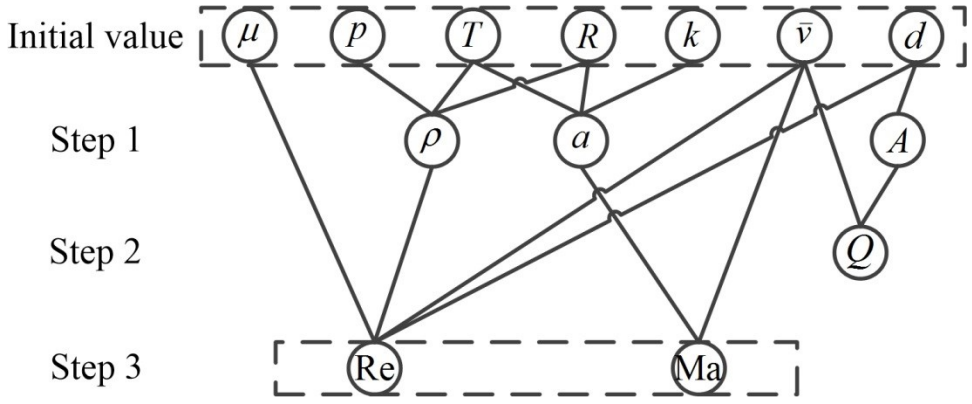


Figure 3.1: Data processing module.

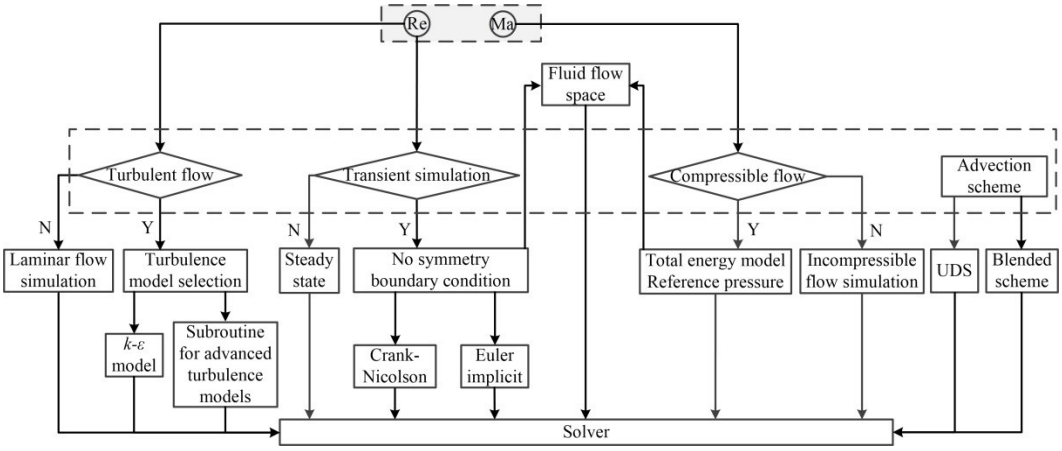


Figure 3.2: Physics model selection module.

The root-mean-square (RMS) of normalized residuals is used as the convergence criteria for individual CFD runs (RMS < $10^{-4}$). As shown in Figure 3.3, the index i (iteration), C (Convergence) and D (Divergence) will be updated after each simulation run. All the solver setup and the convergence status are recorded no matter whether the simulation is converged or not. If a simulation converged, post-processing will be conducted to check whether the solution matches the initial assumptions and expected accuracy. If not, grid adaption will be activated based on the existing simulation result. According to the peak value of Reynolds number and Mach number obtained from the simulation, the flow regime is double checked to see whether the simulation model needs to be changed. If a simulation diverged, the solver setup should be modified to achieve convergence. It should be noted that each time when a new iteration starts, only one change is allowed in the solver configuration to obtain the sensitivity towards different simulation schemes. If the simulation still has convergence problems

after several successive runs, human intervention is needed to diagnose the problem.

Higher order schemes can be applied after rounds of successful simulations because the mesh will be further refined. In such kind of situation, a subroutine will be entered to select one advanced turbulence model if the flow is turbulent. This program stops when the selected turbulence model is able to demonstrate the dominant features observed in the real-world turbulent flow based on the converged simulation. If the flow regime used to judge the fluid physics models is valid, grid independence analysis will be conducted to see whether the simulation is still affected by the grid refinement. By this analysis, the error of the discretization can be estimated if the grid is independent. The detailed description of the subroutine for advanced turbulence models and grid independence analysis will be introduced in subsection 3.3.2 and 3.3.3, respectively. By comparing with the validation result, the accuracy of the simulation result can be obtained, which is the criteria for stopping the loop in the post-processing module. Consequently, the accuracy of the robust simulation model can be guaranteed. If an external validation result is not available, the accuracy of the solution cannot be assessed. In this case, the solution is still precise because the grid independence analysis and the optimized combination of physical models still generate a robust simulation model. During this process, the dynamic physics feature is developed to facilitate the generation of the robust simulation model which is defined as the applicable CFD regime and simulation setup template with validated physics

conditions, and converges into physically reasonable and accurate results (L. Li, Ma, and Lange 2016). More specifically, the robustness of the simulation model means that the model can be used with confidence on a difficult problem and produce physically reasonable results besides the expected accuracy (Venkatakrishnan, Salas, and Chakravarthy 1998).

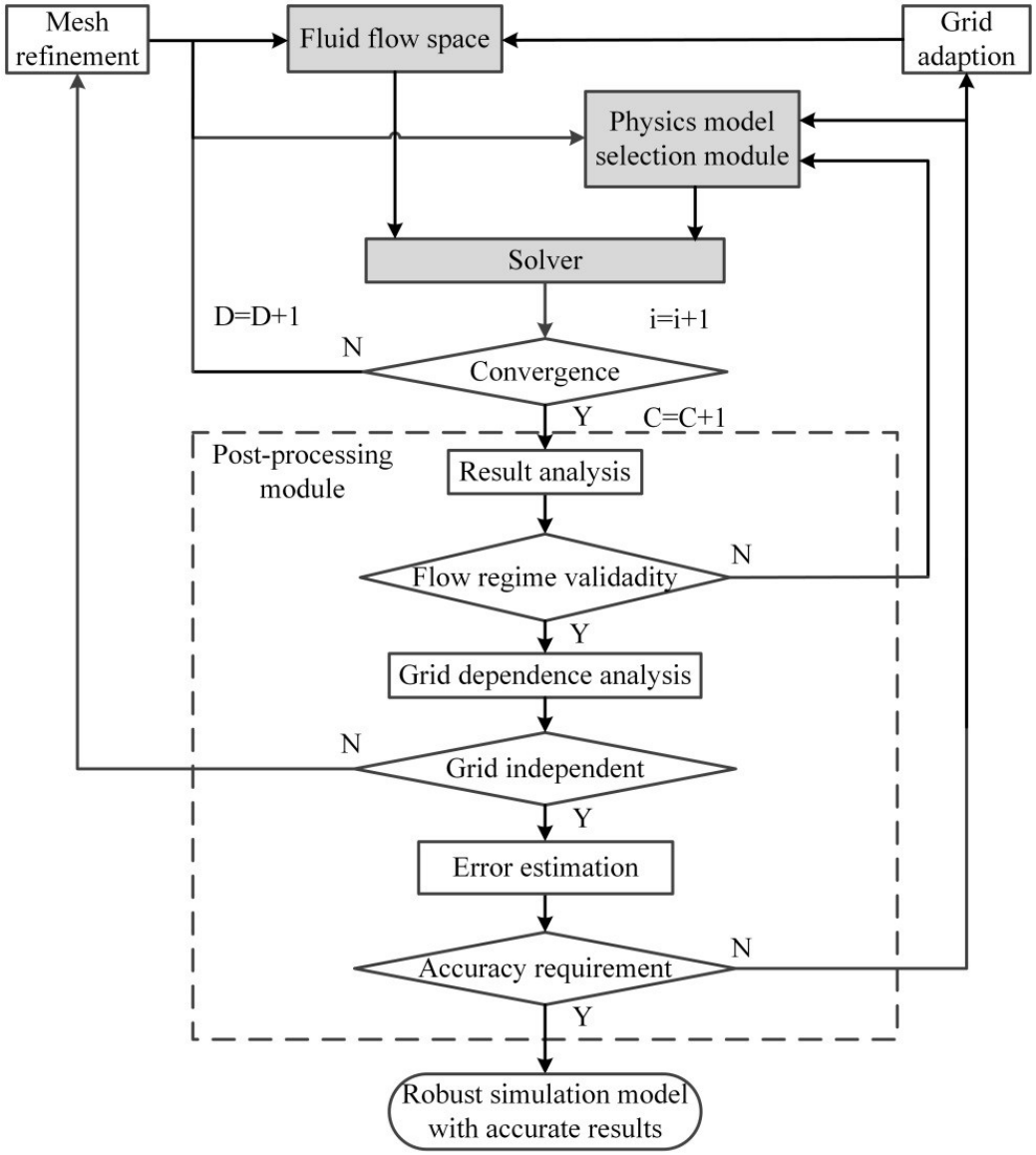


Figure 3.3: Post-processing module.

In this system, the physical parameters are the component of the object-oriented fluid physics feature which also embeds a set of rules to select the proper CFD solver regime. Therefore, the proposed intelligent solver functions are built toward a rule-based system, and the CFD analysis view in this system is a feature based model which contains CAE boundary features, fluid physics features, and dynamic physics features. The knowledge of engineering, physics, and numerical method is applied in this CAD/CFD interaction process, which contributes to the smooth feature conversion and automation.

### 3.3.2 Subroutine for Advanced Turbulence Models

There are several methods available to model the turbulence, such as Reynolds-averaged Navier-Stokes equations (RANS), large eddy simulation (LES), and direct numerical simulation (DNS). In DNS, the Navier-Stokes equations are solved for all the motions in a turbulent flow, which provides very detailed information of the flow. However, DNS is too computationally expensive making it hard to be a design tool. LES is good for transient large-scale fluctuating flows. Though less costly than DNS, LES is still computationally expensive because it is three dimensional and time-dependent (Ferziger and Perić 2002; Sanderse, Pijl, and Koren 2011). So the advanced turbulence models used in the subroutine focus on RANS models including $k$-$\omega$, Reynolds Stress Models (RSM), and Scale-Adaptive Simulation (SAS).

The structure of the subroutine for advanced turbulence models is shown in Figure 3.4. When the subroutine for advanced turbulence models is entered, after an initial solution with the *k-ε* model, the *k-ω* model will be selected first as the turbulence model. If it is not capable of modeling the turbulence accurately, RSM or SAS will be selected according to the flow regime obtained from the initial simulation result with the *k-ε* model. If the result is still not acceptable, the fluid physics models will be updated to achieve better cooperation with the turbulence model. If none of the models in the subroutine is applicable, the *k-ε* model will be reselected with updated fluid physics models.

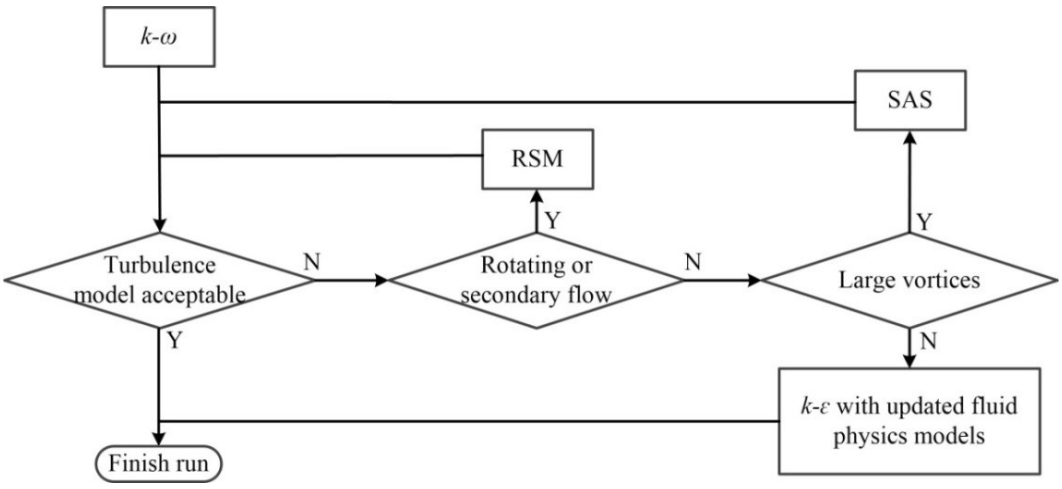


Figure 3.4: Subroutine for advanced turbulence models.

### 3.3.3 Grid Independence Analysis and Error Estimation

In order to estimate the discretization error, grid independence analysis needs to be conducted first to see whether the solution will change fundamentally with the further refinement of the grid. Three successively refined grids with different

refinement levels are needed to conduct the grid independence analysis. If the characteristic parameter approaches the exact value asymptotically, then the order of discretization can be calculated. In this case, assume that the grid spacing of the coarse, medium, and fine mesh is $\Delta z_1$, $\Delta z_2$, and $\Delta z_3$, respectively, then the refinement rate $\alpha$ can be calculated by Equation (9).

$$\alpha = \frac{\Delta z_1}{\Delta z_2} = \frac{\Delta z_2}{\Delta z_3} \tag{9}$$

CFD uses discretized equations to approximate the differential equation. Usually, the exact solution $\phi(x)$ in CFD simulation is not known. Incorporating the refinement rate $\alpha$, the value of $\phi$ in each grid level is used to estimate the order $\tau$ of the discretization scheme by Equation (10).

$$\tau \approx \frac{\log(\frac{\emptyset_{\Delta z_2} - \emptyset_{\Delta z_1}}{\emptyset_{\Delta z_3} - \emptyset_{\Delta z_2}})}{\log \alpha} \tag{10}$$

Grid independence can be claimed if $\tau$ is close to 2 for 2nd order discretization schemes or between 0.8 to 2.2 for a combination of 1st and 2nd order discretization schemes. Neither negative nor very large $\tau$ values can be accepted as grid independence. By Richardson extrapolation (Ferziger and Perić 2002), the discretization error $\varepsilon_h^d$ can be estimated using Equation (11) and a better approximation of the exact value can be found by Equation (12).

$$\varepsilon_h^d = \frac{\emptyset_{\Delta z_3} - \emptyset_{\Delta z_2}}{\alpha^\tau - 1} \tag{11}$$

$$\emptyset_{\text{exact}} \approx \emptyset_{\Delta z_3} + \varepsilon_h^d \tag{12}$$

Typically, in the grid independence analysis, an integral parameter, which is relevant and sensitive to the entire flow field, should be chosen as the characteristic parameter $\phi(x)$. Because the grid independence can be expected only on sufficiently fine grids, the mesh needs to be refined further if the grid independent solution is not reached. If the accuracy of the simulation is not acceptable, grid adaption will be conducted and the physical models in the selection module, including advection scheme, turbulence model, transient simulation model, and compressible flow simulation model, will be adjusted to achieve better results.

### 3.3.4 Wet Steam Simulation Module

In practice, wet steam is commonly represented as a medium formed by a mixture of water vapor and liquid water. This mixture represents two different thermodynamic phases of water in which both phases are at saturation temperature. So the simulation of wet steam falls into multiphase flow simulation. As shown in Figure 3.5, the wet steam exhibits various flow regimes depending on the relative concentration of the two phases and the flow rate. Each regime requires different modeling approaches. The dominant interactions between liquid and vapor change their character from one regime to another.

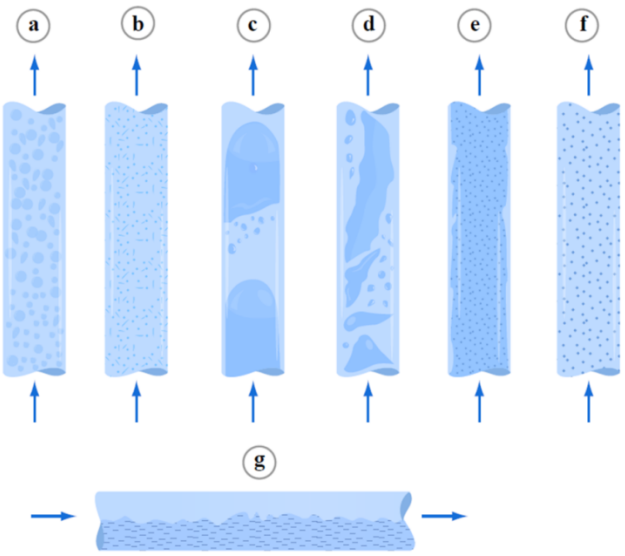


Figure 3.5: Various regimes in wet steam.

(a) Bubbly flow, (b) Dispersed bubbly flow, (c) Slug flow, (d) Churn flow, (e) Annular flow, (f) Mist flow, (g) Stratified flow. (Buongiorno 2010)

In CFX specifically, there are two main multiphase models, namely the Lagrangian particle tracking model and the Eulerian-Eulerian model ("ANSYS CFX-Solver Modeling Guide" 2013). To model the phase change, both equilibrium and non-equilibrium phase change models are available. The equilibrium phase change model is a single fluid, multicomponent phase change model which assumes the phase change occurs instantaneously. Therefore, the two phases have the same temperature. This model is especially suitable for wet steam simulation with a small liquid mass fraction ("ANSYS CFX-Solver Modeling Guide" 2013). The non-equilibrium phase change model is available when using Eulerian multiphase and Particle Transport, which allows the two

phases to go beyond the saturation dome. The focus of this module lies in the equilibrium phase change model as an initial investigation attempt.

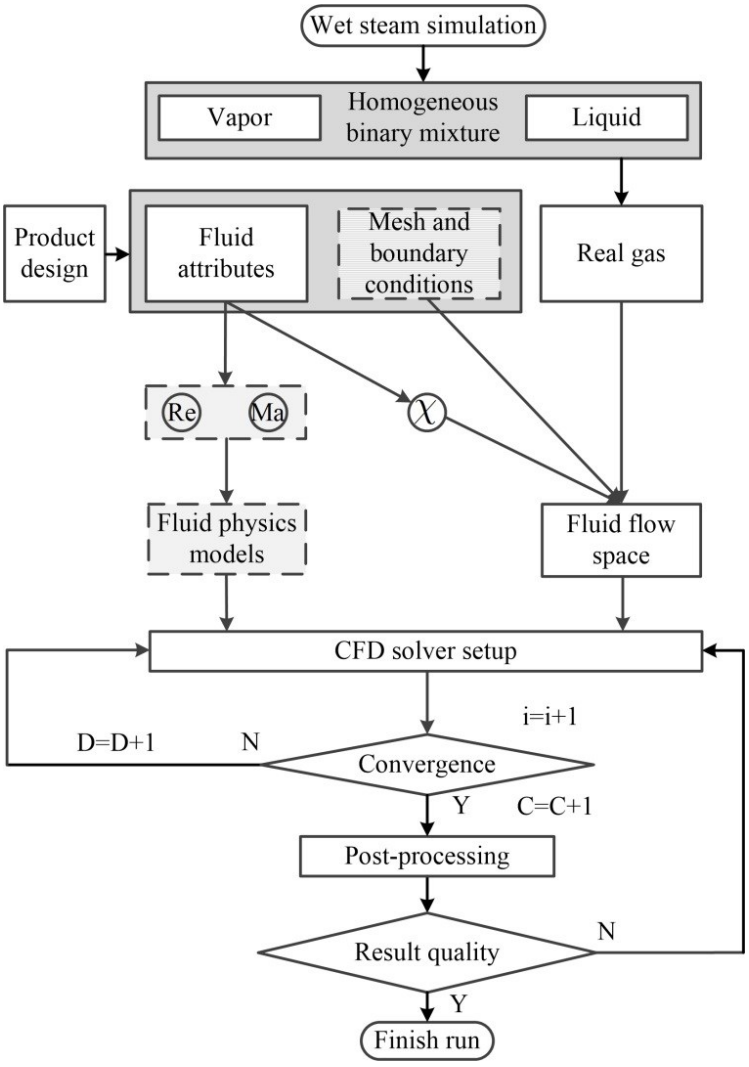


Figure 3.6: Structure of the wet steam simulation module.

As shown in Figure 3.6, if the wet steam simulation module is entered, the homogeneous binary mixture including water vapor and liquid water is created as a real gas which is treated as the fluid of the flow space. Similar to the dry steam simulation, the fluid domain is abstracted from the product and meshed with

boundary conditions attached. Again, by forward-chaining, the fluid attributes derived from the design are used to estimate the non-dimensional Reynolds number and Mach number to select suitable fluid physics models. Especially, the pre-defined steam quality $\chi$ is used as an additional boundary condition of the fluid flow space. The rules in configuring the solver are the same as the intelligent solver functions for dry steam simulation. If a simulation diverged, the solver setup should be tweaked to achieve convergence. Still, only one change is allowed in the solver configuration. If a simulation converged, the post-processing module including result analysis, flow regime validation, grid independence analysis, and error estimation will be executed. If any of the checks failed or the quality of the simulation result is not satisfactory, the flow regime with corresponding physics models, order of the schemes, and mesh refinement level will be checked to improve the simulation quality. The program ends when the simulation result meets the requirement.

## 3.4 Case Study

### 3.4.1 Design and Analysis of Contracted Pipe

Figure 3.7(a) shows a section of a pipe with a contraction which induces flow separation and mixing. The design and analysis of the piping system are selected as the case study. The reason is that the pressure drop under a certain flow rate in the piping system can be determined by head loss calculation (Çengel and Cimbala 2006), and it can be used as a benchmark for the simulation results. The

fluid domain is created by feature conversion and is shown in Figure 3.7(b). Under the control of CAE boundary features, the mesh is generated as shown in Figure 3.7(c). The initial value of the design parameter *d* (small inner diameter of the pipe) in this sample case is 70 mm.

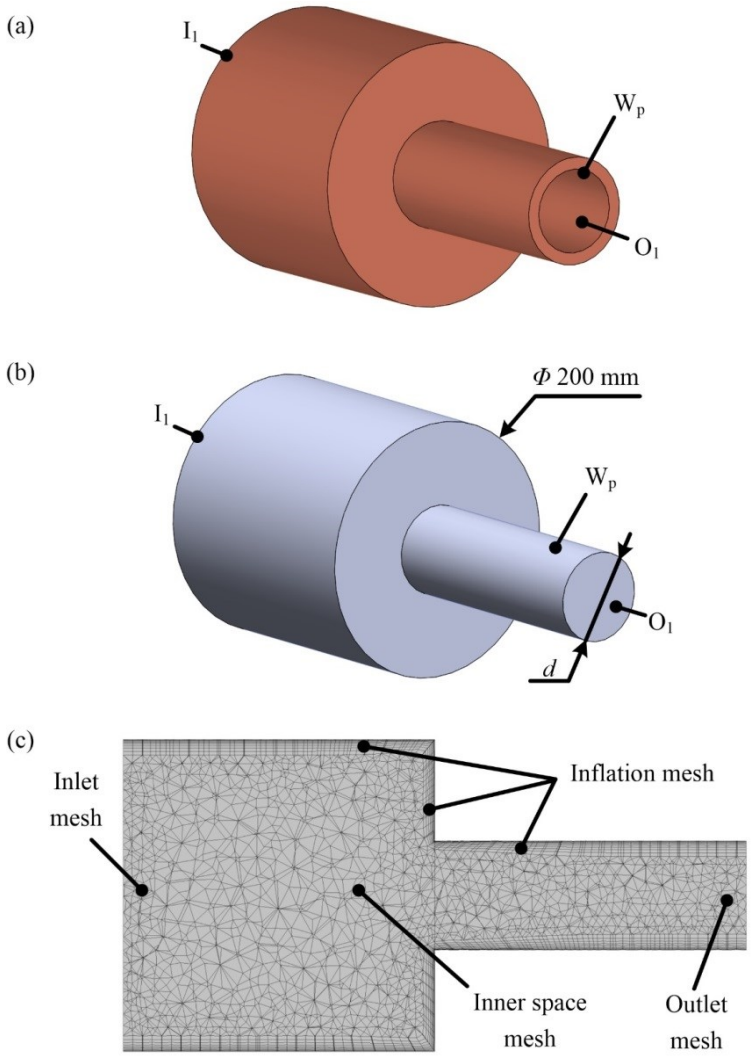


Figure 3.7: Model conversion in the pipe analysis.

(a) Contracted pipe, (b) Fluid domain, (c) Mesh generation.

At the inlet of the fluid domain, dry steam flows at 1 m/s. The pressure of 101325 Pa is assigned to the outlet. The other initial physical parameters are collected in Table 3.1. Using equations, the physical parameters in Table 3.2 are derived. The flow rate is calculated to be 0.031 $m^3/s$ in step 2. The Reynolds number and Mach number are 9561 and 0.002, respectively. Therefore, the flow is assumed to be incompressible turbulent flow. Then the physics models are selected accordingly through the intelligent solver functions. The mesh generated by the adaptive method is shown in Figure 3.8(a). To conduct the grid independence analysis, this grid is systematically refined at the rate of 1.1. Based on those 3 grids and the physics models, the simulation is conducted. In the analysis of pipe flow, one of the important quantities is the pressure drop. The number of nodes and the value of pressure drop corresponding to each refinement level are tabulated in Table 3.3. The pressure drop is selected as the characteristic parameter and its trend towards the number of nodes is depicted in Figure 3.8(b). Apparently, all the pressure drops are in the asymptotic region of the solution space. By Equation (10), the order $\tau$ is calculated to be 1.87. Because the blended scheme is applied as the advection scheme, which corresponds to a weighted average between UDS and Central Differencing Scheme (CDS), the calculated $\tau$ value corresponds to the discretization scheme used. Therefore, grid independence is achieved. Using Equation (11) and Equation (12), the discretization error and the approximated exact solution is found to be -1.025 and 29.156, respectively. The pressure and velocity vectors obtained from the robust simulation model are shown in Figure 3.9.

Table 3.1: The initial values of the physical parameters.

| Physical parameter | Value | Unit |
|---|---|---|
| $\mu$ | $1.23\times10^{-5}$ | kg/(m·s) |
| $p$ | $1.013\times10^{5}$ | Pa |
| $T$ | 373.15 | K |
| $R$ | 461.5 | J/(kg·K) |
| $k$ | 1.327 | N/A |
| $\bar{v}$ | 1 | m/s |
| $d$ | 0.2 | m |

Table 3.2: The values of physical parameters calculated in step 1.

| Physical parameter | Value | Unit |
|---|---|---|
| $\rho$ | 0.588 | $kg/m^3$ |
| $a$ | 478 | m/s |
| $A$ | 0.031 | $m^2$ |

Table 3.3: Pressure drop calculation based on different grids.

| Refinement level | Number of nodes | $\Delta p$ (Pa) |
|---|---|---|
| Coarse (original mesh) | 83414 | 30.62 |
| Medium | 109238 | 30.381 |
| Fine | 144429 | 30.181 |

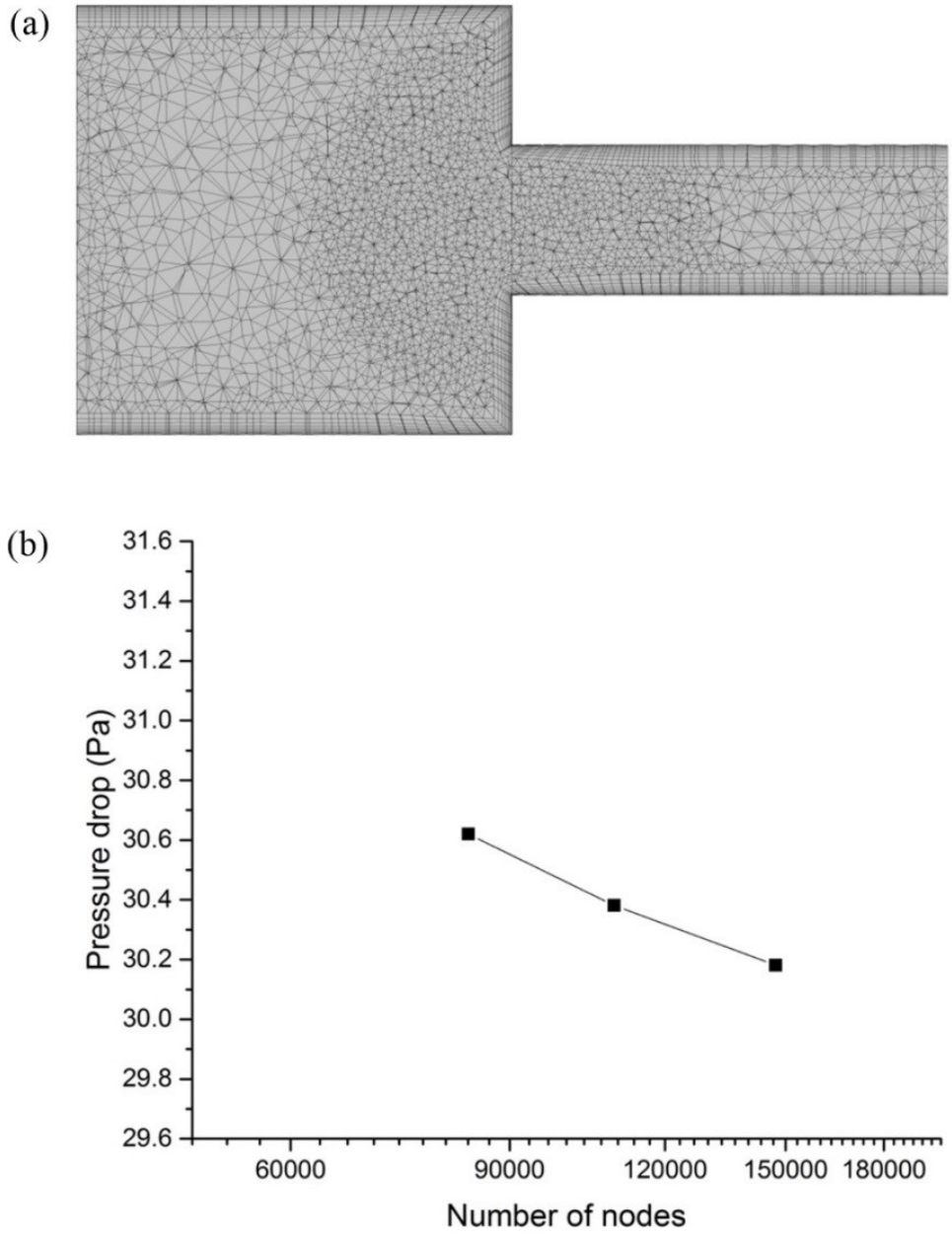


Figure 3.8: Mesh generation and assessment.

(a) Adaptively refined mesh, (b) Grid independence analysis.

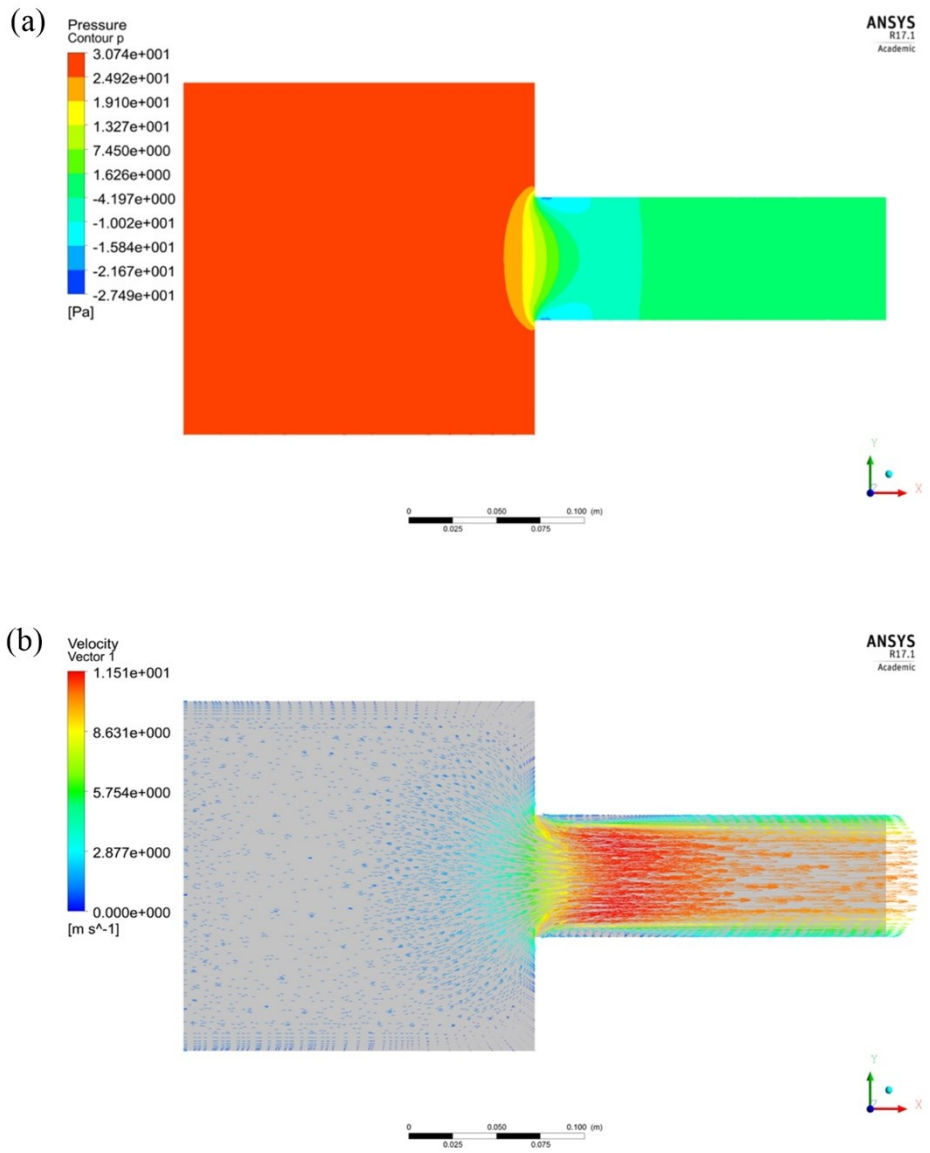


Figure 3.9: Results obtained from the robust simulation model.

(a) Pressure contour, (b) Velocity vectors.

### 3.4.2 Comparison of Results Between Different Designs

With the design parameter *d* decreasing, the pressure drop between the inlet and outlet is calculated in batch mode and by the intelligent solver and tabulated in

Table 3.4 and 3.5, respectively. Here, $\Delta p$ is calculated from the published head loss coefficient plot for flow through contracted pipe (Çengel and Cimbala 2006), $\Delta p_1$ is calculated by ANSYS CFX under the batch mode, which is a kind of routine analysis using the default setup for each design point. $\delta_1$ is the relative error between $\Delta p_1$ and $\Delta p$. Correspondingly, $\Delta p_2$ is calculated using the intelligent solver functions, and $\delta_2$ is the relative error between $\Delta p_2$ and $\Delta p$. Seen from Table 3.4 and 3.5, the pressure drop increases with the decreased small inner diameter. The $\delta_2$ error of the intelligent solver scheme is in the order of the uncertainty of $\Delta p$ obtained from the empirical method which cannot be improved further. Analyzing the results obtained from the batch mode, the $\delta_1$ error is significantly bigger especially when much higher velocity occurs with very small $d$, which means the compressibility effect is already not negligible. In comparison, the error of the intelligent solver is 2 to 3 times smaller than the batch mode error.

Table 3.4: Pressure drop calculation in the batch mode.

| Design point | $d$ (mm) | $\Delta p$ (Pa) | $\Delta p_1$ (Pa) | $\delta_1$ (%) | No. of nodes |
|---|---|---|---|---|---|
| DP1 | 70 | 29.05 | 32.18 | 10.77 | 59297 |
| DP2 | 60 | 54.32 | 60.81 | 11.94 | 57853 |
| DP3 | 50 | 113.45 | 129.64 | 14.27 | 56296 |
| DP4 | 40 | 278.35 | 325.01 | 16.76 | 56220 |
| DP5 | 30 | 882.52 | 1065.67 | 20.75 | 59466 |
| DP6 | 20 | 4478.13 | 6156.05 | 37.46 | 65952 |

Table 3.5: Pressure drop calculated by the intelligent solver.

| Design point | $d$ (mm) | $\Delta p$ (Pa) | $\Delta p_2$ (Pa) | $\delta_2$ (%) | No. of nodes |
|---|---|---|---|---|---|
| DP1 | 70 | 29.05 | 30.62 | 5.40 | 83414 |
| DP2 | 60 | 54.32 | 57.39 | 5.65 | 80573 |
| DP3 | 50 | 113.45 | 120.04 | 5.81 | 77486 |
| DP4 | 40 | 278.35 | 296.57 | 6.55 | 76353 |
| DP5 | 30 | 882.52 | 959.09 | 8.68 | 76235 |
| DP6 | 20 | 4478.13 | 5057.10 | 12.93 | 78895 |

The physics models selected for the batch mode are shown in Table 3.6. All the models remain to be unchanged during the design updating process. In the intelligent solver, the changes in physics models shown in Table 3.7 and Table 3.8 respond to the compressibility effect occurs in design point 6. Hence, the reason for the difference in the error control is that the intelligent solver functions support the validation of the CFD results and the reselection of correct solver regimes if there is any validity issue. And for each design, the robust simulation model can be derived to guarantee the quality of CFD simulation results. Therefore, the proposed CFD analysis view achieves the automatic feature conversion from the design view and provides a convincible input for another view, for example, the optimization view (L. Li, Lange, and Ma 2017), in product development process.

Table 3.6: Physics models selected for the batch mode.

| Physics models in batch mode | Selection |
|---|---|
| Turbulence model | *k-ε* |
| Advection scheme | UDS |
| Transient model | No |
| Compressible flow model | No |

Table 3.7: Model selection in the first round of simulation for design point 6.

| Physics models in intelligent solver (i=1; C=1; D=0) | Selection |
|---|---|
| Turbulence model | *k-ε* |
| Advection scheme | UDS |
| Transient model | No |
| Compressible flow model | No |

Table 3.8: Model selection in the last round of simulation for design point 6.

| Physics models in intelligent solver (i=5; C=5; D=0) | Selection |
|---|---|
| Turbulence model | RSM |
| Advection scheme | Blended scheme |
| Transient model | No |
| Compressible flow model | Yes |

### 3.4.3 Wet Steam Simulation

The mesh used in the wet steam simulation is the adaptively refined mesh shown in Figure 3.8(a). The gas phase named H2ORKv and the liquid phase named H2ORKl are used to create the homogeneous binary mixture which is treated as the fluid of the domain. The saturation properties of this mixture are set to Redlich Kwong, which is a real gas model in CFX ("ANSYS CFX-Solver Modeling Guide" 2013). The Reynolds number and Mach number derived from the fluid attributes indicate that the flow is incompressible turbulent flow. In addition, the steam quality at the inlet is 80%. Then, the boundary conditions are specified as follows:

(1) Inlet: velocity at 1 m/s, steam quality at 80%, temperature at 373.15 K;

(2) Outlet: relative pressure at -40 Pa;

(3) Wall: no-slip wall at 273.15 K;

(4) Reference pressure: 101325 Pa.

After several runs, the robust simulation model with satisfactory result is obtained. The mass fraction of the H2ORKv is exactly the steam quality which is shown in Figure 3.10. In order to verify the result, the steam quality is calculated by the intelligent solver and the empirical method (Çengel and Ghajar 2014) at the cross-sectional area where the big and small pipe connects and at the outlet. The results are collected in Table 3.9. It is obvious that the relative error between

the two methods is quite small at both locations. The error at the outlet is slightly bigger because of the entry effects for the second stage calculation. These results demonstrate the successful implementation of the wet steam simulation module in the intelligent solver.

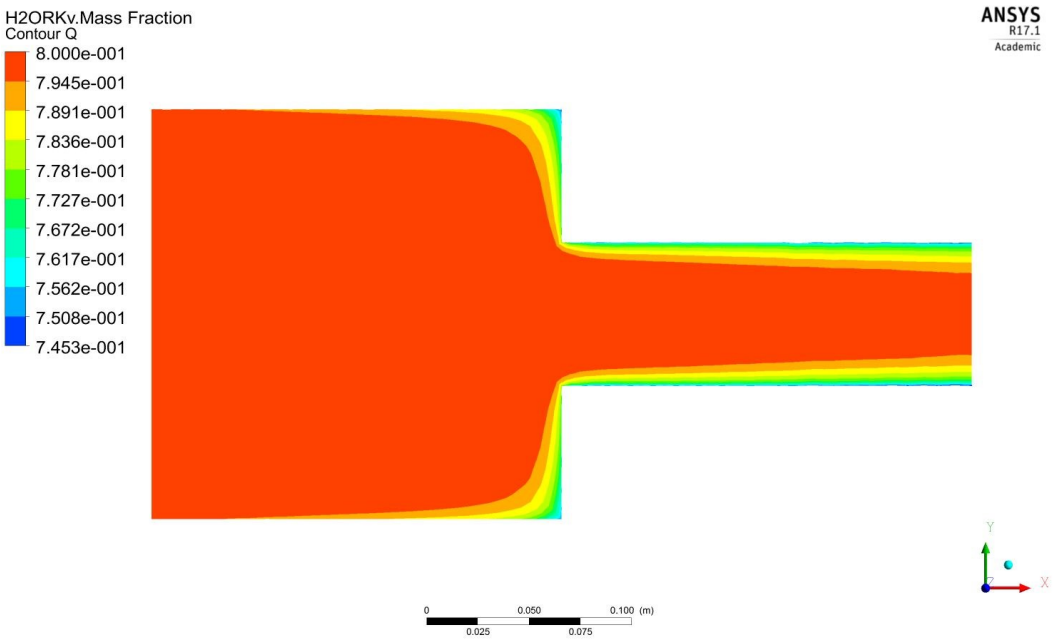


Figure 3.10: Contour of steam quality.

Table 3.9: Comparison of steam quality.

| Location | Intelligent solver | Empirical calculation | $\delta_3$ |
|---|---|---|---|
| Inlet | 80% | 80% | - |
| Connection | 79.6% | 79.9% | 0.39% |
| Outlet | 78.7% | 79.6% | 1.13% |

### 3.4.4 Implementation of the System

The proposed intelligent CFD solver functions are implemented based on ANSYS Workbench which provides two scripting levels. For task automation at the application level, in CFX specifically, CFX Command Language (CCL) ("Workbench Scripting Guide" 2013) is applied as a session to manipulate CFX-Pre and CFD-Post. Consequently, the physical model selection can be executed using CCL. After the simulation is done, the post-processing can be automated by CCL as well.

For task automation at the project level, Workbench scripting ("Workbench Scripting Guide" 2013) is used to create the whole project and invoke various applications to complete the created project. The actions performed via the GUI are recorded as journals which are Python-based scripts. Such kind of scripts can be customized according to a specific purpose. Thus, the functions of the whole system are greatly extended without too much scripting effort.

Based on the tools provided, the fluid physics features and dynamic physics features are implemented by programs to edit CCL. Further, the intelligent solver functions are fitted into the CAD/CFD integration system through Workbench scripting.

## 3.5 Summary

This chapter proposes intelligent CFD solver functions toward an expert system for both dry and wet steam simulation. The CAE interface protocol is used to convert the fluid functional features in the design view into the CAE boundary features in the CFD analysis view. Then, the intelligent CFD solver is able to select the right module to model the steam flow. Based on the derived non-dimensional numbers, appropriate physics models can be selected to run the simulation. Grid adaption, higher order schemes, and a subroutine for advanced turbulence models help to improve the accuracy of the CFD model after rounds of simulation. In this process, the fluid physics feature and dynamic physics feature are developed to generate the robust simulation model. The accuracy of this model is guaranteed by flow regime validation, grid independence analysis, and error estimation. Consequently, the consistency is kept properly in the view conversion process and the CFD analysis view can be fully fulfilled. The effectiveness of the proposed system is demonstrated by the analysis of a contracted pipe. In dry steam simulation scenario, the error induced by the intelligent solver is smaller than that of the traditional ANSYS batch mode. The results obtained by the intelligent solver also match well the empirical results when it comes to wet steam simulation.

# Chapter 4 : Optimization of Flow Control Device Using the Integration System

## 4.1 Introduction

In the oil industry, steam assisted gravity drainage (SAGD) is applied as a practical method to extract heavy oil from tar sands. As shown in Figure 4.1, there are two horizontal wells in the SAGD completion. The injection well continuously injects high-pressure steam to heat the bitumen and reduce its viscosity. As a result of the steam expansion, a steam saturated zone called the steam chamber forms. Steam condenses at the edge of the chamber. Driven by gravity, the condensed water and low viscosity bitumen move to the lower production well which is drilled in parallel with the injection well (Butler 1994). Due to the dissipation along the injection well and to the formation inhomogeneity, uneven steam distribution may form, which reduces production dramatically.

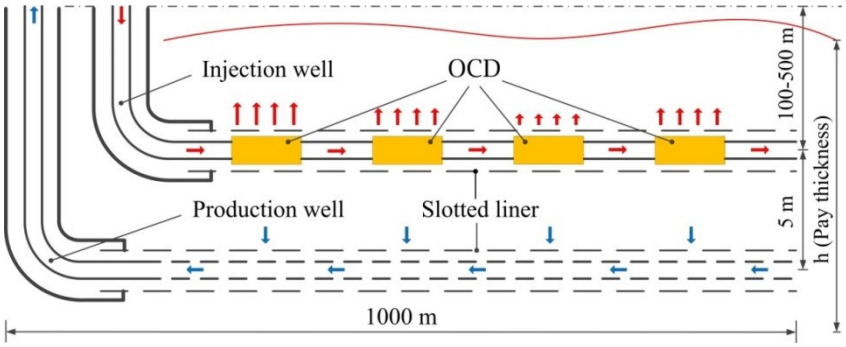


Figure 4.1: SAGD well completion.

Steam injection control has proven to be an important method for SAGD performance improvement (B. Robinson et al. 2005). As a commonly used tool for steam control, the OCD regulates the flow rate of steam flowing to the formation under a given pressure drop. The slotted liner covering the OCD is used to protect the device against the sand surrounding the well (J. Liu and Ma 2017). OCDs coupled with slotted liners or screens are applied in the injection well to control the steam injected into the system and to maintain an optimized steam distribution (Cavender, Hunter, and Pipkin 2011). When steam flows into the device, a portion of it flows to the annular space through the nozzles radially located on the device. Packers separate the annular spaces controlled by each device. The majority of steam continues flowing downstream. By adding steam injection points between the heel and toe of the injection well, OCDs contribute to creating an even distribution, which alleviates the barbell-shaped steam chamber induced by the traditional two injection tubing design (Bedry and Shaw 2012). Furthermore, the use of OCDs enables the conformance of the steam injection profile with the reservoir "pay thickness" (height of oil sands layer) along the well, which promotes steam chamber growth and reduces steam-oil ratio (SOR) (Medina 2015).

The performance of OCDs is significant to the SAGD process efficiency. Some research has been done to optimize the number and locations of OCDs (Kyanpour and Chen 2013; Kyanpour and Chen 2014; Noroozi et al. 2014). However, the design optimization of a single OCD device through physically

realistic CFD simulations is still needed. Actually, the OCD is applied with the slotted liner. There has also been some work dedicated to the optimization of the slotted liner (Kumar, Srivastava, and Kumar 2010; Etesami and Ahsan 2013; Xie 2015; J. Liu and Ma 2017). However, the optimization carried out in this chapter is focused on the OCD design improvement to achieve a better steam distribution through a fixed conventional slotted liner design.

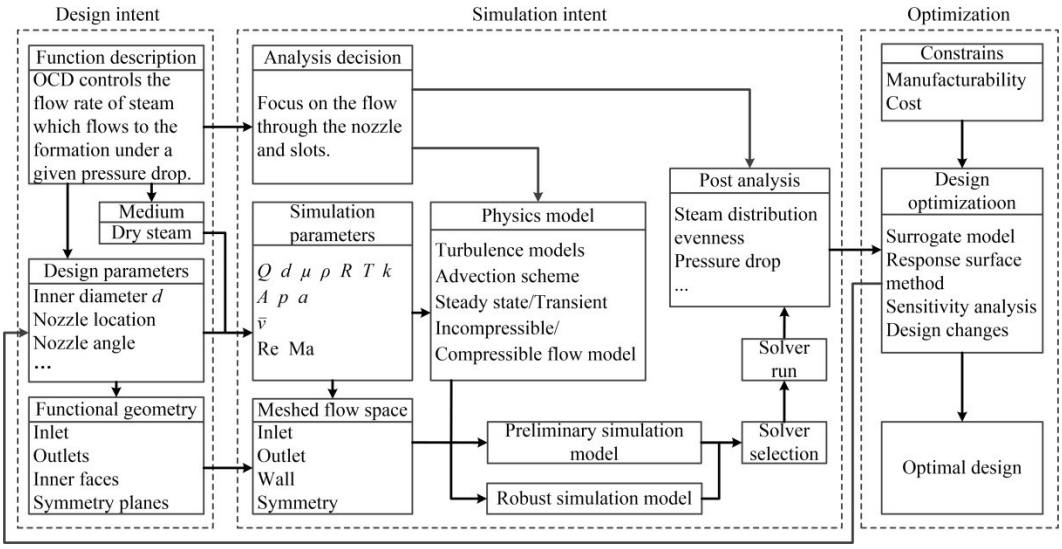


Figure 4.2: Association of design and simulation intent in OCD optimization.

This case study will demonstrate how the proposed CAD/CFD integration system works. Figure 4.2 shows the overall data flow in the OCD optimization based on the proposed CAD/CFD integration system. The design intent and simulation intent are associated seamlessly by the fluid functional features and CAE boundary features generated in section 4.2 and fluid physics features and dynamic physics features generated in section 4.3. The design optimization of OCD is demonstrated in section 4.4.

## 4.2 Generation of Fluid Functional Features and CAE Boundary Features

Though the two-phase wet steam is applied in SAGD, the single-phase flow should be able to provide sufficient approximation to the behavior of steam that has a quality higher than 70% (Lastiwka et al. 2017). As a result, water ideal gas (dry steam) at the temperature of 500 K is assumed to be pumped into the injection well at the flow rate of 0.24 $m^3/s$. Figure 4.3 (a) shows that the functional fluid geometry is itemized as the inlet, outlets, inner faces and symmetry planes. In this way, the fluid functional feature is fully defined, which conveys the design intent to the next stage in the integration loop.

In order to reduce the process time, the fluid domain can be established using SolidWorks parametrically, as shown in Figure 4.3 (b). Beneficially, the flow space can be easily updated subject to design changes. Tags with attributes, similar to named selections, are assigned to the fluid geometrical faces to transmit boundary information in CAD/CFD conversion. By using the CAD Configuration Manager provided by ANSYS Workbench, the simulation platform can visit and modify the geometry file constructed by SolidWorks. The attributes attached by tags are used to guide the mesh generation as shown in Figure 4.3 (c). Consequently, CAE boundary features are established, resulting in the generation of the fluid flow space, which is the input of the intelligent CFD solver.

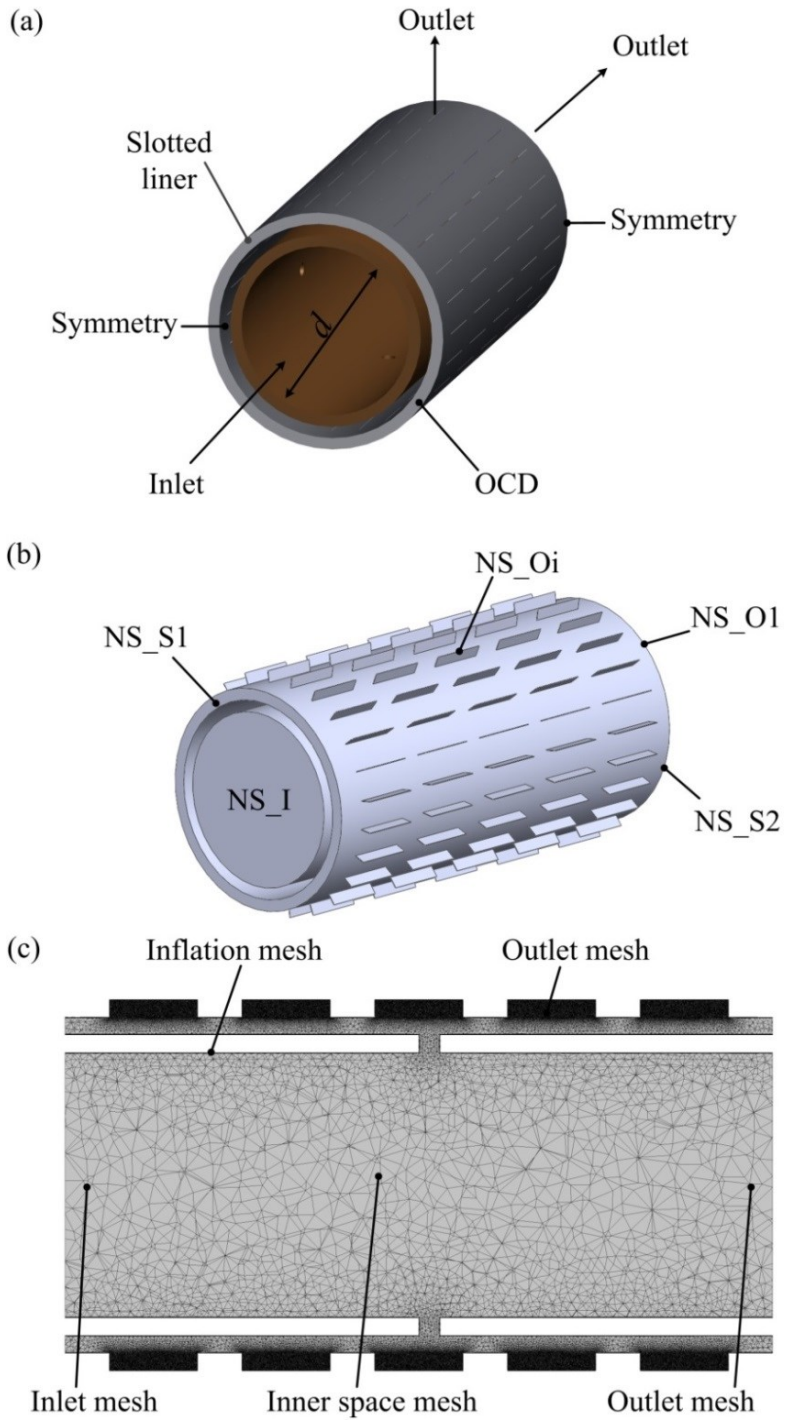


Figure 4.3: Model conversion in CAD and CFD.

(a) OCD and slotted liner, (b) Fluid domain, (c) Initial mesh generation.

The initial values of the physical parameters are given in Table 4.1. Table 4.2 shows the parameters calculated in step 1. The pressure derived in this step is assigned as the pressure inside the tool which is treated as the reference pressure. According to the OCD working conditions (Das 2005), the outlet boundary condition is allocated to NS_Oi and NS_O1 in Figure 4.3 (b) as -50 kPa and 0 respectively. Here, i is the number of the slots. The inlet velocity is found to be 13.5 m/s in step 2 and it is assigned to NS_I as the inlet boundary condition. In step 3, the Reynolds number is calculated to be $1.32\times10^{6}$, which is much bigger than the turbulence transition Reynolds number in a pipe. The Mach number is 0.02, which is much less than 0.3. So, the flow is assumed to be incompressible turbulent flow.

Table 4.1: Initial value of physical parameters.

| Physical parameter | value | Unit |
|---|---|---|
| $Q$ | 0.24 | $m^3/s$ |
| $d$ | 0.15 | m |
| $\mu$ | $1.66\times10^{-5}$ | kg/(m·s) |
| $\rho$ | 10.83 | $kg/m^3$ |
| $R$ | 461.5 | J/(kg·K) |
| $T$ | 500 | K |
| $k$ | 1.327 | N/A |

Table 4.2: Value of physical parameters in step 1.

| Physical parameter | value | Unit |
|---|---|---|
| $A$ | 0.0177 | $m^2$ |
| $p$ | 2500 | kPa |
| $a$ | 553 | m/s |

## 4.3 Generation of Fluid Physics Features and Dynamic Physics Features

The $k$-$\varepsilon$ turbulence model and the UDS advection scheme are selected at this initial stage to facilitate convergence. The simulation type is steady state. The fluid physics models selected in this simulation are shown in Table 4.3. Using ANSYS CFX as the solver, the simulation converges and the Mach number contour obtained from this initial run is shown in Figure 4.4.

Table 4.3: Fluid physics models of the initial run.

| Fluid physics model (i=1; C=1; D=0) | Selection |
|---|---|
| Turbulence model | $k$-$\varepsilon$ |
| Advection scheme | UDS |
| Transient model | No |
| Compressible flow model | No |

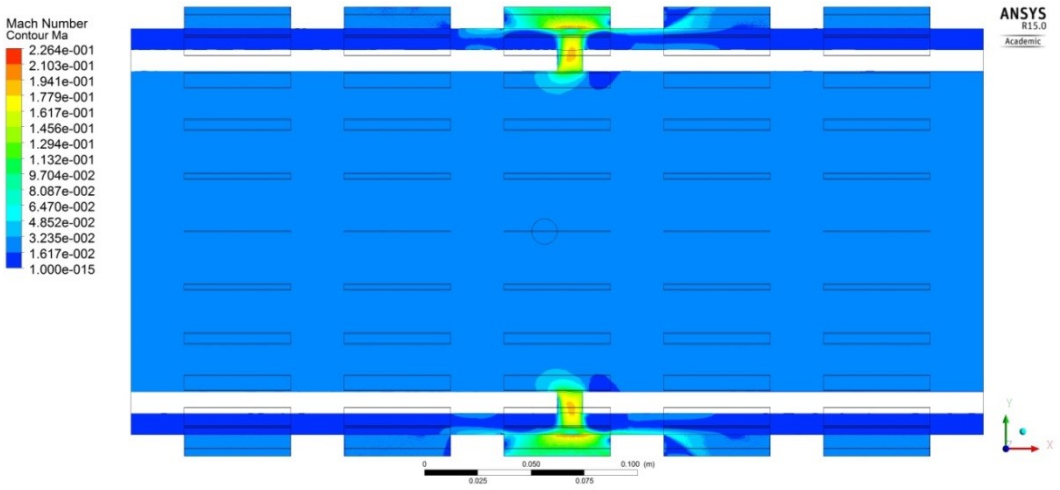


Figure 4.4: Mach number contour of the initial run.

Though the initial run converged, it is found that the maximum Mach number is close to 0.3 which means the compressibility effects cannot be ignored. Based on the simulation result, grid adaption is conducted, which is shown in Figure 4.5. The total energy model is selected to activate the compressible flow simulation. The other solver setup parameters remain unchanged in the next run.

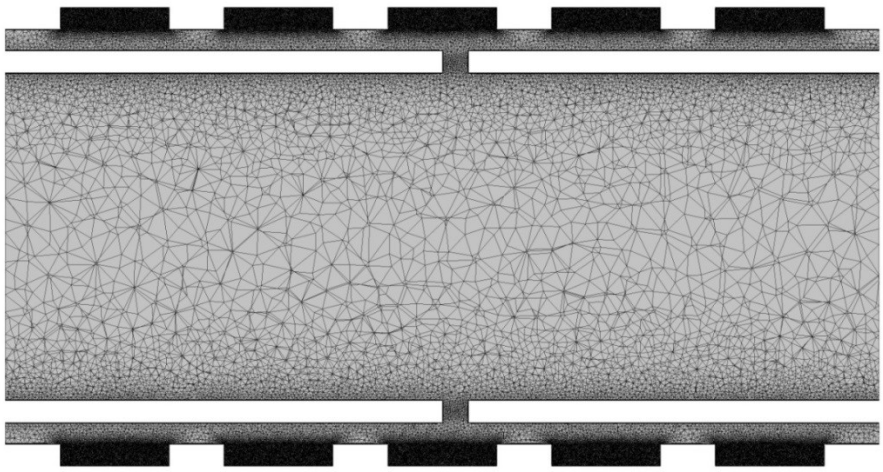

Figure 4.5: Grid adaption.

After a few iterations, the dynamic physics feature is developed to enable the acquisition of sensitivity towards different physical models. Consequently, a robust simulation model is obtained. The physics models selected for this model is shown in Table 4.4. The velocity vectors derived from this final run are shown in Figure 4.6.

Table 4.4: Fluid physics models of the final run.

| Fluid physics model (i=4; C=4; D=0) | Selection |
|---|---|
| Turbulence model | *k-ω* |
| Advection scheme | Blended scheme |
| Transient model | No |
| Compressible flow model | Yes |

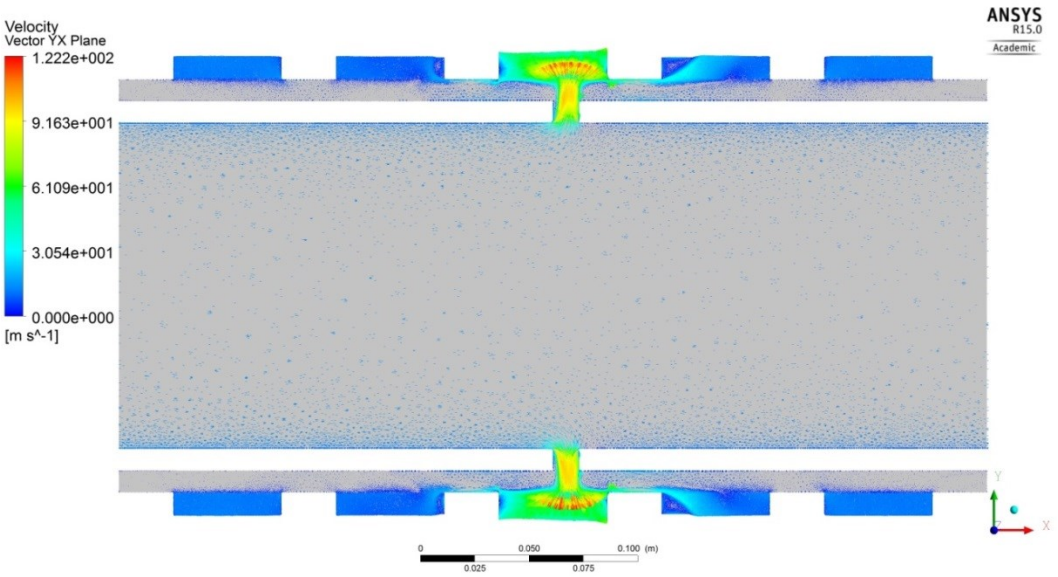


Figure 4.6: Velocity vectors of the final run.

## 4.4 Design Optimization

### 4.4.1 Evenness Factor for Quantifying Steam Distribution

The steam going through the slots is expected to evenly distribute, in order to form the steam cavern more precisely in the SAGD completion. To quantify the evenness of the steam distribution, the function $E_s$ is defined by calculating the deviation of mass flow rate through a specific slot from the perfectly even distribution situation, which has the expression as:

$$E_s = \iint_{A_s} (\rho \vec{v} \cdot \vec{n}) \mathrm{d}s - \psi \dot{m}_{in} / N \tag{13}$$

in which, $\rho$ is the density of steam, $\vec{v}$ is the steam velocity, $\vec{n}$ is the normal of slot opening surface, $A_s$ is the single slot opening area, $\psi$ is the steam outflow ratio, $\dot{m}_{in}$ is the total mass flow into the device, $N$ is the total number of slots. The value of $E_s$ ranges from $-\psi\dot{m}_{in}/N$ to $\dot{m}_{in}-\psi\dot{m}_{in}/N$. Depending on the sign of $E_s$, the steam distribution in the slot can be categorized as excess steam flow or insufficient steam flow.

Correspondingly, $E_0$ is defined as the variance of the mass flow rate through all $N$ slots over a set length and it is called the evenness factor.

$$E_0 = \frac{1}{N} \sum_{i=1}^{N} E_{s_i}^2 \tag{14}$$

Ideally, $E_0$ is 0, i.e. the steam flow through the slots complies with the even steam distribution scenario. Hence, a smaller $E_0$ means better overall evenness,

which is treated as the optimization objective derived from the design intent. $E_0$ is calculated in CFX-Post as an expression and it turned out to be $2.89\times10^{-6}$ $kg^2/s^2$ in the final run. $E_0$ can be normalized by dividing by the average mass flow rate through the slots.

### 4.4.2 Design of Numerical Experiments Based on CFD Simulation

In order to optimize the OCD performance, five design variables are selected to investigate their effect on the steam evenness factor while the other design parameters remain fixed. Four of the variables are shown in Figure 4.7, where $L_1$ and $\theta_1$ control the two nozzles pointing in the same direction with the flow inside the pipe while $L_2$ and $\theta_2$ control the two nozzles pointing in the opposite direction. The fifth parameter is the conical angle $\gamma$ which applies to all the four nozzles.

Central composite design (CCD) (Montgomery 2012) is applied to design the experiments, which forms 44 sets of experiments subjected to the 5 design variables with 5 levels each. The values of the design variables are coded, as shown in Table 4.5.

In the integrated environment, the fluid geometry can be easily updated to conduct the 44 sets of numerical experiments. The simulated objective values are recorded accordingly. For each design point, the robust simulation model is used to conduct the simulation and ensure the result is trustable. Meanwhile, it should be noted that every time an updated fluid domain occurs, the validity of the robust simulation model is checked according to the method described in chapter 3. If

the simulation model failed in a new design, another robust simulation model will be generated for this design point specifically. As a result, the accuracy of each design point can be guaranteed, which provides effective inputs for the optimization process.

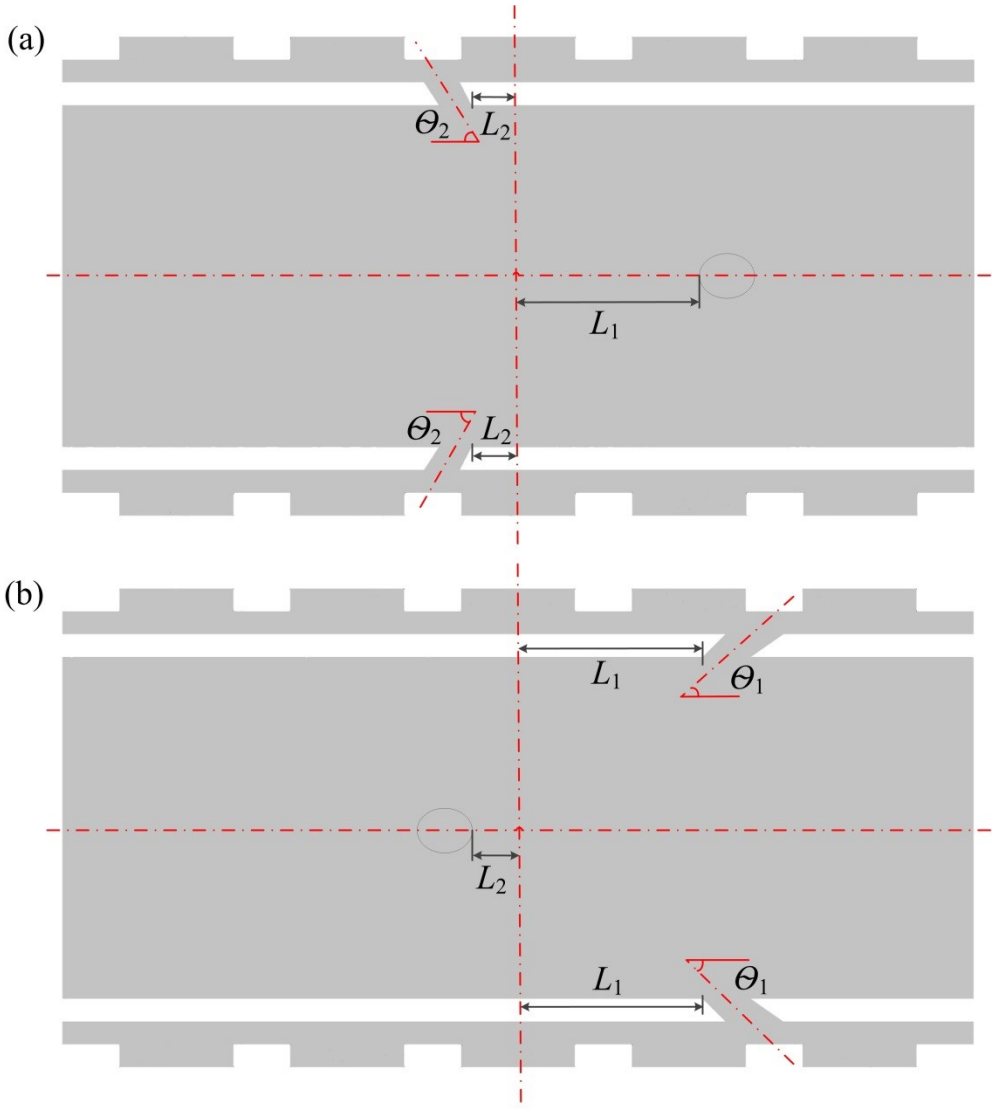


Figure 4.7: Design variables.

(a) Horizontal plane cross-section view, (b) Vertical plane cross-section view.

Table 4.5: Levels of design variables.

| | $L_1$ (mm) | $\theta_1$ (º) | $L_2$ (mm) | $\theta_2$ (º) | $\gamma$ (º) |
|---|---|---|---|---|---|
| -2.3784 | 0 | 40 | 0 | 40 | 0 |
| -1 | 11.59 | 54.49 | 11.59 | 54.49 | 1.45 |
| 0 | 20 | 65 | 20 | 65 | 2.5 |
| 1 | 28.41 | 75.51 | 28.41 | 75.51 | 3.55 |
| 2.3784 | 40 | 90 | 40 | 90 | 5 |

### 4.4.3 Optimization Result

Finally, the log file recording the simulation results is post-processed in MATLAB. Judging the optimization result obtained, it is found that the error between the derived minimal point's normalized evenness factor and the value from simulation validation at the same point is not acceptable. This is due to insufficient data input while the OCD flow is complex.

In order to obtain accurate optimization result, more design points are added adaptively based on the initial metamodel (Yang and Xue 2014). To achieve this, the evenness factor of the derived optimal point through RSM is calculated by simulation and treated as the new input for the next round of approximation. Eventually, the full data collected is shown in the appendix of this thesis. By regression analysis, the response function can be obtained as

$$y = (0.4397 - 0.0984x_1 + 0.0355x_2 - 0.141x_3 + 0.0942x_4 + 0.0071x_5 - 0.1096x_1x_2 + 0.0056x_1x_3 - 0.0117x_1x_4 - 0.0199x_1x_5 - 0.0014x_2x_3 + 0.0089x_2x_4 + 0.0185x_2x_5 - 0.117x_3x_4 - 0.0049x_3x_5 + 0.0161x_4x_5 + 0.117x_1^2 + 0.0326x_2^2 + 0.0895x_3^2 + 0.0432x_4^2 + 0.0099x_5^2) \times 2.7027 \times 10^{-4} \quad (15)$$

where y is the normalized evenness factor while $x_1$, $x_2$, $x_3$, $x_4$, $x_5$ are variables which represent the coded value of $L_1$, $\theta_1$, $L_2$, $\theta_2$, and $\gamma$ respectively. The average approximation error of this function is 6.7%. Using this function, the minimal normalized evenness factor is found to be $0.9776\times10^{-4}$ kg/s at the design point shown in Table 4.6. In this table, the coded values are obtained first by the response function. Then the actual values are calculated based on the coded values under the coding scheme presented in Table 4.5. The derived optimum design point is validated by simulation, and the simulation result of the normalized evenness factor is $1.0032\times10^{-4}$ kg/s, which leads to a relative error of 2.6%.

Table 4.6: Values of design variables at the optimum point.

| | $L_1$ | $\theta_1$ | $L_2$ | $\theta_2$ | $\gamma$ |
|---|---|---|---|---|---|
| Coded value | 0.7466 | 0.7216 | 0.5216 | -0.3784 | 0.1216 |
| Actual value | 26.28 mm | 72.58° | 24.39 mm | 61.02° | 2.63° |

The influence of each design variable on the evenness factor is analyzed graphically, as shown in Figure 4.8. The green line shows the contour of the

response surface against a single variable while all the other variables remain fixed at the point shown in the figure. The two red curves indicate a 95% simultaneous confidence band for the fitted response surface. Obviously, the evenness factor is most affected by the first and third variables, namely the nozzles' distances to the central plane. The effect of the conical angle and slant angles is relatively small. The streamlines flowing through the four nozzles are generated to show how the flow develops in the optimized OCD, as demonstrated in Figure 4.9.

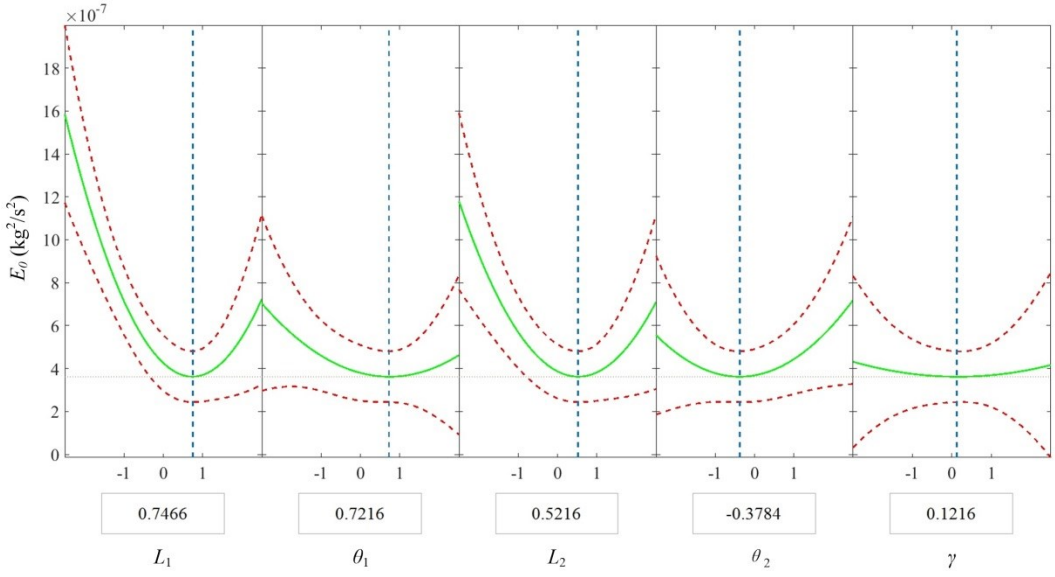


Figure 4.8: Influence of design variables.

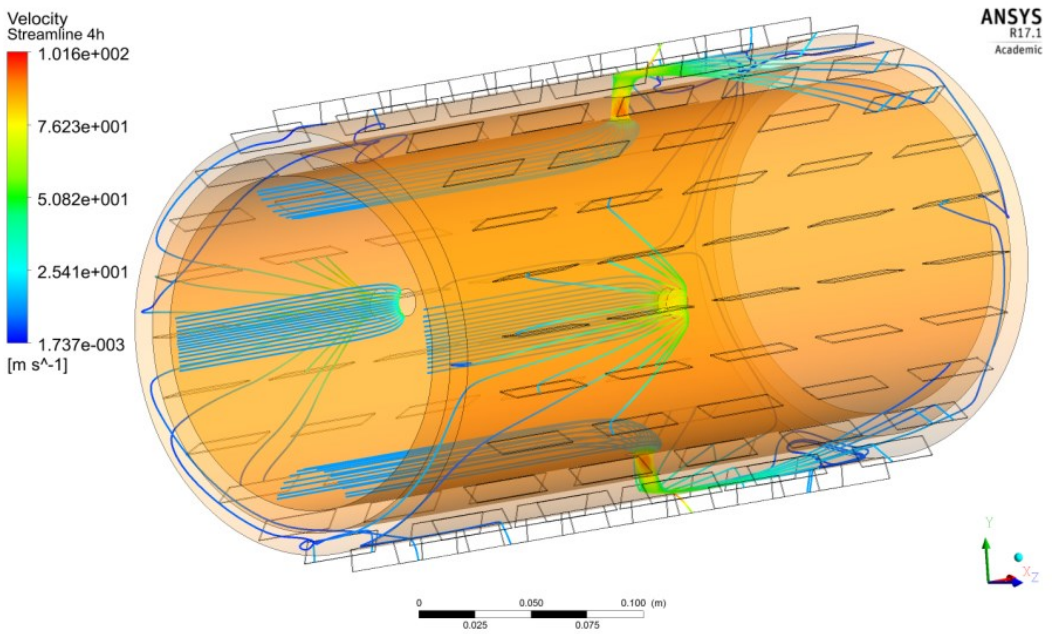


Figure 4.9: Streamlines through the four nozzles of the optimized design.

## 4.5 Summary

The application of OCD is important to the steam conformance in SAGD. The design of OCD needs to be improved to achieve better heating efficiency, which is significant to the oil sand industry considering the massive steam injection. As a result, the OCD is a good case to show the effectiveness of the proposed CAD/CFD integration system.

Based on the OCD design, the fluid functional features in the design view are abstracted with the design intent fully defined. Then, the fluid functional features are converted into CAE boundary features through feature conversion. Following that, the intelligent CFD solver functions help to generate fluid physics features

and dynamic physics features. Thus, the simulation intent is defined with the fulfillment of the analysis view. The robust simulation model provides accurate simulation results to the optimization algorithm. Using metamodeling, the response to the five design variables is derived. The minimal evenness factor is obtained, which shows a 75% improvement from an early design concept. The model corresponding to this minimal evenness factor is also validated by CFD simulation. The CAE effect features are generated according to the influence of design variables, which can be used to guide the design modification.

# Chapter 5 : Translation of the Optimization Result into the Realistic Design

## 5.1 Introduction

As shown in chapter 4, the steam distribution through the slots can be greatly affected by the OCD design. It is significant to research the OCD performance in order to achieve optimum design and thus guarantee high production rate in practice. Only a few studies have been done to investigate OCD aiming to optimize steam distribution and reduce energy consumption. Among them, the majority of the research work focuses on the OCD's effect on the whole reservoir (Medina 2015). However, the OCD flow characteristics are rarely studied, which is not sufficient to understand the fundamentals of the flow. In addition, the existing research on OCD performance and its effect on the reservoir is not sufficiently accurate.

On the other hand, the optimization of OCD is conducted in a simplified domain in chapter 4. The result needs to be validated in the realistic design to show the effectiveness. The mechanism and flow characteristics of OCD are studied first to build the suitable simulation model for the real OCD design. In the following section, the geometry and application conditions of OCD are introduced. Different domain sizes are tested in section 5.3 to investigate the effect of pressure drop, steam distribution and interaction between the nozzles, respectively.

Based on the understanding of the flow, the full-scale domain is established to test the effectiveness of the optimization result which are obtained from the simplified model.

## 5.2 OCD Geometry and Application Conditions

The OCD analyzed here is a commercial product, which has been applied in practice. As shown in Figure 5.1, the OCD functions based on the nozzles annularly located on it. There are four nozzles divided into two groups pointing to opposite directions with the help of the ring which covers them. When there is steam flowing through the OCD, a fraction of the steam will inject to the annular space through the nozzles due to the pressure drop. The rest of the steam will progress to the next OCD downstream. The working conditions for the OCD are listed as follows:

(1) Nozzle size: 1/4 in - 1 in (mainly depends on the desired pressure drop and flow rate);

(2) Steam quality: 92.5% - 95%;

(3) Flow rate: 200 - 300 $m^3$/d in cold water equivalent (CWE);

(4) Pressure inside the tool: determined by the program at each location;

(5) Annular pressure (max. operating pressure): 1500 - 2500 kPa;

(6) Pressure drop per nozzle: 20 - 100 kPa;

(7) Flow velocity per nozzle: < 30 m/s.

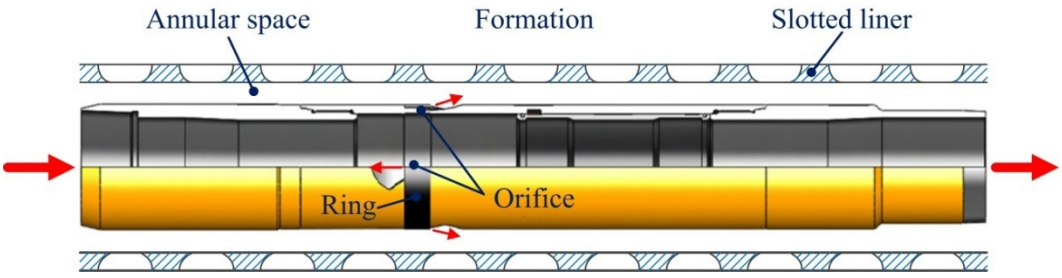


Figure 5.1: OCD and slotted liner configuration.

The fluid is assumed to be dry steam at 2500 kPa. According to the steam table ("Steam Table" 2017), under this pressure, the steam saturation temperature is 226.1 ºC, the steam density is 13 kg/m$^3$ and the steam dynamic viscosity is $1.66\times10^{-5}$ kg/(m·s). With the given steam flow rate in CWE and the inner diameter of the OCD, the average steam velocity in the device can be calculated to be 13.5 m/s using Equation (16), (3) and (6). In Equation (16), $Q_{\mathrm{w}}$ and $\rho_{\mathrm{w}}$ are the volumetric flow rate and density of the equivalent cold water, respectively.

$$Q = \frac{Q_{\mathrm{w}}\rho_{\mathrm{w}}}{\rho} \tag{16}$$

The Reynolds number can be calculated using Equation (7), and it is found to be $1.68\times10^{6}$, which means the flow is fully turbulent (White 2011). For ideal steam, the Mach number can be calculated using Equation (5) and (8). The Mach number is calculated to be 0.024 which is much less than 0.3. This means the flow in the tubing can be treated as incompressible. With the calculation done and the

simplification of the real condition, the boundary conditions are specified in the next section.

## 5.3 Simulation of OCD Based on Different Domain Sizes

### 5.3.1 Boundary Conditions and Effect of Pressure Drop

At the starting phase of the OCD simulation, a small region of interest is investigated to learn the flow characteristics quickly. A high gradient is expected in the region close to the nozzle, so the flow near the nozzle can be closely studied. Because of the different directions of steam flow distributed by the four nozzles, the OCD geometry is not perfectly symmetric. However, balancing the accuracy and computational cost, a quarter of the OCD domain is still selected to be studied first. Considering that the OCD can operate in subcritical or critical conditions (Medina 2015), it is time-effective to test the OCD performance under different pressure drops with the simulation of a quarter-domain, even though the simplification on the OCD geometry does not strictly comply with the symmetric requirement for flow.

The total length of the OCD is 1.78 m. Since the simulation of the device in full length would be time-consuming and is not necessary at the initial stage, a shortened quarter-domain including a single nozzle, which is shown in Figure 5.2, is extracted to conduct the simulation first.

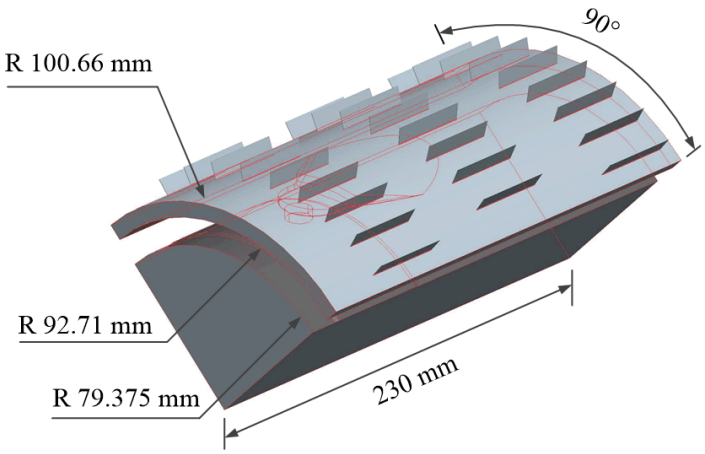


Figure 5.2: Quarter OCD flow space extraction.

The mesh of the flow space is generated by the ANSYS Mesh module. Local mesh refinement is implemented in the nozzle and channel regions, where high gradients are expected. Inflation layers are applied along the wall boundaries to capture the boundary layer accurately. The result of mesh generation is shown in Figure 5.3.

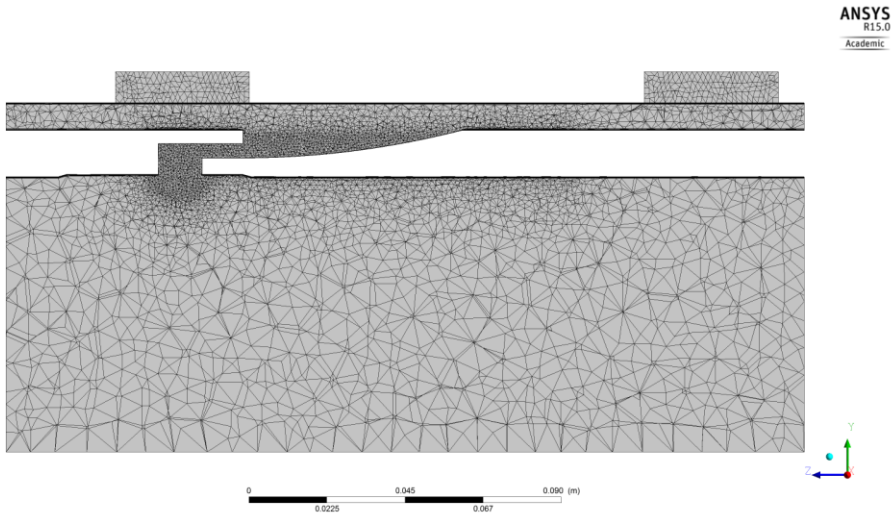


Figure 5.3: Sectional view of the meshed flow space.

Because a number of OCDs are installed along the injection well in practice, both of the ends of the annular space are assigned symmetrical boundary conditions to approximate the interaction between different OCDs. With the calculation done in section 5.2 and the simplification of the real conditions, the boundary conditions are specified as follows:

(1) Inlet average velocity: 13.5 m/s;

(2) Pressure of inner outlet: 2500 kPa;

(3) Pressure of outer outlet (slots): 2450 kPa (Das 2005);

(4) Six symmetry boundaries;

(5) The other surfaces are defined as the wall boundary.

The boundary conditions above are assigned to the corresponding regions as shown in Figure 5.4. ANSYS/CFX has an International Association for the Properties of Water and Steam (IAPWS) library integrated into the system, and it has shown great capabilities in the simulations conducted in previous chapters. Therefore, it is still selected as the solver for this study. The reference pressure is set to 2500 kPa and total energy is selected to be the heat transfer option. In this way, CFX can be configured to conduct compressible flow simulation if the compressibility effect is not negligible. The turbulence model used in this simulation is SST $k$-$\omega$ while water ideal gas is used as the fluid. The simulation

converges successfully after a few iterations and the streamlines through the nozzle are obtained, which are shown in Figure 5.5.

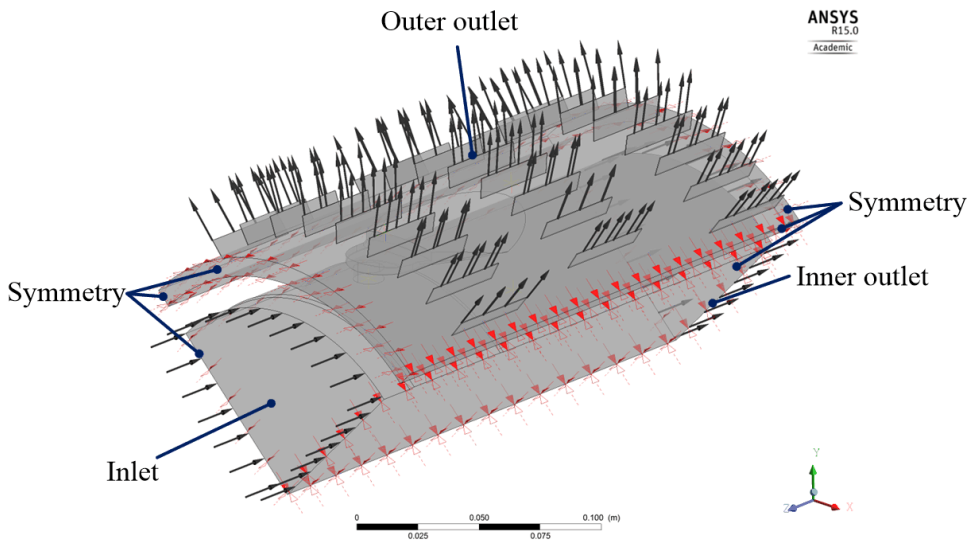


Figure 5.4: Boundary condition setup in the quarter-domain.

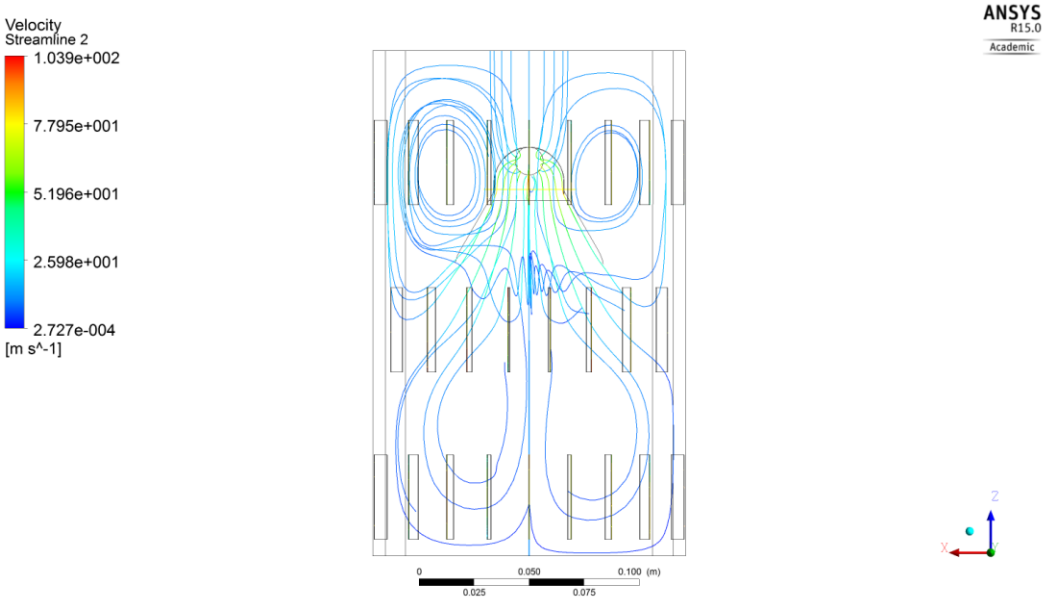


Figure 5.5: Streamlines through the nozzle in the quarter-domain.

The quarter-domain is very useful to check the flow behavior under different pressure drop values, which is important to the OCD working criteria investigation. To analyze the effect of pressure drop on the steam flow, the outflow ratio is defined as the fraction of steam flowing to the annular space from the total amount of steam. A series of simulations are conducted to calculate the outflow ratio. As shown in Figure 5.6, the simulation results indicate that outflow ratio increases with the increase of pressure drop. This trend slows down as the flow becomes compressive across the nozzle and approaches choked condition with the increasing pressure drop. It can be concluded that the pressure drop is the key driving force in the OCD flow. The streamlines in the annular space show that too many artificial effects are imposed on the solution because of the restricted flow area induced by the symmetry boundary. Thus, the quarter-domain should be extended in order to reveal more realistic flow.

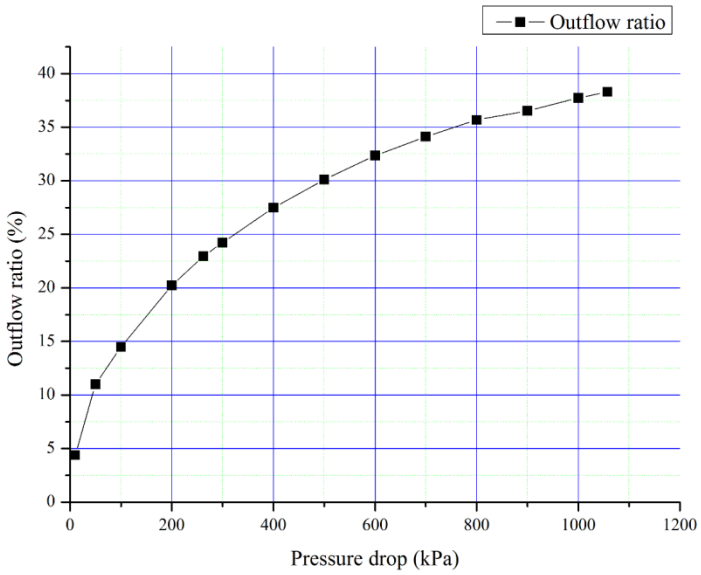


Figure 5.6: Outflow ratio with different pressure drops.

### 5.3.2 Steam Distribution Investigation

As aforementioned, the symmetry boundary on the sides restricts the development of the flow in the earlier simulation trial. Therefore, those two boundaries are moved away from the nozzle to alleviate this artificial effect. In this subsection, the simulation of the expanded half-domain is to be introduced. As shown in chapter 4, the OCD design affects the flow phenomena. Attempting to investigate the other affecting factors, the size of the annular space is doubled in the half-domain to check the impact on the flow.

In this half-domain simulation, the advanced meshing functions, proximity and curvature, are applied to obtain high-quality mesh in slots. Figure 5.7 shows the refined mesh generated in the half-domain.

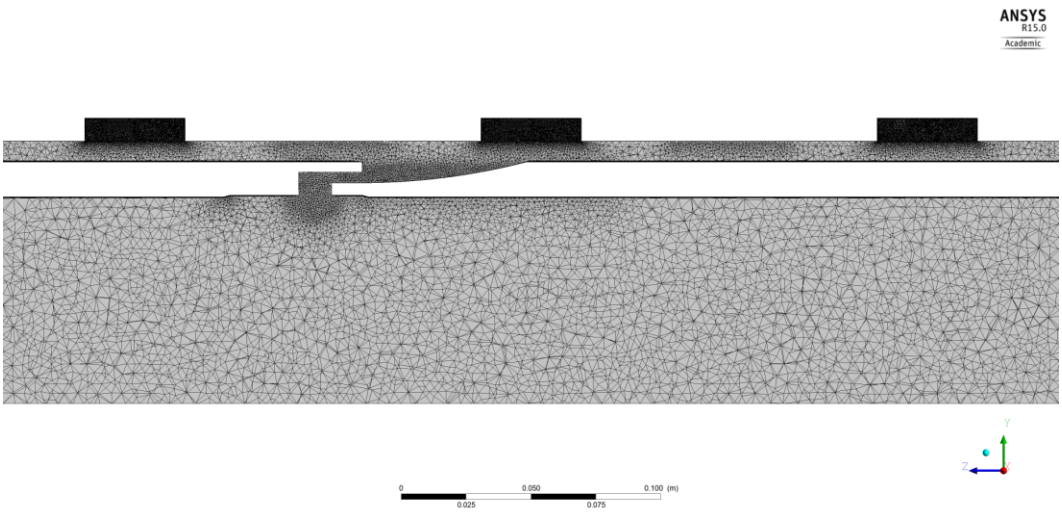


Figure 5.7: Sectional view of the meshed half-domain.

Regarding the geometry, the angle between the two sides is increased to 180° and the number of slots is also increased, but the boundary and solver configuration used are the same as the quarter-domain case. After the simulation, Figure 5.8 is obtained to show the velocity vectors in the channel, revealing Dean vortices caused by the curvature of the nozzle channel.

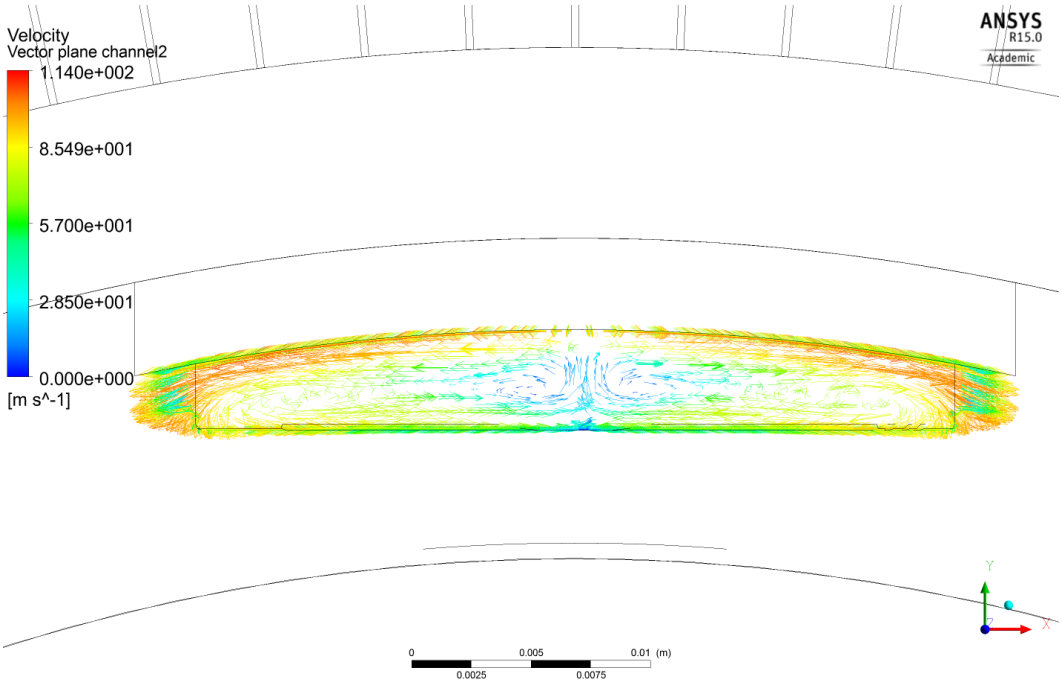


Figure 5.8: Velocity vectors in the channel.

In order to acquire the doubled annular space, both the inner and outer diameters of the slotted liner are increased correspondingly. The radial length of the doubled annular space is 15.9 mm. Using the same method applied in the regular annular space case, the mesh is generated and the solver setup remains the same. Figure 5.9 is captured to show the steam velocity vectors within the slot opening areas. This figure represents the steam distribution on the slots, which is

an important indicator to compare different OCD designs. The more evenly distributed is the steam injection over the slots, the better for an even growth of the steam chamber, especially at the initial stages.

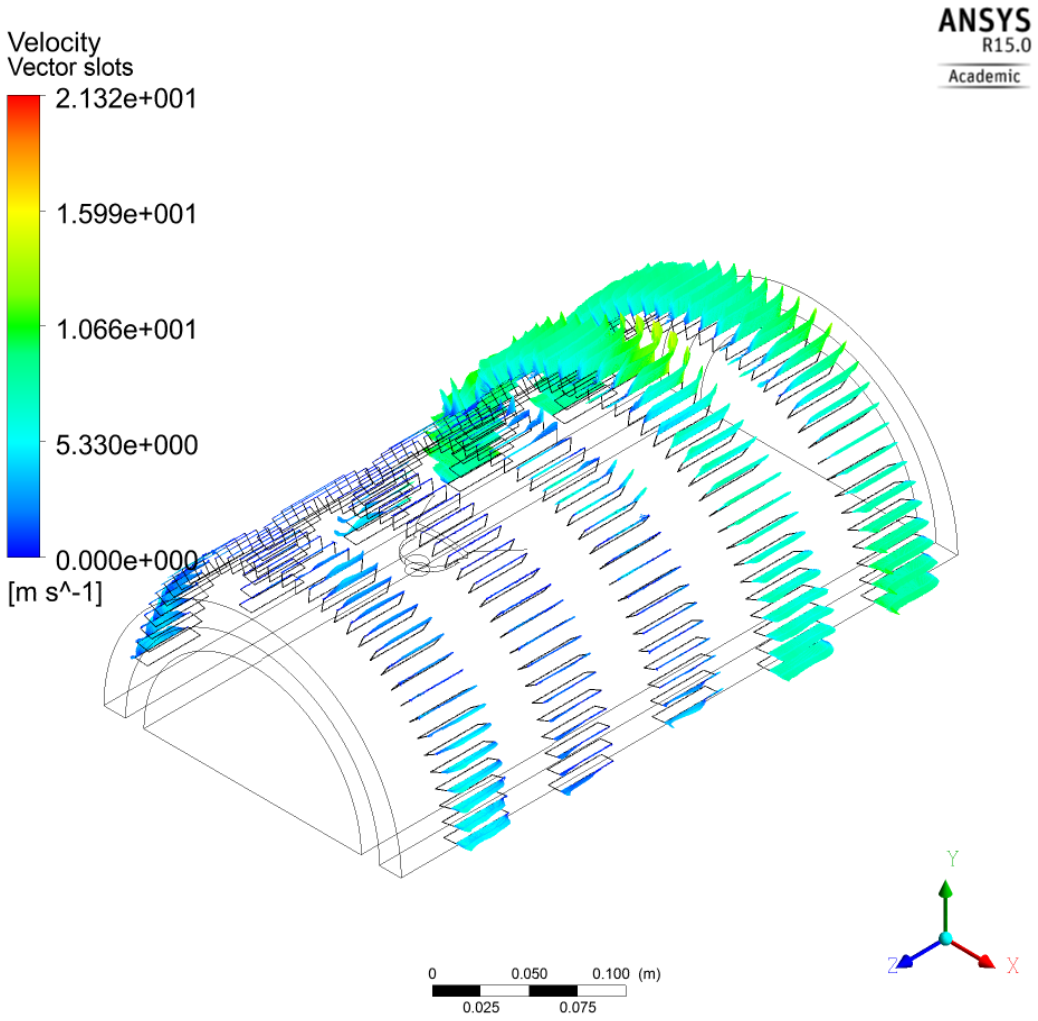


Figure 5.9: Velocity vectors on slots.

The top of Figure 5.10 shows the velocity vectors in the doubled annular space case while the regular annular space result is shown on the bottom. The velocity distribution is noticeably more uniform with the doubled annular space.

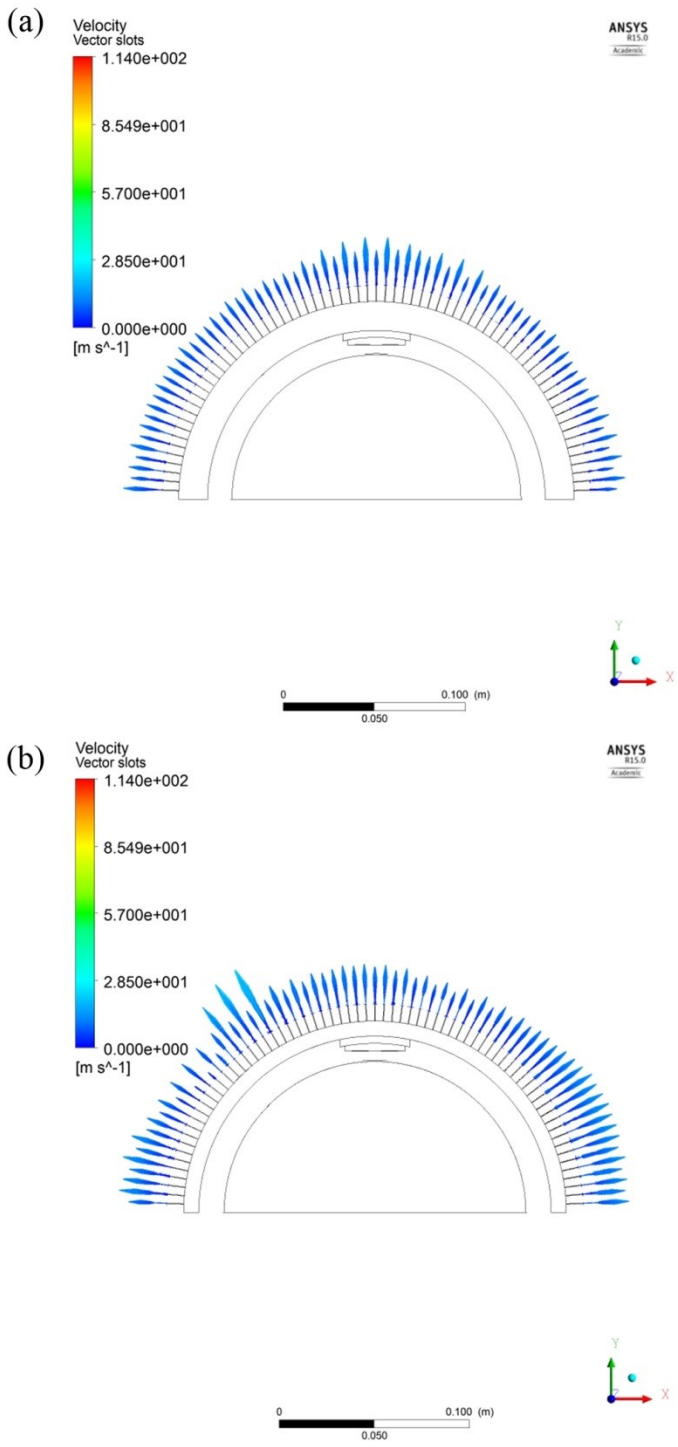


Figure 5.10: Comparison of steam distribution with different annular sizes.

(a) Doubled annular space, (b) Regular annular space.

### 5.3.3 Interactions Between Nozzles

The simulation of half-domain relieves the boundary effect occurred in the quarter-domain. However, the interactions between the four nozzles have not been considered in that simulation because of the simplification of the geometry. The simulation of a full-domain is needed to study these interactions.

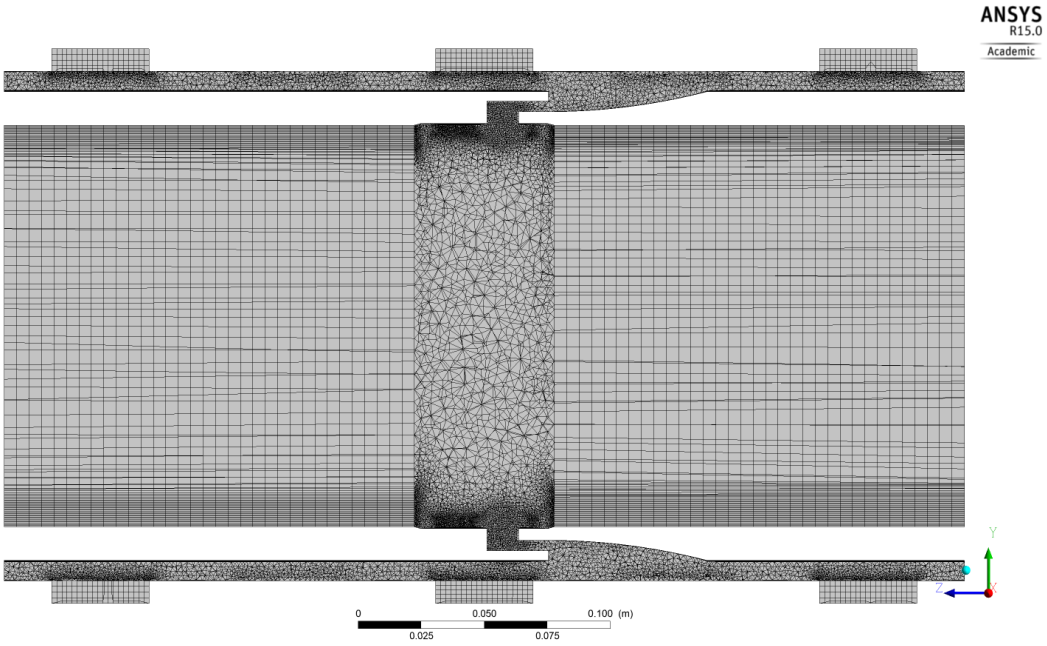


Figure 5.11: Sectional view of the meshed full-domain.

Because the aim of this study is to investigate the interactions between the nozzles, the central plane of the two sets of nozzles is located in the center of the full-domain intentionally. Using the previous mesh generation method, the total number of nodes would be very large because of the greatly increased domain size, so applying hexahedral mesh is a wise choice to balance the computational cost and accuracy. The geometry is divided into different zones to apply the

hexahedral mesh, which is shown in Figure 5.11. As can be seen, the slots and parts of the base pipe are discretized by hexahedral elements while the other parts are still discretized by tetrahedral elements, which lead to a reduced number of nodes and accurate results at the same time.

Because the domain is increased to 360°, there are only two symmetry boundaries at the ends of the annular space, which are shown in Figure 5.12. The other boundary conditions and solver setup remain the same as before.

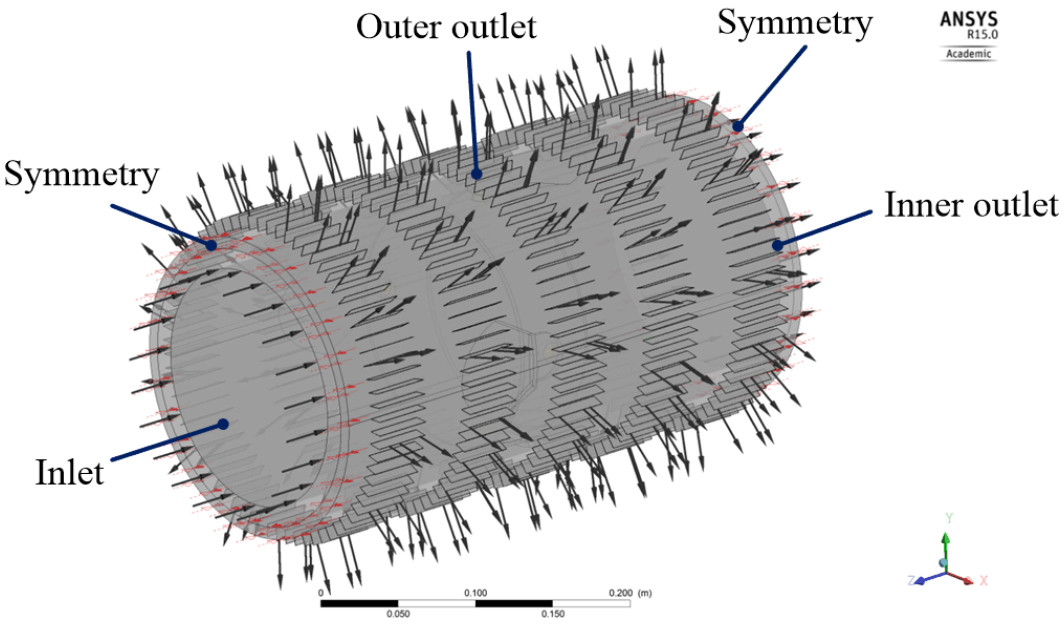


Figure 5.12: Boundary condition setup in the full-domain.

Figure 5.13 shows the velocity vectors on the mid-plane. It can be seen that some slots prevent steam from flowing into the domain as indicated by the solver. This phenomenon may be caused by the solver blocking a potential reverse flow at the slots' specific locations relative to the nozzle. Considering the environment

in which the OCD is applied, it may lead to sand production or plugging in those corresponding slots.

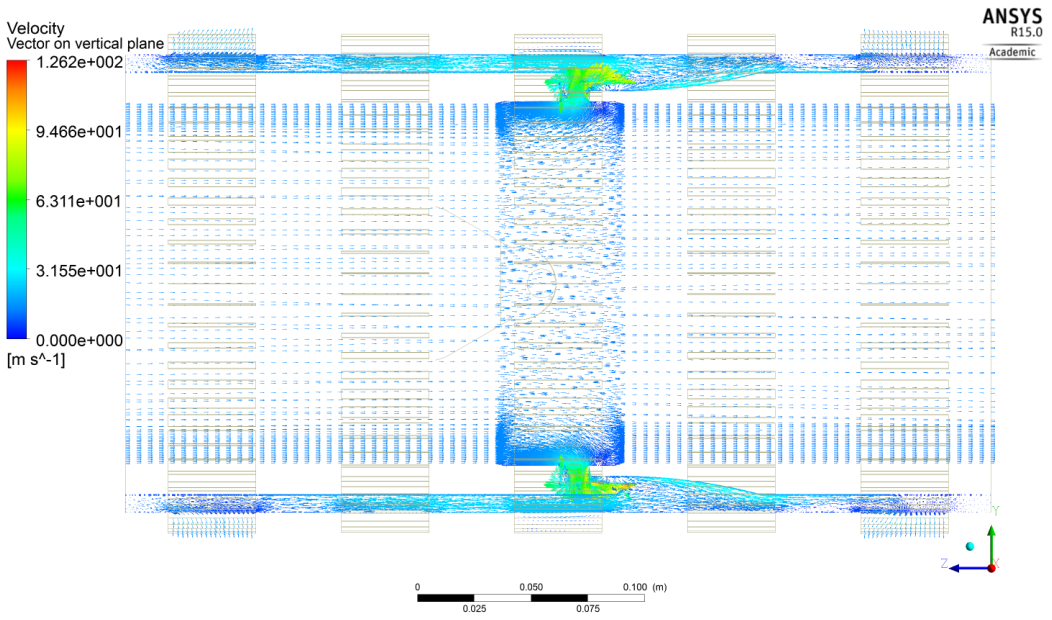


Figure 5.13: Velocity vectors on the mid-plane.

The streamlines through the four nozzles are shown in Figure 5.14. Instead of showing the velocity, the streamlines are denoted by four different colors to represent the flow traveling through the four nozzles correspondingly. Though the domain is expanded to 360°, the development of the streamlines is still restricted by the length of the domain because of the symmetry boundary imposed on the ends of annular space. Thus, the domain needs to be elongated to mitigate this effect.

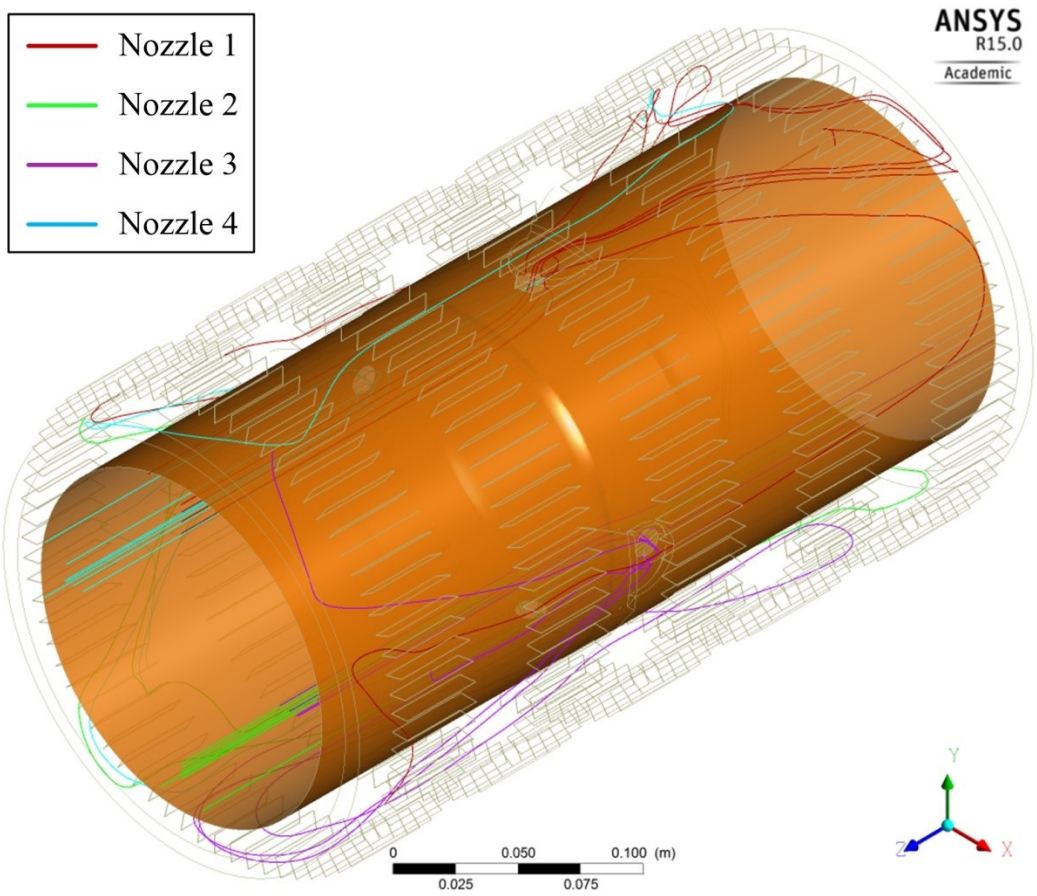


Figure 5.14: Streamlines through the four nozzles.

The outflow ratio under the pressure drop of 50 kPa is tested to be 10.7%, compared with 10.5% in the half-domain and 10.2% in the quarter-domain. The relatively small difference confirms the previous results, and the pressure drop is confirmed to be the decisive factor, regardless of the domain size. In addition, the mass flow rates through the four nozzles are calculated and the results are tabulated in Table 5.1. It is found that there is more flow through the two channels which are opposite to the steam flow direction in the base pipe, which is quite counter-intuitive. Because the pressure drop is the key driving force, further

investigation on the pressure field before and after entering the nozzle is needed to discover the reason for this flow behavior.

Table 5.1: Mass flow rates through the four nozzles.

| Property | Nozzle 1 | Nozzle 2 | Nozzle 3 | Nozzle 4 |
|---|---|---|---|---|
| $\dot{m}$ (kg/s) | 0.0751 | 0.0751 | 0.0796 | 0.0802 |
| $C_d$ | 0.52 | 0.52 | 0.55 | 0.56 |

## 5.4 Translation of the Optimization Result

### 5.4.1 Simulation of the Full-Scale Domain Without Porous Media

Because of the complexity of the fluid domain, the optimization of OCD is conducted using a simplified model shown in chapter 4 to reduce the computational time. The optimization result indicates that the evenness factor is mostly affected by the nozzles' distance to the central plane. This result needs to be tested to show its effectiveness in the realistic design.

Based on the detailed investigation of OCD in the previous sections, an in-depth understanding of the device is achieved. To reveal all the flow characteristics in the annular space, the length of the domain is extended to 3 meters to eliminate the domain effect. In SAGD completion, a margin for drilling is made in the formation to accommodate the wells. In the startup phase of the heating cycle, as shown in Figure 5.15, the margin leaves a gap between the formation and the slotted liner, which will be filled with the steam pumped from

the injection well. In addition to the steam in the base pipe and annular space, in order to model the steam in the gap, a cylindrical fluid domain is added to the outer bound of the slots. Thus, the full-scale simulation domain is generated. Because of the addition of this cylindrical region, it is hard to mesh the domain with different types of element. As shown in Figure 5.16, besides the inflation layers applied along the walls, the entire domain is discretized by tetrahedral elements with refinement made at the nozzles, channels, and the five columns of slots where the evenness factor is measured.

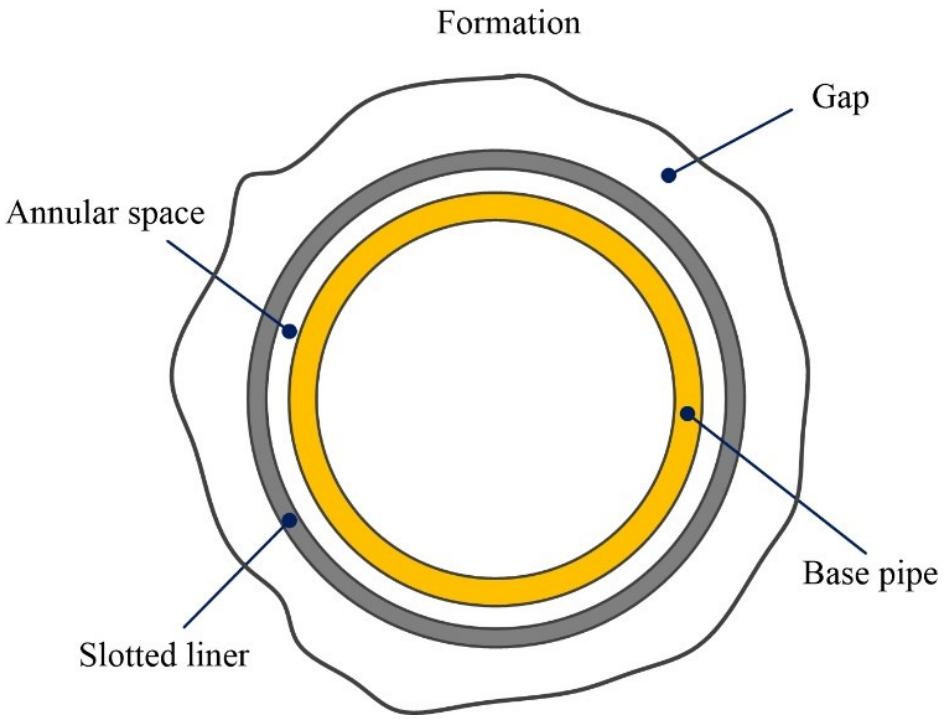


Figure 5.15: The gap between the formation and slotted liner during startup.

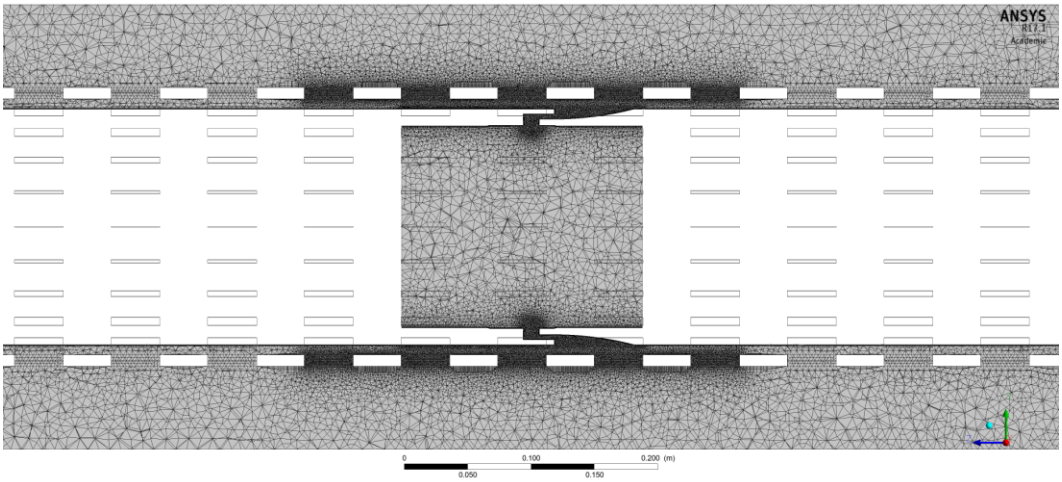


Figure 5.16: Sectional view of the mesh generated in the full-scale domain.

The inlet velocity, reference pressure, and the pressure at the inner outlet remain the same as the previous configuration. The pressure at the formation outlet (gap surface) is set to be -50 kPa intentionally to be consistent with the pressure at the slot openings in the simplified optimization case. The full-scale domain with boundary conditions setup is shown in Figure 5.17.

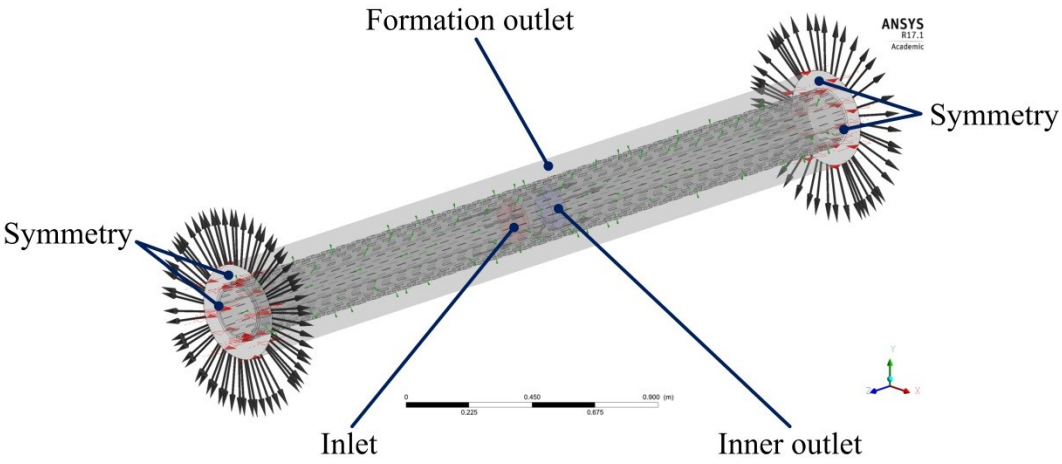


Figure 5.17: Full-scale fluid domain and boundary conditions.

The advection scheme used for this simulation is High Resolution, and the turbulence model is SST $k$-$\omega$. Figure 5.18 shows the velocity vectors above the top slots with a few streamlines. It is obvious that there are reverse flows in the slots adjacent to the nozzle, which confirms the nozzle's effect on the flow in the slots. This flow behavior corresponds to the slots without outgoing flow shown in Figure 5.13. The normalized evenness factor in this case is calculated to be $5.52\times10^{-8}$ kg/s.

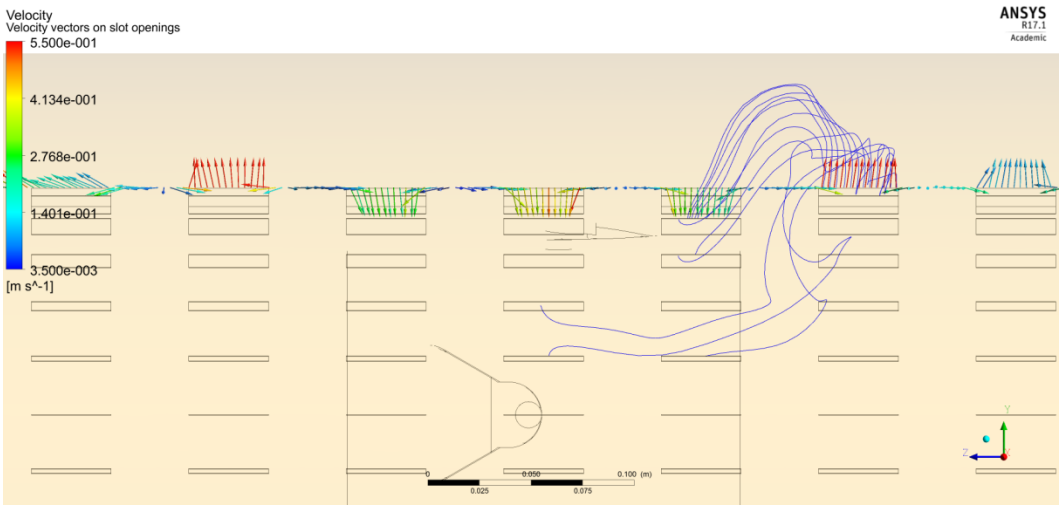


Figure 5.18: Velocity vectors above the top slots associated with the original design with the gap region surrounding the slots.

(Size of vector arrows is constant; velocity varies with colors)

### 5.4.2 Simulation of the Full-Scale Domain with Porous Media

After the heating of the well is conducted for a certain time, the formation will collapse and attach to the slotted liner (Kaiser, Wilson, and Venning 2002;

Carlson 2003). In order to investigate the flow injected into the formation in this scenario, the cylindrical domain outside of the slotted liner is configured as a porous domain which has a porosity of 35% and the permeability of 3.6 darcy. The pressure at the outlet is set as -56 kPa to impose an averaged pressure at the slot opening areas of approximately -50 kPa. Except for this, the other boundary conditions are the same as the none porous media case. The mesh, advection scheme and turbulence model used are also the same as the previous case.

The plot of velocity vectors on the slots is also obtained as shown in Figure 5.19. In comparison with Figure 5.18, the reverse flows are replaced by outflows with higher velocity than the flows through other slots. Besides, the overall velocity magnitude is reduced because the porous media acts as a fluidic resistor. The streamlines across the vertical mid-plane are shown in Figure 5.20. Seen from the streamlines, the addition of the porous media has a homogenizing effect on the distribution of the steam. The normalized evenness factor in this case is calculated to be $3.74\times10^{-9}$ kg/s, which is much smaller than that in the none porous case. This makes the effect of the porous media more convincible in a quantitative manner.

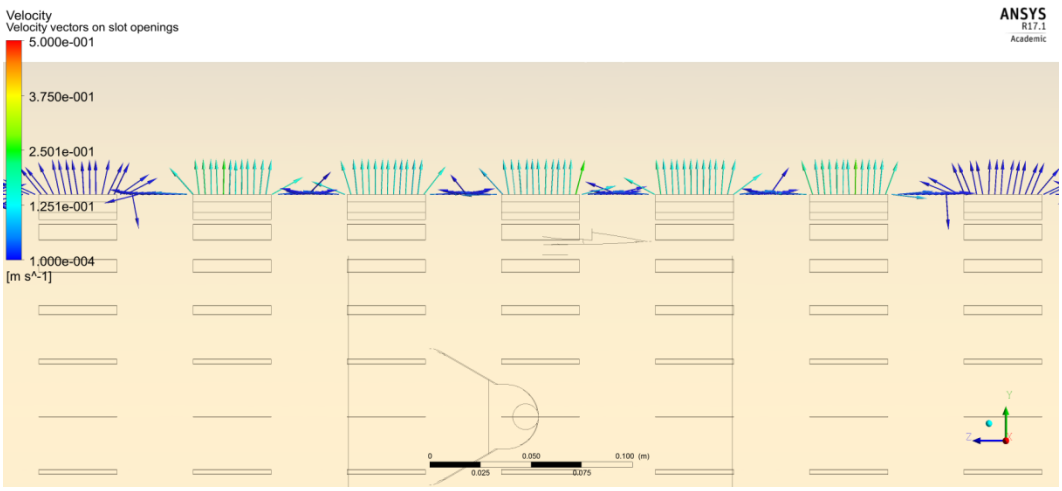


Figure 5.19: Velocity vectors above the top slots associated with the original design with the porous media surrounding the slots.

(Size of vector arrows is constant; velocity varies with colors)

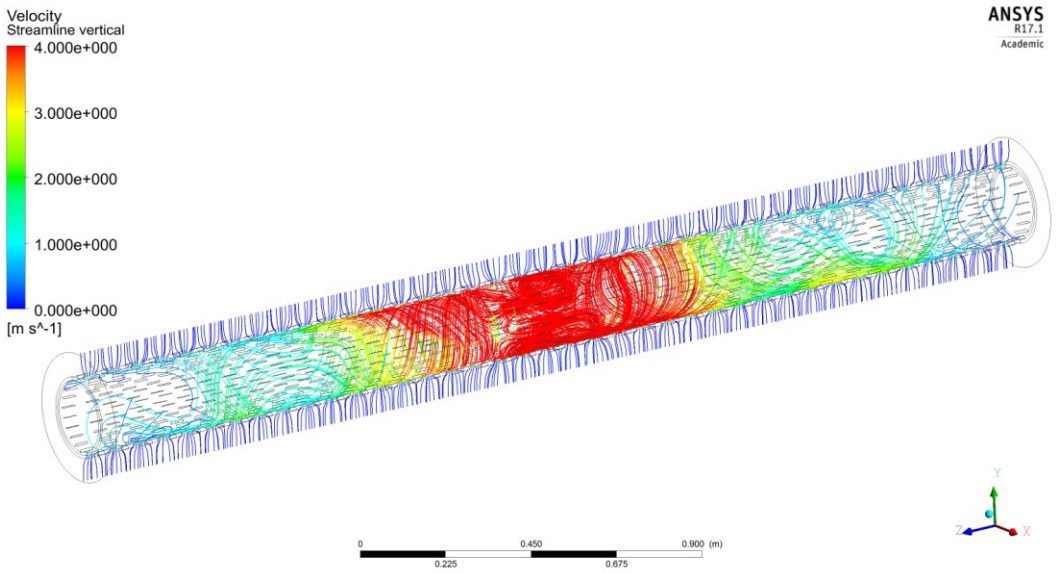


Figure 5.20: Streamlines across the vertical mid-plane.

### 5.4.3 Simulation of the Optimized Design Without Porous Media

The optimum design point in the simplified OCD case study shows a 50 mm distance between the two sets of nozzles approximately. In order to translate this result into the realistic design, the distance between the two nozzles in the full-scale domain is extended from almost 0 to 50 mm as shown in Figure 5.21 to run the simulation firstly conducted without porous media.

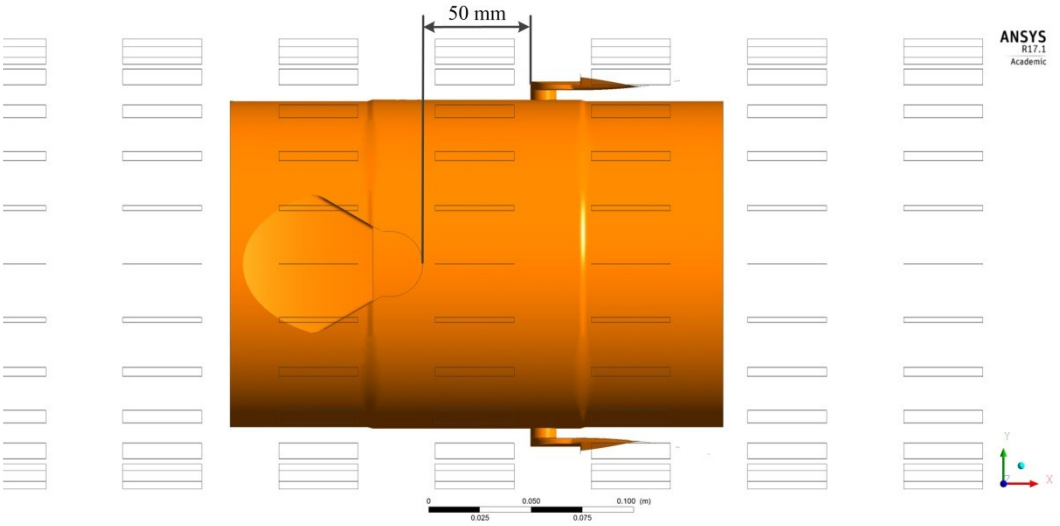


Figure 5.21: Extended distance between the nozzles.

In this case, the domain properties, boundary conditions, and physical models used are the same as the simulation presented in subsection 5.4.1. The velocity vectors in Figure 5.22 show that the reverse flow phenomenon is not eliminated. However, it is worth noting that the velocity magnitudes in the affected region are much smaller than those in the original design. Therefore, the optimized design is able to transport the momentum further in the annular space and distribute the

steam injection more evenly. The normalized evenness factor calculated in this case is $4.83\times10^{-8}$ kg/s, which results in a 12.5% improvement compared with the case shown in subsection 5.4.1.

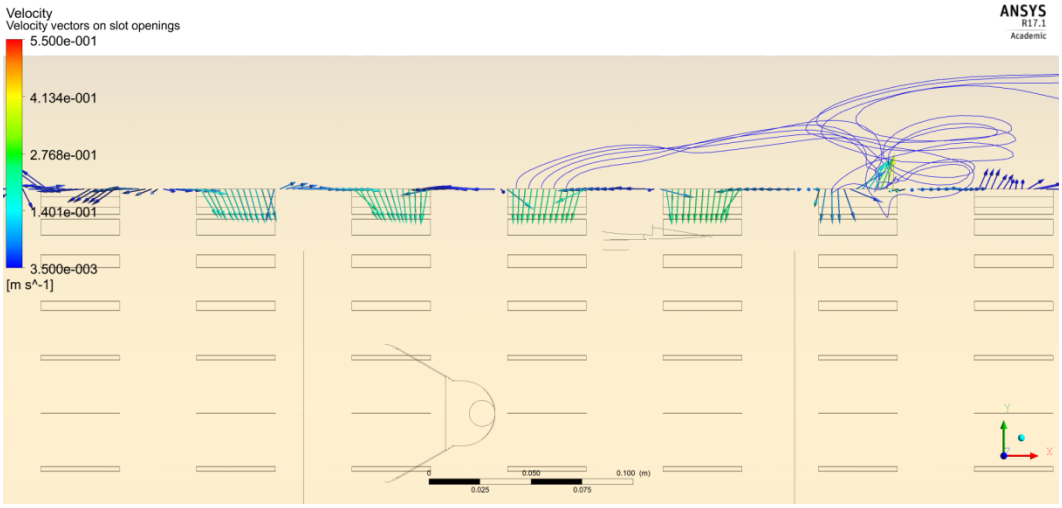


Figure 5.22: Velocity vectors above the top slots associated with the optimized design with the gap region surrounding the slots.

(Size of vector arrows is constant; velocity varies with colors)

### 5.4.4 Simulation of the Optimized Design with Porous Media

Since the SAGD well runs at the stable stage for a long time, it is very meaningful to compare the evenness factor when there are porous media attached to the slotted liner. In this simulation with the porous formation, the domain properties, boundary conditions, and physical model used are the same as the simulation presented in subsection 5.4.2.

As shown in Figure 5.23, because of the addition of the porous media, the reverse flows are absent as expected. The normalized evenness factor calculated in this case is $3.02\times10^{-9}$ kg/s. Consequently, the steam distribution is improved by 19.3% from the original design, which is significant considering the total amount of steam injected into the formation. This is enough to show the effectiveness of the optimization result. The evenness factor can be improved further by modifying the bend angle and shape of the flow channel as indicated by the previous optimization result obtained from the simplified domain.

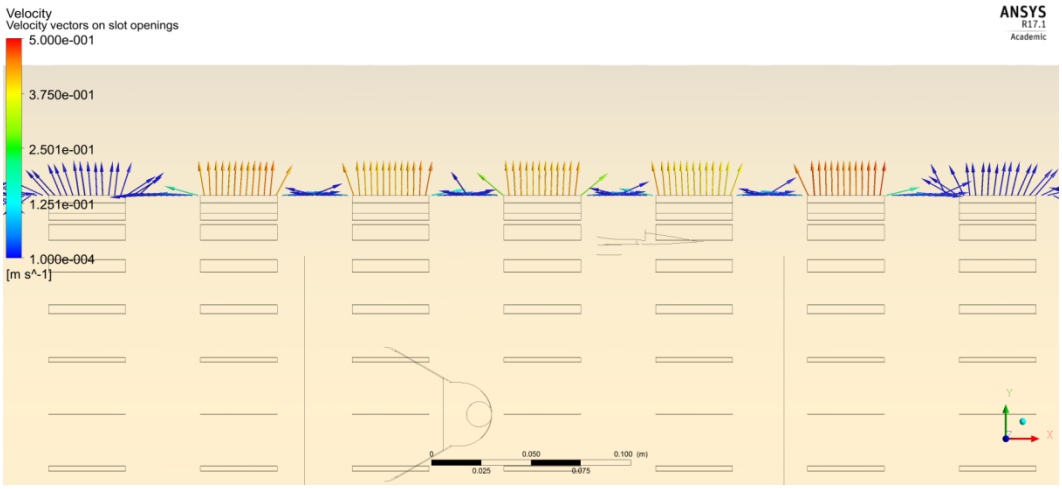


Figure 5.23: Velocity vectors above the top slots associated with the optimized design with the porous media surrounding the slots.

(Size of vector arrows is constant; velocity varies with colors)

## 5.5 Summary

The fluid mechanics of the flow involved in the OCD and the slotted liner is investigated through a detailed CFD analysis. The simulation conducted in the quarter-domain shows that the pressure drop across the nozzle is the driving force of the flow to the formation. The half-domain is used to compare the steam distribution through the slots in different annular sizes. Besides the influence of the design variables shown in chapter 4, the size of the annular space also has an effect on the steam distribution. The interaction between the nozzles is revealed by the simulation conducted in the full-domain. It is found that the outflow ratio under the same pressure drop in different domains is almost the same. Interestingly, there is more flow through the nozzles that are opposite to the flow direction to the downstream.

Intuitively, the nozzles are gathered together to provide more evenly distributed steam flow across the slots. However, the aformentioned optimization result does not support this assumption. A small axial separation (50mm) between the nozzles gives a better (lower) evenness factor in the idealized model, which is confirmed in the realistic model.

At the beginning of the heating cycle, when there is a gap between the formation and the slotted liner, reverse flows are found in some specific slots adjacent to the nozzles, which could potentially cause sand production or slot plugging. At the stable stage of oil production, when the formation is attached to

the slotted liner, the steam injected from the slots goes directly into the porous formation. The simulation of the flow in the formation is also conducted and it is shown that the reverse flows are eliminated due to the addition of the porous media. Actually, the porous media has a homogenizing effect on the distribution of steam. This is confirmed by comparing the normalized evenness factor quantitatively. The distance between the two sets of nozzles is extended to 50 mm to verify the effectiveness of the optimization result obtained from the simplified model. When there is a gap between the formation and the liner, even though the reverse flow phenomenon is not eliminated, the velocity magnitudes in the affected region are much smaller than those in the original design in which the distance between the two sets of the nozzles is almost zero. The normalized evenness factor shows that the steam distribution can be improved by 12.5% from the original design. When the slotted liner is surrounded by the porous formation, the steam distribution shows a 19.3% improvement compared with the original design.

Overall, the systematically developed CFD model is capable of simulating the complex flow behavior in the OCD, annular space, slots, and porous formation. The evenness factor can be applied effectively to measure the steam distribution quantitatively. The performance of the realistic design can be improved based on the sensitivity results obtained from the simplified domain. It should be noted that the evenness factor is still measured through the five columns of slots located at the center to be consistent with the calculation

conducted in the simplified domain. The evenness factor, based on a representative number of slot columns, should be investigated to improve the steam distribution further.

# Chapter 6 : Conclusions and Future Work

## 6.1 Research Contributions

This research explores a mechanism of CAD/CFD integration based on the innovative application of feature concepts. An overall feature mapping framework for persistent associations for CAD/CFD interactions has been suggested. This framework can effectively represent the engineering knowledge involved in product design, CFD evaluation, optimization, and design change justification. It can be concluded that the associative feature is an effective mechanism for managing not only geometric associations but also semantic portions of the features. The consistency and accuracy in this integration system are maintained by introducing the CAE boundary feature. CAE boundary features model and represent boundary conditions during iterations and achieve associated mesh generation for solver setup. The CAE effect features can be obtained after the optimization process, which reveal the effect of the design variables and guide the design modification.

On top of the design view supported by the CAD fluid functional features, the CFD analysis view is developed as a feature model to respond to the changes in the design view effectively. This feature model consists of CAE boundary features, fluid physics features, and dynamic physics features. The feature conversion between the design view and the CFD analysis view is achieved by the CAE interface protocol. Especially, the application of fluid physics feature and

dynamic physics feature enables artificial intelligence assisted solver regime selection and validation; this method leads to a robust simulation model with accurate or precise results. The quality of the robust simulation model is guaranteed by the grid independence analysis and error estimation. The subroutine for advanced turbulence models is developed to enhance the ability of the intelligent CFD solver to model complex turbulent phenomena.

The effectiveness of the intelligent CFD solver functions is shown by the investigation of pressure drop in a benchmark case of contracted pipe under different designs. By comparing with the empirical results, the error generated by the intelligent solver is generally 2 to 3 times smaller than that of the traditional ANSYS batch mode, which demonstrates that the proposed method has a better control over the errors as expected. The rules used in this system are expanded to make it capable of wet steam modeling. This approach can be applied in other contexts by adapting the relevant knowledge bases. Thus, the proposed method is able to provide a generic approach to integrate CFD analysis into a multiple-view product development environment.

The case study of OCD applied in SAGD is used to test the CAD/CFD integration system. The two evenness factors are introduced for the first time to measure the steam distribution through the slots quantitatively. It should also be highlighted that the robust simulation model is constructed progressively under the scheme proposed. In this process, the intelligent CFD solver functions are implemented through physical knowledge and best practices in CFD. Relying on

the accurate simulation results provided by the robust simulation model, design optimization is conducted using metamodeling. The response to the five design variables is derived by regression analysis. Based on the response function, the minimal evenness factor is derived, leading to a 75% improvement from an early design concept. The CAE effect features are generated, which reveal the influence of design variables. It is shown that the evenness factor is mainly affected by the nozzles' distance to the central plane while the effect of conical angle and slant angles is relatively small. This finding is used to guide the design modification toward a better steam distribution. With the help of the CAD/CFD integration system, the design intent and simulation intent are associated seamlessly in the OCD design optimization process.

In order to validate the optimization result which is obtained based on the simplified OCD model, a detailed study of the flow is conducted to build the proper model for the realistic OCD design. The outflow ratio curve as a function of pressure drops is quite smooth, which confirms the simulation analysis and model configuration. The steam distribution can be strongly affected by the design, for example, the size of the annular space. Under the same pressure drop, the outflow ratio is almost the same regardless of the domain size. Thus, the pressure drop is confirmed to be the driving force of the OCD flow. Counter-intuitively, more steam is found flowing through the two nozzles which are opposite to the steam flow direction in the base pipe.

At the startup phase of SAGD, reverse flows are found in some specific slots adjacent to the nozzles, which may lead to excessive sand production or slot plugging in practice. As the oil production approaches the stable stage, the formation, which is a porous media, will collapse and attach to the slotted liner. The CFD simulation reveals that the reverse flows in the slots can be eliminated by the addition of the porous media. The porous formation has a homogenizing effect on the steam distribution. When the distance between the two set of nozzles is extended from almost zero to 50 mm corresponding to the optimization result obtained from the simplified domain, the steam distribution through the slots surrounded by a gap shows a 12.5% improvement from the original design. Even though the reverse flow phenomenon is not eliminated, the velocity magnitudes in the affected region are much smaller than those in the original design. If the slots are surrounded by the porous formation, the steam distribution can be improved by 19.3% compared with the original design. All these results prove the validity of the optimization result obtained from the CAD/CFD integration system.

## 6.2 Limitations and Future Work

The multiphase model used in the wet steam simulation module of the intelligent CFD solver is only based on the mist flow which is a very specific case in wet steam modeling. Other models which are capable of complex wet steam simulation need to be studied in the future to facilitate the better modeling of the flow through the OCD. In this way, the design optimization can be further

implemented incorporating pressure drop and steam condensation rate as objectives.

As shown in chapter 5, the radial dimension of the annular space shows an obvious effect on the steam distribution through the slots. Besides the design variables investigated in chapter 4, there may be other factors influencing the steam distribution. Those factors need to be explored to improve the OCD design further. The difference in the mass flow rate through the two sets of nozzles is found. More work needs to be done to find the reason for this difference.

Transient behavior is found in the flow in the annular space, which affects the distribution of the steam significantly. The current solution is to make the last simulation stop when the mean of the residuals stabilizes. The transient simulation of the flow needs to be conducted in the future to achieve a better modeling.

Even though the evenness factor is applied to measure the steam distribution quantitatively and used as the objective to improve the design effectively, it is only calculated based on five columns of slots, which is not sufficient to reveal the overall steam distribution across the whole domain. A representative number of slots need to be explored to further improve the overall steam distribution.

# Bibliography

Anderson, D. C., and T. C. Chang. 1990. “Geometric Reasoning in Feature-Based Design and Process Planning.” *Computers & Graphics* 14 (2): 225–35. doi:10.1016/0097-8493(90)90034-U.

ANDREWS, ALISON E. 1988. “Progress and Challenges in the Application of Artificial Intelligence to Computational Fluid Dynamics.” *AIAA Journal* 26 (1): 40–46. doi:10.2514/3.9848.

“ANSYS CFX-Solver Modeling Guide.” 2013. Canonsburg, PA: ANSYS, Inc.

Ayancik, Fatma, Erdem Acar, Kutay Celebioglu, and Selin Aradag. 2017. “Simulation-Based Design and Optimization of Francis Turbine Runners by Using Multiple Types of Metamodels.” *Proceedings of the Institution of Mechanical Engineers, Part C: Journal of Mechanical Engineering Science* 231 (8). SAGE PublicationsSage UK: London, England: 1427–44. doi:10.1177/0954406216658078.

Barton, Russell R., and Martin Meckesheimer. 2006. “Chapter 18 Metamodel-Based Simulation Optimization.” *Handbooks in Operations Research and Management Science* 13 (January). Elsevier: 535–74. doi:10.1016/S0927-0507(06)13018-2.

Bathe, Klaus-Jürgen, and Hou Zhang. 2009. “A Mesh Adaptivity Procedure for

CFD and Fluid-Structure Interactions." *Computers & Structures*, Fifth MIT Conference on Computational Fluid and Solid Mechanics, 87 (11–12): 604–17. doi:10.1016/j.compstruc.2009.01.017.

Bedry, Mark, and Joel Shaw. 2012. "Using a New Intelligent Well Technology Completions Strategy to Increase Thermal EOR Recoveries - SAGD Field Trial." In *SPE EOR Conference at Oil and Gas West Asia*. Society of Petroleum Engineers. doi:10.2118/154760-MS.

Bonte, M H A, A H van den Boogaard, and J Huétink. 2008. "An Optimisation Strategy for Industrial Metal Forming Processes." *Structural and Multidisciplinary Optimization* 35 (6): 571–86. doi:10.1007/s00158-007-0206-3.

Bronsvoort, W F, and A Noort. 2004. "Multiple-View Feature Modelling for Integral Product Development." *Computer-Aided Design* 36 (10): 929–46. doi:10.1016/j.cad.2003.09.008.

Bronsvoort, Willem F., Rafael Bidarra, Maurice Dohmen, Winfried van Holland, and Klaas Jan de Kraker. 1997. "Multiple-View Feature Modelling and Conversion." In *Geometric Modeling: Theory and Practice*, 159–74. Berlin, Heidelberg: Springer Berlin Heidelberg. doi:10.1007/978-3-642-60607-6_11.

Bronsvoort, Willem F, and Frederik W Jansen. 1993. "Feature Modelling and conversion—Key Concepts to Concurrent Engineering." *Computers in Industry* 21 (1): 61–86. doi:10.1016/0166-3615(93)90045-3.

Buongiorno, Jacopo. 2010. “NOTES ON TWO-PHASE FLOW, BOILING HEAT TRANSFER, AND BOILING CRISES IN PWRs AND BWRs.” Engineering of Nuclear Systems, MIT Department of Nuclear Science and Engineering.

Butler, R.M. 1994. “Steam-Assisted Gravity Drainage: Concept, Development, Performance And Future.” *Journal of Canadian Petroleum Technology* 33 (2). Petroleum Society of Canada: 44–50. doi:10.2118/94-02-05.

Carlson, M. 2003. “SAGD and Geomechanics.” *Journal of Canadian Petroleum Technology* 42 (6). Petroleum Society of Canada. doi:10.2118/03-06-DAS.

Cavender, Travis Wayne, Timothy Hunter, and Robert Pipkin. 2011. “Method of Minimizing Liner Expansion Issues in Horizontal Thermal Applications.” In *SPE Heavy Oil Conference and Exhibition*. Society of Petroleum Engineers. doi:10.2118/150493-MS.

Çengel, Yunus A., and John M. Cimbala. 2006. *Fluid Mechanics : Fundamentals and Applications*. McGraw Hill Publication.

Çengel, Yunus A., and Afshin J. Ghajar. 2014. *Heat and Mass Transfer : Fundamentals and Applications*. McGraw-Hill.

Corriveau, Guillaume, Raynald Guilbault, and Antoine Tahan. 2009. “Genetic Algorithms and Finite Element Coupling for Mechanical Optimization.” doi:10.1016/j.advengsoft.2009.03.008.

Cuillière, Jean-Christophe Christophe, and Vincent Francois. 2014. “Integration of CAD, FEA and Topology Optimization through a Unified Topological Model.” *Computer-Aided Design and Applications* 11 (5): 493–508. doi:10.1080/16864360.2014.902677.

Cunningham, J J, and J R Dixon. 1988. “Designing with Features: The Origin of Features.” In *Proceedings of the 1988 ASME International Computers in Engineering Conference and Exhibition*, 1:237–43.

Das, Swapan Kumar. 2005. “Well Bore Hydraulics in a SAGD Well Pair.” In *SPE International Thermal Operations and Heavy Oil Symposium*. Society of Petroleum Engineers. doi:10.2118/97922-MS.

Delap, Damon, Jeff Hogge, and C. Greg Jensen. 2006. “CAD-Centric Creation and Optimization of a Gas Turbine Flowpath Module with Multiple Parameterizations.” *Computer-Aided Design and Applications* 3 (1–4): 175–84. doi:10.1080/16864360.2006.10738454.

Deng, Y.-M., G. A. Britton, Y. C. Lam, S. B. Tor, and Y. S. Ma. 2002. “Feature-Based CAD-CAE Integration Model for Injection-Moulded Product Design.” *International Journal of Production Research* 40 (15). Taylor & Francis Group : 3737–50. doi:10.1080/00207540210141643.

Deng, Y.-M., Y C Lam, S B Tor, and G A Britton. 2002. “A CAD-CAE Integrated Injection Molding Design System.” *Engineering with Computers* 18 (1): 80–92. doi:10.1007/s003660200007.

Edke, M. S., and K. H. Chang. 2006. “Shape Optimization of Heavy Load Carrying Components for Structural Performance and Manufacturing Cost.” *Structural and Multidisciplinary Optimization* 31 (5). Springer-Verlag: 344–54. doi:10.1007/s00158-005-0603-4.

Etesami, D., and S. Ahsan. 2013. “The Optimization of a Slotted Liner Design for a Horizontal Well.” *Petroleum Science and Technology* 31 (21): 2178–90. doi:10.1080/10916466.2010.551807.

Ferziger, Joel H., and Milovan Perić. 2002. *Computational Methods for Fluid Dynamics*. Berlin, Heidelberg: Springer Berlin Heidelberg. doi:10.1007/978-3-642-56026-2.

García, Manuel, Juan Duque, Pierre Boulanger, and Pablo Figueroa. 2015. “Computational Steering of CFD Simulations Using a Grid Computing Environment.” *International Journal on Interactive Design and Manufacturing (IJIDeM)* 9 (3): 235–45. doi:10.1007/s12008-014-0236-1.

Gelsey, Andrew. 1995. “Intelligent Automated Quality Control for Computational Simulation.” *AI EDAM* 9 (5): 387–400. doi:10.1017/S0890060400002717.

Gosavi, Abhijit. 2015. *Simulation-Based Optimization*. Vol. 55. Operations Research/Computer Science Interfaces Series. Boston, MA: Springer US. doi:10.1007/978-1-4899-7491-4.

Grosan, Crina, and Ajith Abraham. 2011. “Rule-Based Expert Systems.” In

*Intelligent Systems*, 149–85. Springer, Berlin, Heidelberg. doi:10.1007/978-3-642-21004-4_7.

Hoffman, Christoph M, and Robert Joan-Arinyo. 1998. "CAD and the Product Master Model." *Computer-Aided Design* 30 (11): 905–18. doi:10.1016/S0010-4485(98)00047-5.

Hoffmann, C. M., and R. Joan-Arinyo. 2000. "Distributed Maintenance of Multiple Product Views." *Computer-Aided Design* 32 (7): 421–31. doi:10.1016/S0010-4485(00)00023-3.

Johansson, Joel. 2014. "A Feature and Script Based Integration of CAD and FEA to Support Design of Variant Rich Products." *Computer-Aided Design and Applications* 11 (5): 552–59. doi:10.1080/16864360.2014.902687.

JOHN DANNENHOFFER, I I I, and JUDSON BARON. 1987. "A Hybrid Expert System for Complex CFD Problems." *8th Computational Fluid Dynamics Conference*. doi:doi:10.2514/6.1987-1111.

Kaiser, T.M.V., S. Wilson, and L.A. Venning. 2002. "Inflow Analysis and Optimization of Slotted Liners." *SPE Drilling & Completion* 17 (4). Society of Petroleum Engineers: 200–209. doi:10.2118/80145-PA.

Kao, Yung-Chou Chou, Hsin-Yu Yu Cheng, and Chen-Hua Hua She. 2006. "Development of an Integrated CAD/CAE/CAM System on Taper-Tipped Thread-Rolling Die-Plates." *Journal of Materials Processing Technology*

177 (1–3): 98–103. doi:10.1016/j.jmatprotec.2006.04.082.

Kraker, Klaas Jan de, Maurice Dohmen, and Willem F Bronsvoort. 1995. "Multiple-Way Feature Conversion to Support Concurrent Engineering." In *Proceedings of the Third ACM Symposium on Solid Modeling and Applications*, 105–14. doi:10.1145/218013.218044.

Kumar, Avinav, Anil Kumar Srivastava, and Ravi Kumar. 2010. "Design Optimization of Slotted Liner Completions in Horizontal Wells of Mumbai High Field." In *SPE Asia Pacific Oil and Gas Conference and Exhibition*. Society of Petroleum Engineers. doi:10.2118/133321-MS.

KUTLER, P., and U. MEHTA. 1984. "Computational Aerodynamics and Artificial Intelligence." In *17th Fluid Dynamics, Plasma Dynamics, and Lasers Conference*. Reston, Virigina: American Institute of Aeronautics and Astronautics. doi:10.2514/6.1984-1531.

Kyanpour, Mohammad, and Zhangxin Chen. 2014. "Design and Optimization of Orifice Based Flow Control Devices in Steam Assisted Gravity Drainage: A Case Study." In *SPE Heavy and Extra Heavy Oil Conference: Latin America*. Society of Petroleum Engineers. doi:10.2118/171109-MS.

Kyanpour, Mohammad, and Zhangxing Chen. 2013. "A New Approach for Designing Steam Splitters and Inflow Control Devices in Steam Assisted Gravity Drainage." In *SPE Heavy Oil Conference-Canada*. Society of Petroleum Engineers. doi:10.2118/165487-MS.

Lastiwka, Marty, Chris Bailey, Bruce James, and Da Zhu. 2017. “A Practical Approach to the Use and Design of Flow Control Devices in SAGD.” In *SPE Canada Heavy Oil Technical Conference*. Society of Petroleum Engineers. doi:10.2118/185005-MS.

Lee, R. J. V. 1998. “Information Supported Design for Manufacture of Injection-Moulded Rotational Products.” *International Journal of Production Research* 36 (12): 3347–66. doi:10.1080/002075498192094.

Lee, Sang Hun. 2005. “A CAD–CAE Integration Approach Using Feature-Based Multi-Resolution and Multi-Abstraction Modelling Techniques.” *Computer-Aided Design*, CAD’ 04 Special Issue: Product Design, Integration and Manufacturing, 37 (9): 941–55. doi:10.1016/j.cad.2004.09.021.

Li, Lei, Carlos F Lange, and Yongsheng Ma. 2017. “Association of Design and Computational Fluid Dynamics Simulation Intent in Flow Control Product Optimization.” *Proceedings of the Institution of Mechanical Engineers, Part B: Journal of Engineering Manufacture*, March. SAGE PublicationsSage UK: London, England, 954405417697352. doi:10.1177/0954405417697352.

Li, Lei, and Yongsheng Ma. 2016. “CAD/CAE Associative Features for Cyclic Fluid Control Effect Modeling.” *Computer-Aided Design and Applications* 13 (2): 208–20. doi:10.1080/16864360.2015.1084190.

Li, Lei, Yongsheng Ma, and Carlos F Lange. 2016. “Association of Design and Simulation Intent in CAD/CFD Integration.” *Procedia CIRP* 56: 1–6.

doi:10.1016/j.procir.2016.10.006.

Li, Yingguang, Xu Liu, James X. Gao, and Paul G. Maropoulos. 2012. “A Dynamic Feature Information Model for Integrated Manufacturing Planning and Optimization.” *CIRP Annals - Manufacturing Technology* 61 (1). CIRP: 167–70. doi:10.1016/j.cirp.2012.03.085.

Lin, Bor-Tsuen Tsuen, and Chun-Chih Chih Kuo. 2008. “Application of an Integrated CAD/CAE/CAM System for Stamping Dies for Automobiles.” *International Journal of Advanced Manufacturing Technology* 35 (9–10): 1000–1013. doi:10.1007/s00170-006-0785-y.

Liu, Jikai, Zhengrong Cheng, and Yongsheng Ma. 2016. “Product Design-Optimization Integration via Associative Optimization Feature Modeling.” *Advanced Engineering Informatics* 30 (4). Elsevier Ltd: 713–27. doi:10.1016/j.aei.2016.09.004.

Liu, Jikai, Kajsa Duke, and Yongsheng Ma. 2015. “Computer-Aided Design–computer-Aided Engineering Associative Feature-Based Heterogeneous Object Modeling.” *Advances in Mechanical Engineering* 7 (12): 1687814015619767. doi:10.1177/1687814015619767.

Liu, Jikai, and Yongsheng Ma. 2017. “Design of Pipeline Opening Layout through Level Set Topology Optimization.” *Structural and Multidisciplinary Optimization* 55 (5). Springer Berlin Heidelberg: 1613–28. doi:10.1007/s00158-016-1602-3.

Liu, Jikai, Yongsheng Ma, Junyu Fu, and Kajsa Duke. 2015. “A Novel CACD/CAD/CAE Integrated Design Framework for Fiber-Reinforced Plastic Parts.” *Advances in Engineering Software* 87 (November). Elsevier Ltd: 13–29. doi:10.1016/j.advengsoft.2015.04.013.

Liu, Xu, Yingguang Li, and Limin Tang. 2015. “A Dynamic Feature–based Operation Planning Method for 2.5-Axis Numerical Control Machining of Complex Structural Parts.” *Proceedings of the Institution of Mechanical Engineers, Part B: Journal of Engineering Manufacture* 229 (7): 1206–20. doi:10.1177/0954405414560621.

Luo, Liheng, Dianzi Liu, Meiling Zhu, and Jianqiao Ye. 2017. “Metamodel-Assisted Design Optimization of Piezoelectric Flex Transducer for Maximal Bio-Kinetic Energy Conversion.” *Journal of Intelligent Material Systems and Structures* 28 (18). SAGE PublicationsSage UK: London, England: 2528–38. doi:10.1177/1045389X17689943.

Ma, Y.-S., G A Britton, S B Tor, and L Y Jin. 2007. “Associative Assembly Design Features: Concept, Implementation and Application.” *The International Journal of Advanced Manufacturing Technology* 32 (5–6): 434–44. doi:10.1007/s00170-005-0371-8.

Ma, Y.-S., G. Chen, and G. Thimm. 2008. “Paradigm Shift: Unified and Associative Feature-Based Concurrent and Collaborative Engineering.” *Journal of Intelligent Manufacturing* 19 (6). Springer US: 625–41.

doi:10.1007/s10845-008-0128-y.

Ma, Y -S., and T Tong. 2003. “Associative Feature Modeling for Concurrent Engineering Integration.” *Computers in Industry* 51 (1): 51–71. doi:10.1016/S0166-3615(03)00025-3.

Martino, T. De, and F. Giannini. 1998. “Feature-Based Product Modelling in Concurrent Engineering.” In *Globalization of Manufacturing in the Digital Communications Era of the 21st Century*, 351–62. Boston, MA: Springer US. doi:10.1007/978-0-387-35351-7_28.

Matin, Ivan, Miodrag Hadzistevic, Janko Hodolic, Djordje Vukelic, and Dejan Lukic. 2012. “A CAD/CAE-Integrated Injection Mold Design System for Plastic Products.” *The International Journal of Advanced Manufacturing Technology* 63 (5–8): 595–607. doi:10.1007/s00170-012-3926-5.

Medina, Max. 2015. “Design and Field Evaluation of Tubing-Deployed Passive Outflow-Control Devices in Steam-Assisted-Gravity-Drainage Injection Wells.” *SPE Production & Operations* 30 (4): 283–92. doi:10.2118/165563-PA.

Merkel, M, and A Schumacher. 2004. “An Automated Optimization Process for a CAE Driven Product Development.” *Journal of Mechanical Design* 125 (4): 694–700. doi:10.1115/1.1631570.

Montgomery, Douglas C. 2012. *Design and Analysis of Experiments, 8th Edition*.

Wiley Global Education.

Mun, Duhwan, Soonhung Han, Junhwan Kim, and Youchon Oh. 2003. "A Set of Standard Modeling Commands for the History-Based Parametric Approach." *Computer-Aided Design* 35 (13): 1171–79. doi:10.1016/S0010-4485(03)00022-8.

Nolan, Declan C., Christopher M. Tierney, Cecil G. Armstrong, and Trevor T. Robinson. 2015. "Defining Simulation Intent." *Computer-Aided Design* 59 (August). Elsevier Ltd: 50–63. doi:10.1016/j.cad.2014.08.030.

Noroozi, Mehdi, Marco Melo, R.P.(Pete) Singbeil, and Blair Neil. 2014. "Investigation of Orifice Type Flow-Control Device Properties on the SAGD Process Using Coupled Wellbore Reservoir Modeling." In *SPE Heavy and Extra Heavy Oil Conference: Latin America*. Society of Petroleum Engineers. doi:10.2118/171131-MS.

Oberkampf, William L, and Timothy G Trucano. 2002. "Verification and Validation in Computational Fluid Dynamics." *Progress in Aerospace Sciences* 38 (3): 209–72. doi:10.1016/S0376-0421(02)00005-2.

Onwubolu, Godfrey C., and B. V. Babu. 2004. *New Optimization Techniques in Engineering*. Vol. 141. Studies in Fuzziness and Soft Computing. Berlin, Heidelberg: Springer Berlin Heidelberg. doi:10.1007/978-3-540-39930-8.

Papalambros, Panos Y. 2002. "The Optimization Paradigm in Engineering Design:

Promises and Challenges." *Computer-Aided Design* 34 (12). Elsevier: 939–51. doi:10.1016/S0010-4485(01)00148-8.

Park, Hong-Seok, and Xuan-Phuong Dang. 2010. "Structural Optimization Based on CAD–CAE Integration and Metamodeling Techniques." *Computer-Aided Design* 42: 889–902. doi:10.1016/j.cad.2010.06.003.

Price, Mark A., Trevor T. Robinson, Danielle Soban, Adrian Murphy, Cecil G. Armstrong, Roisin McConnell, and Rajkumar Roy. 2013. "Maintaining Design Intent for Aircraft Manufacture." *CIRP Annals - Manufacturing Technology* 62 (1). CIRP: 99–102. doi:10.1016/j.cirp.2013.03.124.

Robinson, Bill, Joseph Kenny, Ivan Lazaro Hernandez-Hdez, Jeimy Andrea Bernal, and Rob Chelak. 2005. "Geostatistical Modeling Integral to Effective Design and Evaluation of SAGD Processes of an Athabasca Oilsands Reservoir, A Case Study." In *SPE International Thermal Operations and Heavy Oil Symposium*. Society of Petroleum Engineers. doi:10.2118/97743-MS.

Robinson, Trevor T, Cecil G Armstrong, and Hung Soon Chua. 2012. "Strategies for Adding Features to CAD Models in Order to Optimize Performance." *Structural and Multidisciplinary Optimization* 46 (3): 415–24. doi:10.1007/s00158-012-0770-z.

Rubio, Gonzalo, Eusebio Valero, and Sven Lanzan. 2012. "Computational Fluid Dynamics Expert System Using Artificial Neural Networks." *International*

*Journal of Computer, Electrical, Automation, Control and Information Engineering* 6 (3): 413–17. http://www.waset.org/publications/5734.

Sakawa, Masatoshi. 2002. *Genetic Algorithms and Fuzzy Multiobjective Optimization*. Vol. 14. Operations Research/Computer Science Interfaces Series. Boston, MA: Springer US. doi:10.1007/978-1-4615-1519-7.

Sanderse, B., S.P. Pijl, and B. Koren. 2011. "Review of Computational Fluid Dynamics for Wind Turbine Wake Aerodynamics." *Wind Energy* 14 (7). John Wiley & Sons, Ltd: 799–819. doi:10.1002/we.458.

Sanfilippo, Emilio M., and Stefano Borgo. 2016. "What Are Features? An Ontology-Based Review of the Literature." *Computer-Aided Design* 80 (November). Elsevier Ltd: 9–18. doi:10.1016/j.cad.2016.07.001.

Shah, Jami J. 1991. "Conceptual Development of Form Features and Feature Modelers." *Research in Engineering Design* 2 (2): 93–108. doi:10.1007/BF01579254.

Shelton, M. L., B. A. Gregory, S. H. Lamson, H. L. Moses, R. L. Doughty, and T. Kiss. 1993. "Optimization of a Transonic Turbine Airfoil Using Artificial Intelligence, CFD and Cascade Testing." In *Volume 3A: General*, V03AT15A012. ASME. doi:10.1115/93-GT-161.

Shephard, Mark S, Mark W Beall, Robert M O'Bara, and Bruce E Webster. 2004. "Toward Simulation-Based Design." *Finite Elements in Analysis and Design*,

The Fifteenth Annual Robert J. Melosh Competition, 40 (12): 1575–98. doi:10.1016/j.finel.2003.11.004.

Simpson, T.W. W, J.D. D Poplinski, P. N. Koch, and J.K. K Allen. 2014. "Metamodels for Computer-Based Engineering Design: Survey and Recommendations." *Engineering with Computers* 17 (2): 129–50. doi:10.1007/PL00007198.

Smit, M. Sypkens, and W. F. Bronsvoort. 2009. "Integration of Design and Analysis Models." *Computer-Aided Design and Applications* 6 (6): 795–808. doi:10.3722/cadaps.2009.795-808.

"Steam Table." 2017. Accessed December 11. http://www.spiraxsarco.com/Resources/Pages/Steam-Tables/saturated-steam.aspx.

Stremel, Paul, Michael Mendenhall, and Martin Hegedus. 2007. "BPX - A Best Practices Expert System for CFD." In *45th AIAA Aerospace Sciences Meeting and Exhibit*. Reston, Virigina: American Institute of Aeronautics and Astronautics. doi:10.2514/6.2007-974.

Suh, Yong Seok, and Michael J. Wozny. 1997. "Interactive Feature Extraction for a Form Feature Conversion System." In *Proceedings of the Fourth ACM Symposium on Solid Modeling and Applications - SMA '97*, 111–22. SMA '97. ACM. doi:10.1145/267734.267762.

Sun, Jian Xiang, Ye Yang, and Jing Yi Tian. 2013. “Structural Topology Optimization for Improvements of Some Shell Structures’ Rib Design Process.” *Applied Mechanics and Materials* 385–386 (August). Trans Tech Publications: 1927–32. doi:10.4028/www.scientific.net/AMM.385-386.1927.

Tang, S.-H., Gang Chen, and Y.-S. Ma. 2013. “Fundamental Concepts of Generic Features.” In *Semantic Modeling and Interoperability in Product and Process Engineering*, 89–115. Springer, London. doi:10.1007/978-1-4471-5073-2_4.

Tierney, Christopher M., Declan C. Nolan, Trevor T. Robinson, and Cecil G. Armstrong. 2014. “Managing Equivalent Representations of Design and Analysis Models.” *Computer-Aided Design and Applications* 11 (2): 193–205. doi:10.1080/16864360.2014.846091.

TONG, S. 1985. “Design of Aerodynamic Bodies Using Artificial Intelligence/expert System Technique.” In *23rd Aerospace Sciences Meeting*. Vol. 14. Reston, Virigina: American Institute of Aeronautics and Astronautics. doi:10.2514/6.1985-112.

Uddin, Md M., and Yongsheng Ma. 2015. “A Feature-Based Engineering Methodology for Cyclic Modeling and Analysis Processes in Plastic Product Development.” *Computer-Aided Design and Applications* 12 (6): 772–83. doi:10.1080/16864360.2015.1033343.

Venkatakrishnan, V., Manuel D. Salas, and Sukumar R. Chakravarthy. 1998.

*Barriers and Challenges in Computational Fluid Dynamics*. Vol. 6. ICASE/LaRC Interdisciplinary Series in Science and Engineering. Dordrecht: Springer Netherlands. doi:10.1007/978-94-011-5169-6.

Vosniakos, George-Christopher, Panorios Benardos, and Virginia Lipari. 2014. "Multi-Disciplinary Design Optimisation of Mechanical Parts with Freeform Surfaces: Case Study Encompassing Manufacturing Criteria." *Proceedings of the Institution of Mechanical Engineers, Part B: Journal of Engineering Manufacture* 229 (2): 954405414527957. doi:10.1177/0954405414527957.

Wang, G. Gary, and S. Shan. 2007. "Review of Metamodeling Techniques in Support of Engineering Design Optimization." *Journal of Mechanical Design* 129 (4). American Society of Mechanical Engineers: 370. doi:10.1115/1.2429697.

Wang, Wenwei, Fengling Gao, Yuting Cheng, and Cheng Lin. 2017. "Multidisciplinary Design Optimization for Front Structure of an Electric Car Body-in-White Based on Improved Collaborative Optimization Method." *International Journal of Automotive Technology* 18 (6). The Korean Society of Automotive Engineers: 1007–15. doi:10.1007/s12239-017-0098-1.

Wesley, Leonard, Janet Lee, Laura Rodman, and Robert Childs. 1998. "Toward an Integrated CFD Expert System Environment." In *36th AIAA Aerospace Sciences Meeting and Exhibit*. Reston, Virigina: American Institute of Aeronautics and Astronautics. doi:10.2514/6.1998-1005.

White, Frank M. 2011. *Fluid Mechanics*. 7thed. New York, NY: McGraw-Hill.

"Workbench Scripting Guide." 2013. Canonsburg, PA: ANSYS, Inc.

Xie, Jueren. 2015. "Slotted Liner Design Optimization for Sand Control in SAGD Wells." In *SPE Thermal Well Integrity and Design Symposium*. Society of Petroleum Engineers. doi:10.2118/178457-MS.

Yang, Qinwen, and Deyi Xue. 2014. "Comparative Study on Influencing Factors in Adaptive Metamodeling." *Engineering with Computers* 31 (3). Springer London: 561–77. doi:10.1007/s00366-014-0358-x.

Zhang, Chaoyang, Weidong Li, Pingyu Jiang, and Peihua Gu. 2016. "Experimental Investigation and Multi-Objective Optimization Approach for Low-Carbon Milling Operation of Aluminum." *Proceedings of the Institution of Mechanical Engineers, Part C: Journal of Mechanical Engineering Science*, August, 954406216640574. doi:10.1177/0954406216640574.

Zheng, L Y, Christopher a McMahon, L Li, Lian Ding, and J Jamshidi. 2008. "Key Characteristics Management in Product Lifecycle Management: A Survey of Methodologies and Practices." *Proceedings of the Institution of Mechanical Engineers, Part B: Journal of Engineering Manufacture* 222 (8): 989–1008. doi:10.1243/09544054JEM1045.

# Appendix: The Full Set of Design Variables and Corresponding Response

| Run No. | $x_1$ | $x_2$ | $x_3$ | $x_4$ | $x_5$ | Normalized $E_0$ (kg/s) |
|---|---|---|---|---|---|---|
| DP1 | -1 | -1 | -1 | -1 | -1 | 1.9498E-04 |
| DP2 | -1 | -1 | -1 | -1 | 1 | 1.5906E-04 |
| DP3 | -1 | -1 | -1 | 1 | -1 | 2.7853E-04 |
| DP4 | -1 | -1 | -1 | 1 | 1 | 3.0530E-04 |
| DP5 | -1 | -1 | 1 | -1 | -1 | 1.6914E-04 |
| DP6 | -1 | -1 | 1 | -1 | 1 | 1.3918E-04 |
| DP7 | -1 | -1 | 1 | 1 | -1 | 1.2757E-04 |
| DP8 | -1 | -1 | 1 | 1 | 1 | 1.4775E-04 |
| DP9 | -1 | 1 | -1 | -1 | -1 | 2.2295E-04 |
| DP10 | -1 | 1 | -1 | -1 | 1 | 2.6967E-04 |
| DP11 | -1 | 1 | -1 | 1 | -1 | 3.6906E-04 |
| DP12 | -1 | 1 | -1 | 1 | 1 | 4.0617E-04 |
| DP13 | -1 | 1 | 1 | -1 | -1 | 2.2148E-04 |
| DP14 | -1 | 1 | 1 | -1 | 1 | 2.3743E-04 |
| DP15 | -1 | 1 | 1 | 1 | -1 | 2.3243E-04 |
| DP16 | -1 | 1 | 1 | 1 | 1 | 2.3686E-04 |

| Run No. | $x_1$ | $x_2$ | $x_3$ | $x_4$ | $x_5$ | Normalized $E_0$ (kg/s) |
|---|---|---|---|---|---|---|
| DP17 | 1 | -1 | -1 | -1 | -1 | 1.9764E-04 |
| DP18 | 1 | -1 | -1 | -1 | 1 | 1.5014E-04 |
| DP19 | 1 | -1 | -1 | 1 | -1 | 2.9911E-04 |
| DP20 | 1 | -1 | -1 | 1 | 1 | 2.8789E-04 |
| DP21 | 1 | -1 | 1 | -1 | -1 | 1.7822E-04 |
| DP22 | 1 | -1 | 1 | -1 | 1 | 1.5453E-04 |
| DP23 | 1 | -1 | 1 | 1 | -1 | 1.4087E-04 |
| DP24 | 1 | -1 | 1 | 1 | 1 | 1.3308E-04 |
| DP25 | 1 | 1 | -1 | -1 | -1 | 1.1927E-04 |
| DP26 | 1 | 1 | -1 | -1 | 1 | 1.4458E-04 |
| DP27 | 1 | 1 | -1 | 1 | -1 | 2.5307E-04 |
| DP28 | 1 | 1 | -1 | 1 | 1 | 2.5576E-04 |
| DP29 | 1 | 1 | 1 | -1 | -1 | 1.1409E-04 |
| DP30 | 1 | 1 | 1 | -1 | 1 | 1.1088E-04 |
| DP31 | 1 | 1 | 1 | 1 | -1 | 1.0360E-04 |
| DP32 | 1 | 1 | 1 | 1 | 1 | 1.0109E-04 |
| DP33 | -2.3784 | 0 | 0 | 0 | 0 | 3.3097E-04 |
| DP34 | 2.3784 | 0 | 0 | 0 | 0 | 2.3299E-04 |
| DP35 | 0 | -2.3784 | 0 | 0 | 0 | 1.3610E-04 |
| DP36 | 0 | 2.3784 | 0 | 0 | 0 | 1.5534E-04 |

| Run No. | $x_1$ | $x_2$ | $x_3$ | $x_4$ | $x_5$ | Normalized $E_0$ (kg/s) |
|---|---|---|---|---|---|---|
| DP37 | 0 | 0 | -2.3784 | 0 | 0 | 3.0759E-04 |
| DP38 | 0 | 0 | 2.3784 | 0 | 0 | 1.5942E-04 |
| DP39 | 0 | 0 | 0 | -2.3784 | 0 | 1.2290E-04 |
| DP40 | 0 | 0 | 0 | 2.3784 | 0 | 2.0310E-04 |
| DP41 | 0 | 0 | 0 | 0 | -2.3784 | 1.0398E-04 |
| DP42 | 0 | 0 | 0 | 0 | 2.3784 | 1.2480E-04 |
| DP43 | 0 | 0 | 0 | 0 | 0 | 1.1560E-04 |
| DP44 | 0 | 0 | 0 | 0 | 0 | 1.1560E-04 |
| DP45 | 1.5716 | 2.3216 | 2.3716 | 2.3216 | -2.3784 | 1.0385E-04 |
| DP46 | -0.4994 | -2.3784 | 2.3716 | 2.3216 | 2.3216 | 1.4051E-04 |
| DP47 | 1.0466 | 1.4216 | 0.5966 | -0.2784 | -0.2784 | 1.4029E-04 |
| DP48 | 0.8216 | 0.9216 | 0.7966 | 0.0216 | -0.1784 | 1.0352E-04 |
| DP49 | 0.8466 | 0.9216 | 0.1466 | -0.9784 | 0.4216 | 1.0135E-04 |
| DP50 | 0.7216 | 0.7216 | 0.9716 | 0.3216 | -0.2784 | 1.0865E-04 |
| DP51 | 0.8966 | 0.9216 | -0.7534 | -2.3784 | 1.4216 | 1.0576E-04 |
| DP52 | 0.7716 | 0.8216 | 0.9716 | 0.3216 | -0.3784 | 1.0904E-04 |
| DP53 | 0.7716 | 0.8216 | 0.8466 | 0.1216 | -0.2784 | 1.0445E-04 |
| DP54 | 0.7716 | 0.8216 | 0.7716 | 0.0216 | -0.1784 | 1.0833E-04 |
| DP55 | 0.7716 | 0.8216 | 0.6466 | -0.1784 | -0.0784 | 1.0202E-04 |